A Comprehensive Mechanistic Analysis of Palladium- and Nickel-Catalyzed α,β-Dehydrogenation of Carbonyls via Organozinc Intermediates

Alexandra K. Bodnar, Suzanne M. Szewczyk, Yang Sun, Yifeng Chen, Anson X. Huang, and Timothy R. Newhouse*

Department of Chemistry, Yale University
225 Prospect St., New Haven, Connecticut 06520-8107
*E-mail: timothy.newhouse@yale.edu

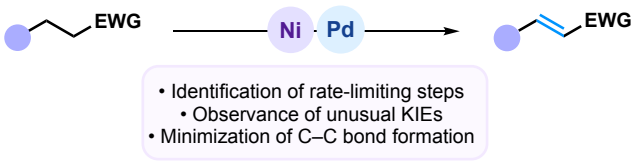

A Comprehensive Mechanistic Analysis of Palladium- and Nickel-Catalyzed α,β-Dehydrogenation of Carbonyls via Organozinc Intermediates

Alexandra K. Bodnar, Suzanne M. Szewczyk, Yang Sun, Yifeng Chen, Anson X. Huang, and Timothy R. Newhouse*

Department of Chemistry, Yale University, 225 Prospect Street, New Haven, Connecticut 06520-8107, United States.

ABSTRACT: Introducing degrees of unsaturation into small molecules is a central transformation in organic synthesis. A strategically useful category of this reaction type is conversion of alkanes into alkenes for substrates with an adjacent electron withdrawing group. An efficient strategy for this conversion has been deprotonation to form a stabilized organozinc intermediate that can be subject to α,β-dehydrogenation through palladium or nickel catalysis. This general reactivity blueprint presents a window to uncover and understand the reactivity of Pd- and Ni-enolates.

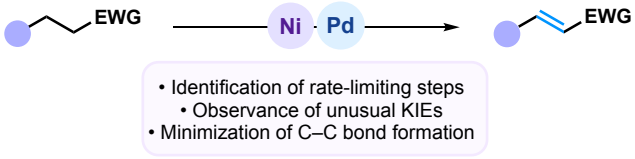

Within this context, it was determined that β-hydride elimination is slow and proceeds via a concerted *syn*-elimination. One interesting finding is that β-hydride elimination can be preferred to a greater extent than C–C bond formation for Ni more so than with Pd, which defies the generally assumed trends that β-hydride elimination is more facile with Pd than Ni. Discussion of these findings are informed by KIE experiments, DFT calculations, stoichiometric reactions, and rate studies.

Additionally, this report details an in-depth analysis of a methodological manifold for practical dehydrogenation and should enable its application to challenges in organic synthesis.

INTRODUCTION

Polarized alkenes are regularly employed functional groups for enabling regioselective addition reactions. Their utility and versatility lead to their widespread occurrence as synthetic intermediates in multistep synthesis of natural products, pharmaceuticals, and other complex small molecules. While numerous building blocks can give rise to polarized alkenes, one particularly advantageous approach is to desaturate the positions adjacent to electron-withdrawing groups. In particular, the goal to introduce an olefin next to a carbonyl has propelled the development of several methodologies.[1]

To access this vital class of α,β-unsaturated compounds, direct α,β-dehydrogenation from ubiquitous saturated counterparts is a straightforward strategy. Classic approaches for carbonyl dehydrogenation typically involve two steps: introduction of the necessary oxidation state at the carbonyl α-position, followed by an elimination reaction (e.g. α-halocarbonyl elimination, selenoxide sigmatropic rearrangement, etc.).[2]

The global strategy to pre-functionalize and in a subsequent operation generate an alkene has also been employed in transition metal catalysis. In pioneering dehydrogenation studies in 1978, Saegusa demonstrated that enoxysilanes could undergo transmetalation to provide palladium enolates that yield enones upon β-hydride elimination.[3] Relatedly, Tsuji showed that allyl-Pd enolates generated from either allyl β-keto esters or allyl enol carbonates could also form enones through decarboxylation (Figure 1A).[4] More recently, Stahl developed a single-step aerobic dehydrogenation of aldehydes and ketones using catalytic Pd.[5]

The general challenge with these approaches has been that they are either limited to more acidic carbonyls (e.g. ketones and aldehydes) or that they require multiple steps. We addressed this key challenge by inventing a mechanistic approach to dehydrogenate a wide range of electron-deficient molecules in a single operation.[6] To date, numerous elegant one-step α,β-dehydrogenations of ketones and aldehydes have been developed,[7] while our group reported several methods for less acidic functionalities, including esters, amides, carboxylic acids, nitriles, and heterocycles.[8] Other methods have also emerged that complement our approach and the accompanying scope. Dong and co-workers reported a Pd- or Pt-catalyzed desaturation of lactams using boron enolates, and shortly thereafter reported a strategy utilizing Cu-catalyzed enolization followed by oxidative elimination to access unsaturated lactones, lactams, and ketones (Figure 1B).[9] Huang has reported a dehydrogenation of amides and carboxylic acids, which proceeds through an allyl-Ir intermediate to generate dienes (Figure 1C).[10] A one-pot electrophilic activation followed by selective selenium(IV)-mediated α,β-dehydrogenation of amides has also been reported by Maulide.[11] Yu and co-workers achieved the Pd-catalyzed dehydrogenation of carboxylic acids via their weak coordination approach and β-C–H activation (Figure 1D).[12] Additionally, Baran reported an electrochemical desaturation of carbonyl-containing compounds, highlighting the complementarity of this approach to reported metal-catalyzed methodologies.[13] Specifically, our group showed that Pd- and Ni-catalyzed methods using either stoichiometric allyl or aryl oxidants could be developed to promote α,β-dehydrogenation of ketones, esters, amides, carboxylic acids, nitriles, and heterocycles (Figure 1E).[8] The development of these methodologies has enabled access to synthetically useful unsaturated molecules, as shown in Figure 1F.[6,14] Many transition metal catalyzed dehydrogenation methods are still being developed, underscoring the importance of this transformation.[15]

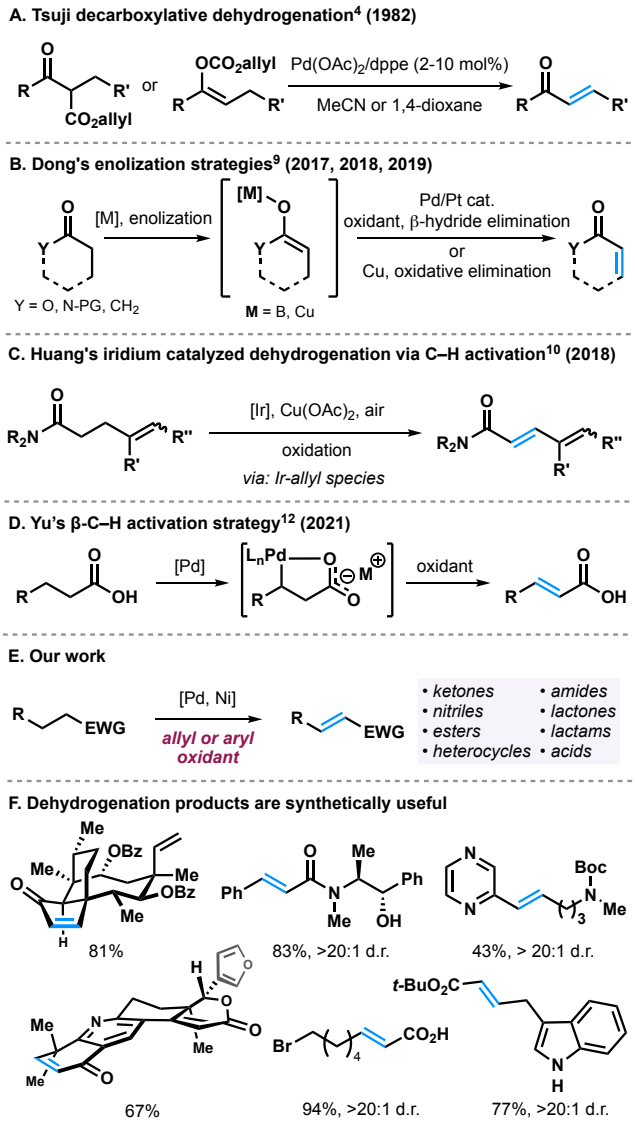

Figure 1. Previous dehydrogenation methodologies.

Questions of mechanistic interest. After successful development of our α,β-dehydrogenation approach, many questions were prompted by the mechanism of these Pd- and Ni-catalyzed reactions. Can dehydrogenation serve as a mechanistic probe to learn about fundamental reactivity differences between Pd and Ni? Does the metal amide base play a role outside of enolate formation (Figure 3)? How can undesired pathways involving incorporation of the oxidant be suppressed (Figure 4)? Which step or steps are turnover limiting and how can they be accelerated (Figures 5, 6, & 7)? In this report we describe insights into the mechanism of our reported allyl-Pd-/Ni-catalyzed α,β-dehydrogenation reactions.

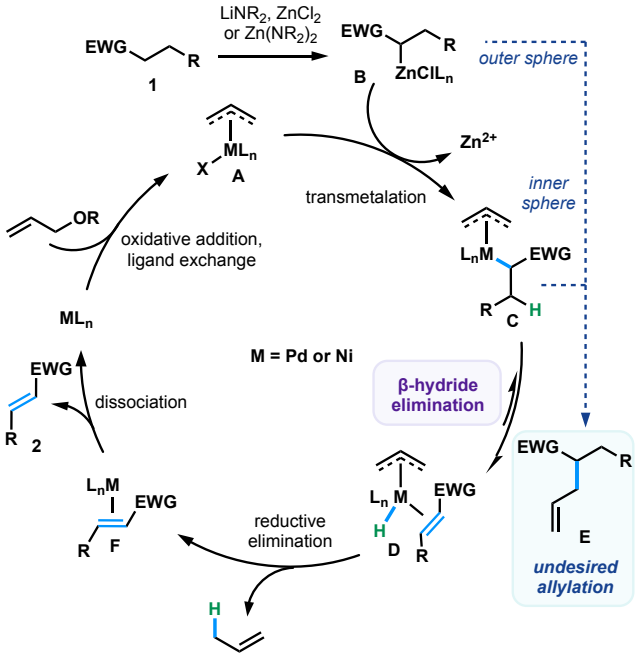

Figure 2. Proposed catalytic cycle.

RESULTS AND DISCUSSION

Mechanistic Blueprint. Throughout the development of our dehydrogenation strategy, we envisioned a plausible mechanism (Figure 2) inspired by Tsuji's pioneering efforts.[4a] It should be noted that the mechanistic blueprint in Figure 2 is meant as a guide for reaction optimization. Allyl-metal complex **A** undergoes transmetalation with zinc enolate **B**, which is formed from *in situ* deprotonation of the substrate, resulting in an allyl-metal enolate **C**. Subsequent β-hydride elimination gives the desired product and allyl-metal hydride species **D**, which undergoes reductive elimination to generate propene gas and a low valent metal species. Oxidative addition with an allyl oxidant regenerates the active allyl-metal catalyst **A**. Alternative reactivity would be observed if intermediate **C** undergoes reductive elimination instead of β-hydride elimination to form allylation product **E**, or if nucleophilic substitution of allyl-metal species **A** occurs with enolate **B**.

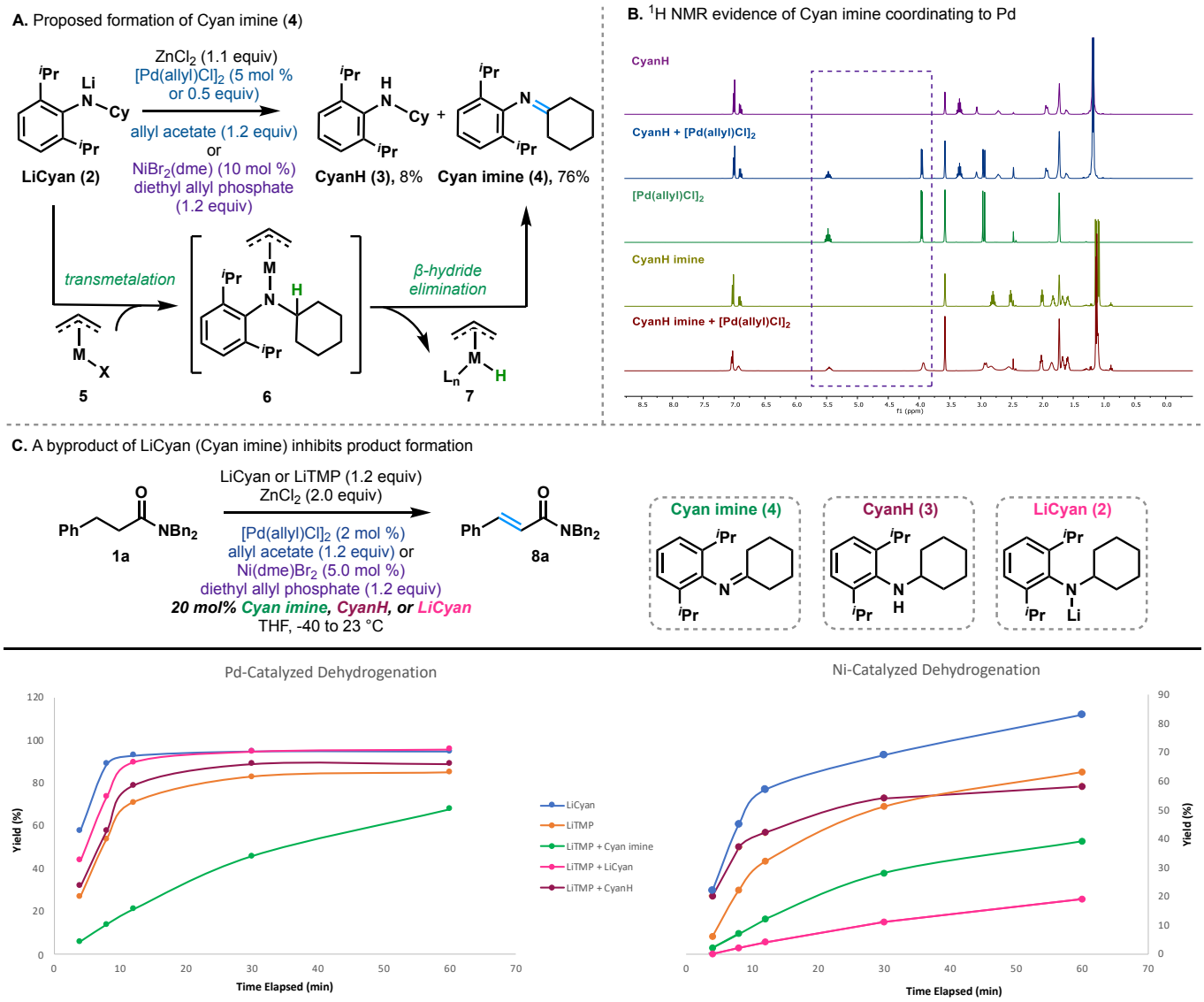

Figure 3. Examination of CyanH and its derivatives as ligands.

A number of variations on this proposed cycle can be envisioned, but our attention focused mostly on the key selectivity questions that relate to β-hydride elimination. One alternative possibility to that elementary step is that species **F** could be formed directly from species **C** via a concerted transfer of the hydride to the allyl ligand. An additional possibility is that instead of β-hydride elimination, a Yu-type directed C–H insertion occurs.[12] Even along the path outlined in Figure 2, there is the potential to form multimetallic intermediates wherein either multiple Pd/Ni catalytic centers are involved, or mixed metallic intermediates with Zn and a catalytically active metal center participate synergistically.[16] Furthermore, the aggregation state of the enolate is not known, and monomers, dimers, tetramers, and other mono- or mixed metallic aggregates are conceivable and even likely.[17] Considerations about the enolate structure and the role of multimetallic intermediates are certainly important, but are beyond the scope of the present study.

Base Effects. The role of the base is complicated in α,β-dehydrogenation by serving the primary function of enolate formation and the secondary function of impacting the speciation of the catalytically active metal. While differences in the base employed can alter enolate structure, and that aggregation state is likely important,[17] we focused our attention on the impact that this reaction component may have on Pd or Ni catalysis.[18] We examined whether lithium amide bases are essential to the reaction and found that they impact the efficiency of the transformation beyond deprotonation (Supporting Information, Table S1). Even for substrates that cannot adopt *E*- and *Z*-diastereomeric enolates, the base impacts the synthetic efficiency to a significant extent. We then determined the extent to which the base impacts the rate of dehydrogenation as evaluated in the Supporting Information (Figure S4). While LiTMP is competent in the reaction, using LiCyan results in an increased initial rate of the reaction, as well as improved yields.

Using amide **1a** as a substrate, we compared the rates of dehydrogenation using lithium cyclohexyl(2,6-diisopropylphenyl)amide (LiCyan, **2**) and LiTMP as the base for both Pd and Ni catalysts. The product was generated significantly faster and in higher yield when Pd was used as the catalyst with LiCyan as the base (Figure S4, gray line vs yellow line). With Ni as the catalyst, the initial reaction rates among LiCyan and LiTMP were approximately comparable, but

LiCyan provided a higher yield of the desired product by more than 20% (Figure S4, blue line vs. orange line). That said, these results do not rule out that the base may influence the aggregation state of the deprotonated substrates.

A byproduct of this transformation is derived from oxidation of CyanH (**3**) to the corresponding imine (**4**). We postulate that Cyan imine (**4**) is formed via β-hydride elimination of an *N*-bound Pd complex. [19,20] In order to test this hypothesis, we subjected LiCyan (**2**) to dehydrogenation reaction conditions using a stoichiometric amount of $[Pd(allyl)Cl]_2$, and 8% of CyanH and 76% of imine **4** was recovered (Figure 3A). This imine (**4**) is formed when LiCyan reacts directly with allyl-Pd/Ni species such as the monomer **5** or the corresponding dimer. This would occur via transmetalation of LiCyan to **6**, followed by β-hydride elimination to yield **4**. Reacting catalytic amounts of $[Pd(allyl)Cl]_2$ or $Ni(dme)Br_2$ with LiCyan under the same conditions at ambient temperature generated a similar ratio of CyanH and imine **4** that was observed in the stoichiometric reaction (9:1, Cyan imine : CyanH). These experiments demonstrate that even though the base is sterically hindered, it is capable of binding to Pd and Ni centers.

In order to determine whether **3** or **4** could bind to the metal center, we evaluated this question by ^{1}H NMR. A solution of CyanH (**3**) and a stoichiometric amount of $[Pd(allyl)Cl]_2$ did not show evidence of complexation (Figure 3B) – even after refluxing in THF-d_8. However, Cyan imine (**4**) was discovered to bind to $[Pd(allyl)Cl]_2$ at ambient temperature, as evidenced by the ^{1}H-NMR spectrum in Figure 3. These spectra show deviated shifts for the allylic protons and significant peak broadening consistent with previously reported amino-Pd-allyl complexes.[21] In the case of LiCyan (**2**), an unstable complex forms as evidenced by the formation of Pd black upon treatment of LiCyan with a Pd(II) source. These results are surprising, as there are sparse examples of monodentate amides binding to transition metals in the context of catalysis.[19]

Given the presence of Pd- and Ni-bound intermediates, we set out to determine if Cyan imine, CyanH, or LiCyan had an influence on the rate or efficiency of catalysis. Three supplementary time-track experiments were carried out with catalytic amounts of Cyan imine (Figure 3C, green line), CyanH (red line), or LiCyan (pink line) with Pd or Ni as the catalyst and LiTMP as base. The addition of 0.20 equivalents of Cyan imine significantly decreased the amount of product formed for both Pd and Ni, presumably via coordination that inhibits catalysis. Based on the data obtained from Figure 3, we conclude that Cyan imine, which can coordinate to the metal center, inhibits Pd- and Ni-catalyzed dehydrogenation.

The addition of 0.20 equivalents of CyanH (red line) did not significantly increase or decrease the yield for either Ni or Pd. These data show that for the Ni-catalyzed dehydrogenation, LiTMP and its TMPH participate less productively in the reaction than LiCyan and its CyanH (orange line vs. blue line).

Interestingly, when 0.20 equivalents of LiCyan (pink line) were added using Pd as the catalyst, the yield could be recovered completely. However, for the analogous experiment with Ni as the catalyst, the yield decreases dramatically. These results suggest that Cyan increases the initial rate and overall yield of the reaction for Pd, but that this effect is not translatable to the Ni-based system.

From the rate experiments in Figure 3, it is evident that Cyan imine acts as an inhibitor in both Pd and Ni dehydrogenation reactions. This may be due to binding of the imine to the metal center. However, alternatives such as the imine impacting speciation of the lithium or zinc enolates cannot be ruled out. At this juncture the structural basis for how the amide base impacts the speciation of the Pd and Ni centers is unknown.

Inhibition Studies. In addition to the imine byproduct, we hypothesized that other reaction components that coordinate to the metal center, such as electron-deficient alkenes, decrease the rate of dehydrogenation. We conducted a series of experiments that demonstrate that alkene products act as inhibitors, reducing yields of dehydrogenation by 20–100% (Supporting Information, Figure S5 and Table S2).[22]

A variety of allyl electrophiles, pre-catalysts, metal salt additives, and Zn sources were examined in comprehensive optimization studies, and the results of those studies can be found in the Supporting Information (Tables S5, S6, S7, and S8). Interestingly, when LiOH or LiCl are added, yields decreased to 84% and 78% (from 91%) under Pd-catalyzed conditions; under Ni-catalyzed conditions, these effects are more pronounced, with yields decreased to 68% and 4% (from 90%). These outcomes are indicative of the greater moisture sensitivity of the Ni-catalyzed reaction relative to the Pd-catalyzed condition.

Avoiding C–C Bond Formation. Allylation is the primary undesired pathway in Pd-catalyzed α,β-dehydrogenation of carbonyls via enolates when allyl oxidants are employed (Figure 4A). Allylation products could arise both from the conventional mechanism wherein the enolate attacks at the electrophilic carbon of the allyl unit, and additionally these could be generated after transmetalation via an inner-sphere reductive elimination of an allyl-metal-enolate intermediate.[23,24] A concern with using this mechanistic approach is that the extent of dehydrogenation can be limited by the possibility of both inner- and outer-sphere reductive elimination.

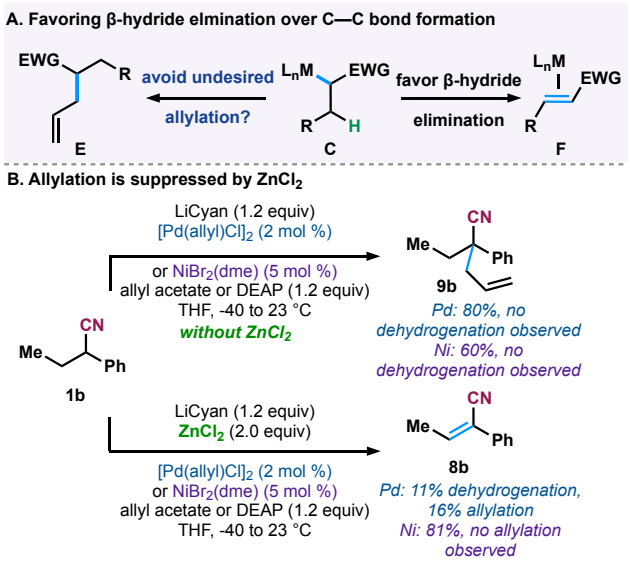

Figure 4. Allylation is suppressed by $ZnCl_2$.

As a representative example, for α-aryl nitrile **1b**, without the addition of $ZnCl_2$, the allylation byproduct **9b** is observed in high yield (Figure 4B, 80% for Pd and 60% for Ni), we attribute to its increased nucleophilicity. However, with the addition of $ZnCl_2$, allylation is observed to a lesser extent under Pd-catalyzed conditions (16%) and is entirely eliminated under Ni-catalyzed conditions. This may be due to the decreased nucleophilicity of the softer zinc enolate compared to the lithium

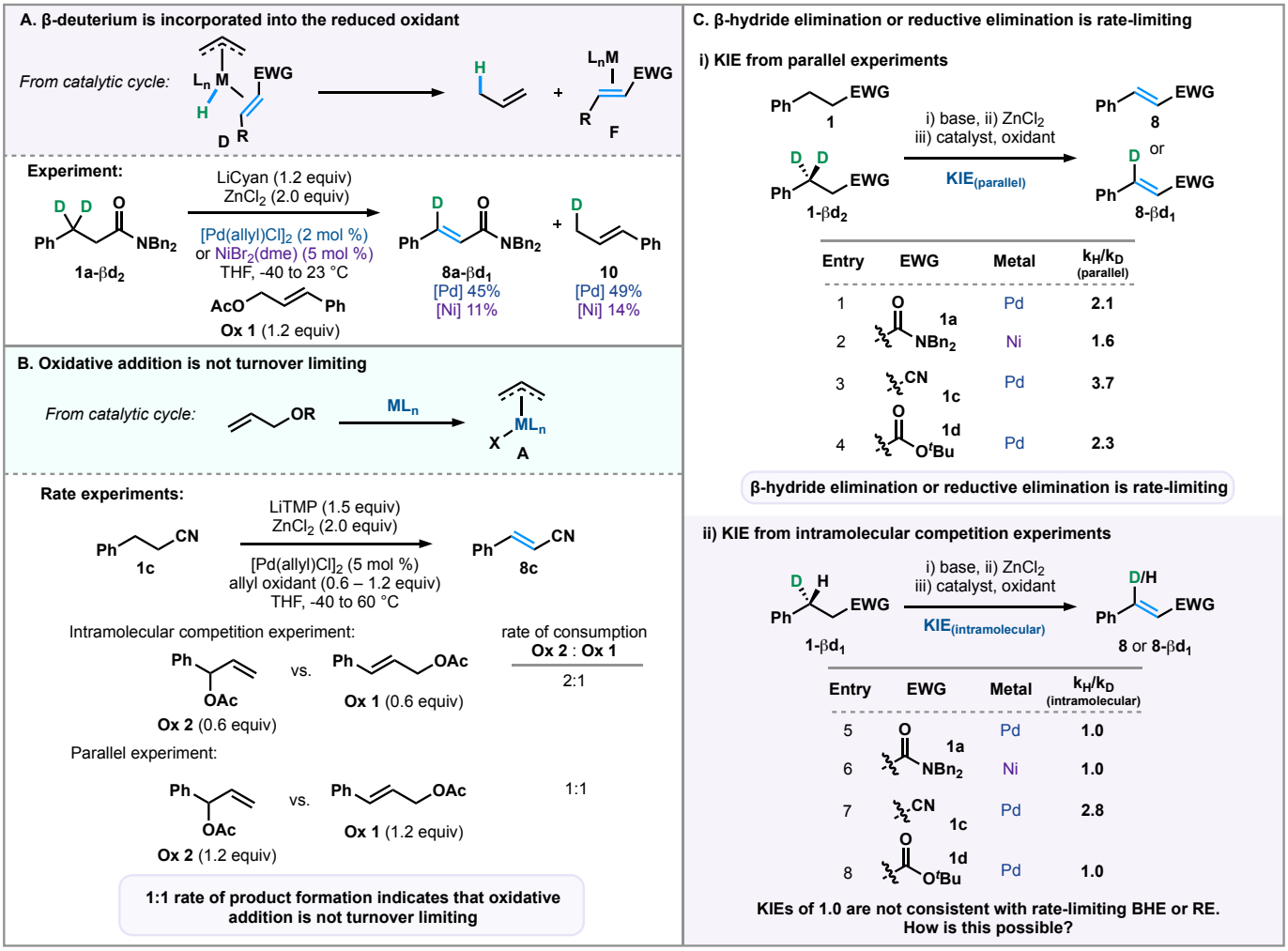

Figure 5. From KIE and competition experiments, β-hydride elimination and/or reductive elimination is turnover limiting.

enolate, and a greater propensity of zinc enolates to undergo transmetalation.[25] The difference in reactivity between Ni and Pd with regard to C–C bond formation may be due to the differential electronegativity of the allyl-metal species.[26]

The degree of allylation is substrate dependent, and the addition of $ZnCl_2$ to form zinc enolates generally overcomes this side reactivity (Supporting Information, Table S4). The decreased propensity for Ni to undergo reductive elimination is beneficial in this reaction by decreasing the likelihood of undesired allylation.[27] A full discussion regarding allylation can be found in the Supporting Information (SI-54–59).

Rate-determining steps. To confirm that the hydride at the β-position is incorporated into propene gas, cinnamyl acetate was substituted for allyl acetate in a typical dehydrogenation reaction (Figure 5A) so that the formation of the reduced oxidant could more easily be monitored. The dehydrogenation was performed with amide **1a-βd$_2$** and less volatile **Ox 1** using both palladium and nickel, which yielded 45% and 11% of unsaturated amide **8a-βd$_1$** and 49% and 14% of **10**. This indicates that the eliminated deuterium is incorporated into the allyl benzene and provides support for our proposed mechanism involving β-hydride elimination followed by reductive elimination.

We designed a competition experiment to evaluate whether oxidative addition is turnover limiting by analyzing differences in rate when branched or linear allyl oxidants are employed (Figure 5B).[28] For a competition experiment where these oxidants are used in equal portions in the same reaction vessel, the extent of conversion for the more reactive branched oxidant (**Ox 2**) was double that of the linear cinnamyl acetate (**Ox 1**, 2:1).[28] Given this difference in rate, if the rate determining step involved oxidative addition, it would be expected that the more reactive branched oxidant would have an overall faster rate of reaction than the linear oxidant. However, a significant rate difference was not observed when these two oxidants were used in parallel reactions (1:1), ruling out oxidative addition as a possibility for the slow step of the reaction.[29]

We questioned whether β-hydride elimination from intermediate **C** and/or reductive elimination from intermediate **D** could be turnover limiting, so we conducted a series of kinetic isotope effect (KIE) studies (Figure 5C, Supporting Information Figures S1, 2, & 3). If a primary KIE were observed when measured by parallel experiments, the turnover-limiting step would involve C–H bond cleavage or formation, either through β-hydride elimination or reductive elimination.[30] These experiments were performed with an amide, ester, and nitrile substrate. Under Pd catalysis primary KIE values were observed and ranged from 2.1–3.7 (entries 1, 3, & 4), whereas under Ni catalyzed conditions a somewhat lower value (1.6, entry 2) was observed. This outcome is consistent with values determined by Hartwig and Alexanian with related Pt-enolate complexes (KIE = 3.2).[31]

These results indicate that C–H bond cleavage and/or formation – here, β-hydride elimination and/or reductive elimination – are slow steps for each of the cases surveyed.[30] This data also rules out transmetallation as the turnover limiting step, as we would not expect a primary KIE to be observed from parallel rate experiments.

An intramolecular competition experiment with a mono-β-deutero-substrate (**1-βd$_1$**) was also used as a mechanistic probe.[31] For the intramolecular competition experiment, during the β-hydride elimination, either C–H or C–D bond cleavage must occur, which was anticipated to result in a normal, primary KIE value given the parallel KIE measurement above. However, in the intramolecular competition experiments, striking KIE values of 1.0 were observed for both the amide (**1a**, entry 5) and the ester (**1d**, entry 8) under Pd-catalyzed conditions. Ni-catalyzed conditions also resulted in a KIE value of 1.0 for **1a** (entry 6). Similarly, for the nitrile substrate (**1c**, entry 7), there is a depreciation of the value of the parallel KIE measurement from 3.7 to a lower value of 2.8 for the intramolecular competition experiment.[31] The unusual outcome that there is a KIE from parallel experiments, but not from the intramolecular measurements, provides a mechanistic opportunity.[32]

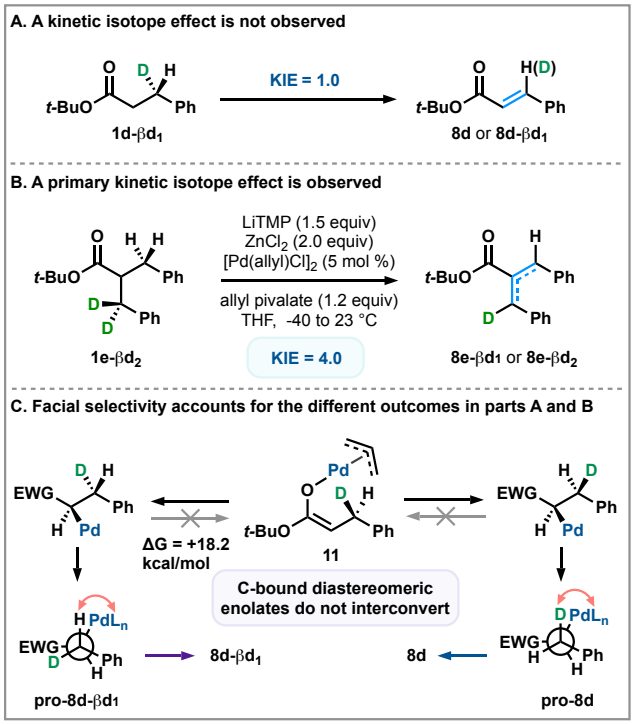

Figure 6. A lack of facial selectivity results in an intramolecular KIE of 1.0.

The peculiar differences in KIE values were reproducible across conditions and substrates, and perplexing such that additional study was warranted to uncover the phenomena underlying these findings. From the observation of this phenomenon for substrate **1d-βd$_1$** (Figure 6A), it was previously proposed that a reversible β-hydride elimination is followed by a turnover-limiting reductive elimination.[8a] Alternatively, the extent of proteo- or deuterio-product formation, **8** or **8-βd$_1$**, for the intramolecular competition experiment could be a function of the facial selectivity of transmetallation to form one of two diastereomeric Pd or Ni C-bound enolates. The metal would either be syn or anti to the deuterium. Via a presumed *syn*-β-hydride elimination, **pro-8** could only lead to **8**, and **pro-8-βd$_1$** could only lead to **8-βd$_1$**, which would obfuscate the attempted isotopic measurement.

This mechanistic suggestion warranted an additional measurement of the intramolecular competition experiment that would eliminate facial selectivity as a potential contributor (Figure 6B). Substrate **1e-βd$_2$** is not subject to the same limitations of **1d-βd$_1$**, and for **1e-βd$_2$** a primary KIE value of 4.0 was observed. This finding is consistent with turnover limiting β-hydride elimination and/or reductive elimination and suggests that if β-hydride elimination is reversible, it does not lead to differentiation of intramolecular and parallel KIE results.

This interpretation requires that interconversion between the C-bound Pd or Ni facial diastereomers (via the O-bound enolate **11**) is less facile than product formation (Figure 6C). Consistent with this view, the energy of the O-bound enolate intermediate is considerably higher than the transition state energies that correspond to β-hydride elimination and reductive elimination (see SI Figures S9–11). Given this mechanistic consideration, the stereoselectivity of C-bound Pd enolate formation would dictate which β-hydrogen undergoes elimination due to the conformational preference about the $\sigma_{C\alpha-C\beta}$ bond, rather than an otherwise equivalent selection between H and D isotopes. Consequently, it would be expected that a 1:1 mixture of products would arise from the experiment, because only subtle differences in agostic interactions could differentiate the energies of these diastereomers.[33] Rotation of **pro-8d** followed by a *syn*-elimination would lead to the *Z*-product. However, only the *E*-alkene product has been observed experimentally. Alternatively, if this rotation were to occur, then an *anti*-elimination would be required to generate the same *E*-product. However, the deuterium labeling experiment shown in Figure 5A wherein allylbenzene is produced as the deuterated product is indicative of a *syn*-elimination pathway. Furthermore, the comparison of the *geminal*-intramolecular KIE value (1.0) and that of the additional intramolecular KIE measurement with **1e-βd$_2$** (4.0) suggests interconversion between the C-bound Pd enolates is less facile than product formation.

Computational Study. In order to gain insight into whether β-hydride elimination and/or reductive elimination is turnover limiting, we used density functional theory (DFT) to calculate the transition states for β-hydride elimination for both Ni- and Pd-catalyzed pathways (Figure 7A). Benzyl groups were truncated to methyl groups to reduce computational cost and calculations were performed at the ωb97X-D/6-311+G(d,p)-LANL2DZ(Ni,Pd)//ωb97X-D/def2TZVP-LANL2DZ(Pd,Ni)-SMD-THF level of theory. Broader examination of other functionals, such as B3LYP-D3 and M06, and basis sets can be found in the Supporting Information (Table S10 and Table S11).

We constrained our analysis to mono-metallic Pd intermediates that proceed via Pd(0/II)-catalysis as this is the simplest scenario that may provide general insight into the elementary steps of interest. Two different mechanistic pathways were examined for the conversion of the C-bound metal enolates to the metal coordinated products, namely from neutral and halide-bound anionic complexes. For the neutral transition state, an (η^3-allyl)-metal complex was lowest in energy, and a transition state for the *syn*-coplanar β-hydride elimination was located. For the anionic transition state, an (η^1-allyl)-metal complex was lowest in energy, and lacks the open coordination site for an inner sphere *syn*-β-hydride elimination, such that direct

transfer of a hydride from the substrate to the allyl group was located (Figure 7A).[34]

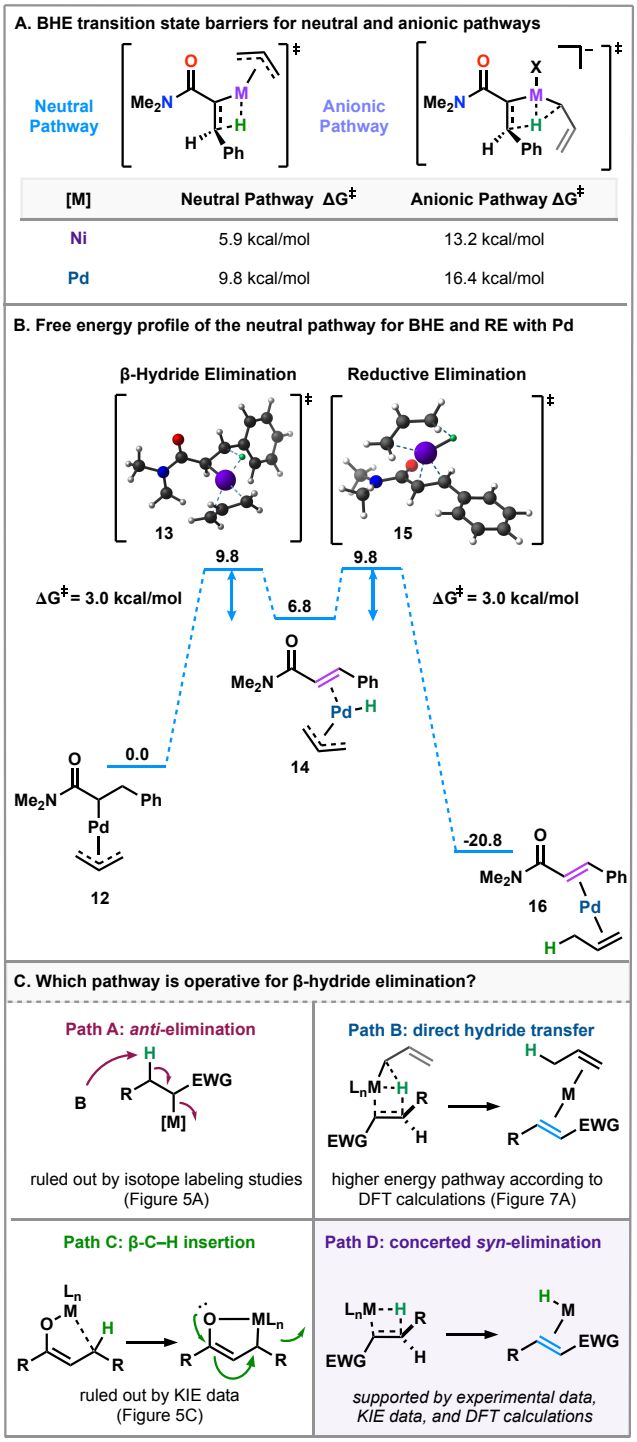

Figure 7. β-hydride elimination is a turnover limiting step and proceeds through a concerted *syn*-elimination. Calculations were performed at the ωb97X-D/6-311+G(d,p)-LANL2DZ(Ni,Pd)//ωb97X-D/def2TZVP-LANL2DZ(Pd,Ni)-SMD-THF level of theory.

These two pathways were each compared for Ni and Pd. The transition state barriers for both Ni and Pd in the neutral pathway are lower than the anionic pathway (Figure 4, $\Delta G^{\ddagger} = 5.9$ vs 9.8 kcal/mol in the neutral pathway, and 13.2 vs 16.4 kcal/mol in the anionic pathway). The higher barrier for the anionic pathway is consistent with the observation that excess salts reduce conversion and yield (Supporting Information, Table S7). More surprisingly, the barriers for β-hydride elimination for the Ni-catalyzed pathways were lower in energy than the barriers for the transition states in the Pd-catalyzed pathways.[35]

For the lower energy neutral pathway, we computed the barrier for reductive elimination for Pd (Figure 7B). We found that the barrier for reductive elimination is significantly lower in energy than the barrier for β-hydride elimination ($\Delta G^{\ddagger} = 3.0$ vs. 9.8 kcal/mol). Additionally, from the allyl-metal hydride intermediate (**14**), the barriers for the reverse pathway showed a value comparable to the reductive elimination step. These calculations were conducted with the ωb97X-D functional and the def2TZVP basis set with implicit solvation correction, and additionally the same conclusions are derived from other levels of theory (see Supporting Information, Figure S6). These calculations are consistent with the KIE data that implicate β-hydride elimination and reductive elimination as turnover limiting steps.

For β-hydride elimination, there are several pathways that could be operative for this elementary step (Figure 7C). An *anti*-elimination (Path A), wherein an exogenous base deprotonates the β-position and eliminates the metal has been proposed for related π-allyl Pd intermediates.[36] However, as shown in Figure 5A, the H (or D) at the β-position is incorporated into the allyl oxidant, which rules out this pathway as a possibility.

A direct hydride transfer pathway (Path B), wherein a metal-hydride species is not formed, and the β-hydrogen is transferred directly to the allyl oxidant, is another mechanistic possibility.[34c,37] However, Figure 7A shows that the transition states for the anionic pathway that proceed via a direct hydride transfer are ~7 kcal/mol higher in energy than the corresponding transition states in the neutral pathway. This significant energetic difference argues against a direct hydride transfer pathway.

A β-C–H insertion pathway could also be operative, similar to the mechanism recently proposed by in Yu and co-workers in their method for the dehydrogenation of carboxylic acids (Path C).[12a] In this mechanism, an O-bound Pd-center could induce C–H functionalization of the β-position, reductively eliminate the hydride and allyl ligands, and then undergo β-elimination by the enolate to give the desired product. Unlike a mechanism involving a concerted *syn*-elimination, it is not expected that the C–H insertion pathway via the O-bound Pd enolate would have the same consequences as the facial selectivity of the C-bound Pd enolate. The C–H insertion pathway (Path C) would not be expected to give rise to the observed intramolecular competition experiment (KIE = 1.0). Therefore, this pathway is ruled out as a possible mechanism.

The final pathway discussed herein is a concerted *syn*-elimination via a 4-membered transition state to give a metal-hydride species that undergoes reductive elimination (Path D). Experimentally, this pathway is supported by the isotope labeling studies described in Figure 5A wherein the deuterium from the substrate is incorporated into the allyl oxidant, suggesting that either *syn*-elimination or direct hydride transfer to the allyl oxidant are operative. Lastly, the DFT calculations show that the *syn*-elimination pathway is lower in energy compared to a direct hydride transfer pathway.

SUMMARY

In summary, a detailed mechanistic study of Pd- and Ni-catalyzed α,β-dehydrogenation of electron-withdrawing groups

has been conducted. There were several key findings that may be useful to those attempting to employ this methodological approach, and perhaps to other reaction types. Based on the KIE measurements (Figure 5 & 6) and computational data (Figure 7), the turnover limiting steps are β-hydride elimination and reductive elimination. C–C bond formation via allylation was identified as the primary side reaction. It was found that zinc enolate intermediates are essential to inhibit allylation and improve the yield of the dehydrogenation (Figure 4).

OUTLOOK

An advantage of concerted efforts to develop first-row transition metal catalysis is their generally more favorable sustainability and costs.[26,38] The complimentary differences in reactivity up or down a periodic group provide opportunities to control selectivity in a predictable fashion. Continued comparative investigations into catalysis will allow for the development of new methods and mechanistic pathways to subvert generally assumed reactivity trends across metals.

ASSOCIATED CONTENT

Data Availability Statement

The data underlying this study are available in the published article and its Supporting Information.

Supporting Information

FAIR Data is available as Supporting Information for Publication and includes the primary NMR FID files for compounds: **(*R*)-1c-βd$_1$**, **8a-*Z***, **SI-2-βd$_2$**, **1c-βd$_2$**, **4**, **9a**, **1a**, **1a-βd$_1$**, **1a-βd$_2$**, **SI-11**, **8a**, **8a-βd$_1$**, **SI-14**, **SI-9**, **SI-8**, **1e-βd$_2$**.

Experimental procedures, spectroscopic data for all new compounds including ^{1}H- and ^{13}C-NMR spectra, XYZ coordinates and full computational details (PDF).

AUTHOR INFORMATION

Corresponding Author

*Timothy Newhouse – Department of Chemistry, Yale University, New Haven, Connecticut 06511, United States; orcid.org/0000-0001-8741-7236;
Email: timothy.newhouse@yale.edu

Authors

Alexandra K. Bodnar – Department of Chemistry, Yale University, New Haven, Connecticut 06511, United States

Suzanne M. Szewczyk – Department of Chemistry, Yale University, New Haven, Connecticut 06511, United States

Yang Sun – Department of Chemistry, Yale University, New Haven, Connecticut 06511, United States; orcid.org/0000-0001-6728-4923

Yifeng Chen – Department of Chemistry, Yale University, New Haven, Connecticut 06511, United States

Anson X. Huang – Department of Chemistry, Yale University, New Haven, Connecticut 06511, United States

Author Contributions

All authors have given approval to the final version of the manuscript.

Notes

The authors declare no competing financial interests.

ACKNOWLEDGMENT

We are grateful for financial support from Yale University, NSF (CHE-1653793 and GRFP to A.K.B), the ACS Petroleum Research Fund, and the NIH (GM118614). Additional support comes from the Swiss National Science Foundation (fellowship to Y.S.). Dr. Fabian Menges is gratefully acknowledged for obtaining the high-resolution mass spectrometry data. Additionally, we would like to thank Prof. Robert H. Crabtree for helpful discussions.

REFERENCES

(1) Knochel, P.; Molander, G. A. *Comprehensive Organic Synthesis*; Newnes, 2014.

(2) (a) Miller, B.; Wong, H.-S. Reactions of 2-Phenylcyclohexanone Derivatives. A Re-Examination. *Tetrahedron* **1972**, *28*, 2369–2376. (b) Stotter, P. L.; Hill, K. A. α-Halocarbonyl Compounds. II. A Position Specific Preparation of α-Bromoketones by Bromination of Lithium Enolates. Position-Specific Introduction of α,β-Unsaturation into Unsymmetrical Ketones. *J. Org. Chem.* **1973**, *38*, 2576–2578. (c) Reich, H. J.; Reich, I. L.; Renga, J. M. Organoselenium Chemistry. A-Phenylseleno Carbonyl Compounds as Precursors for α,β-Unsaturated Ketones and Esters. *J. Am. Chem. Soc.* **1973**, *95*, 5813–5815. (d) Sharpless, K. B.; Lauer, R. F.; Teranishi, A. Y. Electrophilic and Nucleophilic Organoselenium Reagents. New Routes to *α,β*-Unsaturated Carbonyl Compounds. *J. Am. Chem. Soc*. **1973**, *95*, 6137–6139. (e) Reich, H. J.; Wollowitz, S. Preparation of *α,β*-Unsaturated Carbonyl Compounds and Nitriles by Selenoxide Elimination. *Org. React.* **1993**, 44,1–296. (f) Trost, B. M.; Salzmann, T. N.; Hiroi, K. New Synthetic Reactions. Sulfenylations and Dehydrosulfenylations of Esters and Ketones. *J. Am. Chem. Soc.* **1976**, *98*, 4887–4902. For a review, see: (g) Turlik, A.; Chen, Y.; Newhouse, T. R. Dehydrogenation Adjacent to Carbonyls Using Palladium-Allyl Intermediates. *Synlett* **2016**, *27*, 331–336.

(3) (a) Ito, Y.; Hirao, T.; Saegusa, T. Synthesis of *α,β*-Unsaturated Carbonyl Compounds by Palladium(II)-Catalyzed Dehydrosilylation of Silyl Enol Ethers. *J. Org. Chem.* **1978**, *43*, 1011–1013. (b) Theissen, R. A New Method for the Preparation of *α,β*-Unsaturated Carbonyl Compounds. *J. Org. Chem.* **1971**, *36*, 752–757. (c) Larock, R. C.; Hightower, T. R.; Kraus, G. A.; Hahn, P.; Zheng, D. Simple, Effective, New, Palladium-Catalyzed Conversion of Enol Silanes to Enones and Enals. *Tetrahedron Lett.* **1995**, *36*, 2423–2426.

(4) (a) Shimizu, I.; Tsuji, J. Palladium-Catalyzed Decarboxylation−Dehydrogenation of Allyl *β*-Keto Carboxylates and Allyl Enol Carbonates as a Novel Synthetic method for *α*-Substituted *α,β*-Unsaturated Ketones. *J. Am. Chem. Soc.* **1982**, *104*, 5844–5846. (b) Shimizu, I.; Minami, I.; Tsuji, J. Palladium-Catalyzed Synthesis of *α,β*-Unsaturated Ketones from Ketones via Allyl Enol Carbonates. *Tetrahedron Lett.* **1983**, *24*, 1797–1800. (c) Minami, I.; Takahashi, K.; Shimizu, I.; Kimura, T.; Tsuji, J. New Synthetic methods for *α,β*-Unsaturated Ketones, Aldehydes, Esters and Lactones by the Palladium-Catalyzed Reactions of Silyl Enol Ethers, Ketene Silyl Acetals, and Enol Acetates with Allyl Carbonates. *Tetrahedron* **1986**, *42*, 2971–2977.

(5) (a) Diao, T.; Stahl, S. S. Synthesis of Cyclic Enones via Direct Palladium-Catalyzed Aerobic Dehydrogenation of Ketones. *J. Am. Chem. Soc*. **2011**, *133*, 14566–14569. (b) Diao, T.; Wadzinski, T. J.; Stahl. S, S. Direct Aerobic *α,β*-Dehydrogenation of Aldehydes and Ketones with a Pd(TFA)$_2$/4,5-diazafluorenone Catalyst. *Chem. Sci*. **2012**, *3*, 887–891.

(6) Huang, D.; Newhouse, T. R. Dehydrogenative Pd and Ni Catalysis for Total Synthesis. *Acc. Chem. Res.* **2021**, *54*, 1118–1130.

(7) For selected reviews: (a) Muzart, J. One-Pot Syntheses of *α,β*-Unsaturated Carbonyl Compounds through Palladium-Mediated Dehydrogenation of Ketones, Aldehydes, Esters, Lactones and Amides. *Eur. J. Org. Chem.* **2010**, 3779–3790. (b) Stahl, S. S.; Diao, T. Oxidation Adjacent to C=X Bonds by Dehydrogenation in *Comprehensive Organic Synthesis II* (Eds.: Knochel, P.; Molander, G. A.), Elsevier, **2014**, *Vol 7*, pp.178–212. (c) Chen, H.; Liu, L.; Huang, T.; Chen, J.; Chen, T.

Direct Dehydrogenation for the Synthesis of α,β-Unsaturated Carbonyl Compounds. *Adv. Synth. Catal.* **2020**, *362*, 3332–3346. (d) Gnaim, S.; Vantourout, J. C.; Serpier, F.; Echeverria, P. G.; Baran, P. S. Carbonyl Desaturation: Where Does Catalysis Stand? *ACS Catal.* **2021**, *11*, 883–892.

(8) (a) Chen, Y.; Romaire, J. P.; Newhouse, T. R. Palladium-Catalyzed α,β-Dehydrogenation of Esters and Nitriles. *J. Am. Chem. Soc.* **2015**, *137*, 5875–5878. (b) Chen, Y.; Turlik, A.; Newhouse, T. R. Amide α,β-Dehydrogenation Using Allyl-Palladium Catalysis and a Hindered Monodentate Anilide. *J. Am. Chem. Soc.* **2016**, *138*, 1166–1169. (c) Zhao, Y.; Chen, Y.; Newhouse, T. R. Allyl-Palladium-Catalyzed α,β-Dehydrogenation of Carboxylic Acids via Enediolates. *Angew. Chem. Int. Ed.* **2017**, *56*, 13122–13125. (d) Huang, D.; Zhao, Y.; Newhouse, T. R. Synthesis of Cyclic Enones by Allyl-Palladium-Catalyzed α,β-Dehydrogenation. *Org. Lett.* **2018**, *20*, 684–687. (e) Zhang, P.; Huang, D.; Newhouse, T. R. Aryl-Nickel-Catalyzed Benzylic Dehydrogenation of Electron-Deficient Heteroarenes. *J. Am. Chem. Soc.* **2020**, *142*, 1757–1762.

(9) (a) Chen, M.; Dong, G. Direct Catalytic Desaturation of Lactams Enabled by Soft Enolization. *J. Am. Chem. Soc.* **2017**, *139*, 7757–7760; (b) Chen, M.; Rago, A. J.; Dong, G. Platinum-Catalyzed Desaturation of Lactams, Ketones, and Lactones. *Angew. Chem. Int. Ed.* **2018**, *57*, 16205–16209. (c) Chen, M.; Dong, G. Copper-Catalyzed Desaturation of Lactones, Lactams, and Ketones under pH-Neutral Conditions. *J. Am. Chem. Soc.* **2019**, *141*, 14889–14897.

(10) Wang, Z.; He, Z.; Zhang, L.; Huang, Y. Iridium-Catalyzed Aerobic α,β-Dehydrogenation of γ,δ-Unsaturated Amides and Acids: Activation of Both α- And β-C–H Bonds through an Allyl-Iridium Intermediate. *J. Am. Chem. Soc.* **2018**, *140*, 735–740.

(11) Teskey, C. J.; Adler, P.; Gonçalves, C. R.; Maulide, N. Chemoselective α,β-Dehydrogenation of Saturated Amides. *Angew. Chem. Int. Ed.* **2019**, *58*, 447–451.

(12) (a) Wang, Z.; Hu, L.; Chekshin, N.; Zhuang, Z.; Qian, S.; Qiao, J. X.; Yu, J.-Q. Ligand-Controlled Divergent Dehydrogenative Reactions of Carboxylic Acids via C–H Activation. *Science* **2021**, *374*, 1281–1285. (b) Sheng, T.; Zhuang, Z.; Wang, Z.; Hu, L.; Herron, A. N.; Qiao, J. X.; Yu, J.-Q. One-Step Synthesis of β -Alkylidene- γ -lactones via Ligand-Enabled β , γ -Dehydrogenation of Aliphatic Acids. *J. Am. Chem. Soc.* **2022**, *144*, 12924–12933.

(13) Gnaim, S.; Takahira, Y.; Wilke, H. R.; Yao, Z.; Li, J.; Delbrayelle, D.; Echeverria, P. G.; Vantourout, J. C.; Baran, P. S. Electrochemically Driven Desaturation of Carbonyl Compounds. *Nat. Chem.* **2021**, *13*, 367–372.

(14) Zhao, L.-P.; Zhang, S.-Y.; Liu, H.-K.; Cheng, Y.-J.; Liu, Z.-P.; Wang, L.; Tang, Y. Insights into Stereoselectivity Switch in Michael Addition-Initiated Tandem Mannich Cyclizations and Their Extension from Enamines to Vinyl Ethers. *J. Am. Chem. Soc.* **2023**, *145*, 15553–15564.

(15) For additional recently reported metal-mediated carbonyl dehydrogenation methods, see: (a) Wang, M.-M.; Ning, X.-S.; Qu, J.-P.; Kang, Y.-B. Dehydrogenative Synthesis of Linear α,β-Unsaturated Aldehydes with Oxygen at Room Temperature Enabled by ^{t}BuONO. *ACS Catal.* **2017**, *7*, 4000–4003. (b) Shang, Y.; Jie, X.; Jonnada, K.; Zafar, S. N.; Su, W. Dehydrogenative Desaturation-Relay via Formation of Multicenter-Stabilized Radical Intermediates. *Nat. Comm.* **2017**, *8*, 2273. (c) Chen, M.; Dong, G. Platinum-Catalyzed α,β-Desaturation of Cyclic Ketones through Direct Metal-Enolate Formation. *Angew. Chem. Int. Ed.* **2021**, *60*, 7956–7961. (d) Zhang, X.-W.; Jiang, G.-Q.; Lei, S.-H.; Shan, X.-H.; Qu, J.-P.; Kang, Y.-B. Iron-Catalyzed α,β-Dehydrogenation of Carbonyl Compounds. *Org. Lett.* **2021**, *23*, 1611–1615. (e) Yu, W.-L.; Ren, Z.-G.; Ma, K.-X.; Yang, H.-Q.; Yang, J.-J.; Zheng, H.; Wu, W.; Xu, P.-F. Cobalt-Catalyzed Chemoselective Dehydrogenation through Radical Translocation under Visible Light. *Chem. Sci*. **2022**, *13*, 7947–7954. (f) Yang, S.; Fan, H.; Xie, L.; Dong, G.; Chen, M. Photoinduced Desaturation of Amides by Palladium Catalysis. *Org. Lett.* **2022**, *24*, 6460–6465. (g) Li, H.; Yin, C.; Liu, S.; Tu, H.; Lin, P.; Chen, J.; Su, W. Multiple Remote C(sp^3)–H Functionalizations of Aliphatic Ketones via Bimetallic Cu-Pd Catalyzed Successive Dehydrogenation. *Chem. Sci*. **2022**, *13*, 13843–13850.

(16) (a) Pérez-Temprano, M. H.; Casares, J. A.; Espinet, P. Bimetallic Catalysis using Transition and Group 11 Metals: An Emerging Tool for C–C Coupling and Other Reactions. *Chem. Eur. J*. **2012**, *18*, 1864-1884. (b) Pye, D. R.; Mankad, N. P. Bimetallic Catalysis for C–C and C–X Coupling Reactions. *Chem. Sci*. **2017**, *8*, 1705–1718. (c) Ackerman-Biegasiewicz, L. K.; Kariofillis, S. K.; Weix, D. J. Multimetallic-Catalyzed C–C Bond Forming Reactions: From Serendipity to Strategy. *J. Am. Chem. Soc.* **2023**, *145*, 6596–6614.

(17) (a) Reich, H. J. Role of Organolithium Aggregates and Mixed Aggregates in Organolithium Mechanisms. *Chem. Rev*. **2013**, *113*, 7130–7178. (b) Van der Steen, F. H.; Boersma, J.; Spek, A.; Van Koten, G. Synthesis and Properties of Novel Organozinc Enolates of N, N-disubstituted Glycine Esters. Molecular Structure of [cyclic][EtZnOC(OMe):C(H)N(tert-Bu)Me]$_4$. *Organometallics* **1991**, *10*, 2467–2480. (c) Collum, D. B; McNeil, A. J.; Ramirez, A. Lithium Diisopropylamide: Solution Kinetics and Implications for Organic Synthesis. *Angew. Chem. Int. Ed*. **2007**, *46*, 3002–3017. (d) Hall, P. L.; Gilchrist, J. H.; Harrison, A. T.; Fuller, D. J.; Collum, D. B. Mixed Aggregation of Lithium Enolates and Lithium Halides with Lithium 2,2,6,6-tetramethylpiperidide (LiTMP). *J. Am. Chem. Soc.* **1991**, *113*, 9575–9585.

(18) Zhang, P.; Cantrell, R. L.; Newhouse, T. R, Role of Benzylic Deprotonation in Nickel-Catalyzed Benzylic Dehydrogenation. *Synlett* **2021**, *32*, 1652–1656.

(19) Jacobs, B. P.; Wolczanski, P. T.; Lobkovsky, E. B. Oxidatively Triggered Carbon–Carbon Bond Formation in Ene-Amide Complexes. *Inorg. Chem.* **2016**, *55*, 4223–4232.

(20) Muzart, J. On the Behavior of Amines in the Presence of Pd(0) and Pd(II) Species. *J. Mol. Catal. A Chem.* **2009**, *308*, 15–24.

(21) Hegedus, L.S.; Aakermark B.; Olsen, D. J.; Anderson, O. P.; Zetterberg, K. (pi-Allyl) Palladium Complex Ion Pairs Containing Two Different, Mobile. pi-allyl groups: NMR and X-ray Crystallographic Studies. *J. Am. Chem. Soc.* **1982**, *104*, 697–704.

(22) Lau, J.; Sustmann, R. Diethyl-2,2'-bipyridyl-palladium(II), a Case for the Study of Combination vs. Disproportionation Products. *Tetrahedron Lett.* **1985**, *26*, 4907–4910.

(23) For reviews on allylic alkylation: (a) Trost, B.M.; Van Vranken, D. L. Asymmetric Transition Metal-Catalyzed Allylic Alkylations. *Chem. Rev.* **1996**, *96*, 395–422. (b) Trost, B. M.; Crawley, M. L. Asymmetric Transition-Metal Catalyzed Allylic Alkylations: Applications in Total Synthesis. *Chem. Rev*. **2003**, *103*, 2921–2944. (c) Weaver, J. D.; Recio III, A.; Grenning, A. J.; Tunge, J. A. Transition-Metal Catalyzed Decarboxylative Allylation and Benzylation Reactions. *Chem. Rev*. **2011**, *111*, 1846–1913. (d) James, J.; Jackson, M.; Guiry, P.J. Palladium-Catalyzed Decarboxylative Asymmetric Allylic Alkylation: Development, Mechanistic Understanding and Recent Advances. *Adv. Synth. Catal*. **2019**, *361*, 3016–3049.

(24) (a) Steinhagen, H.; Reggelin, M.; Helmchen, G. Palladium-Catalyzed Allylic Alkylation with Phosphinoaryldihydrooxale Ligands: First Evidence and NMR Spectroscopic Structure Determination of a Primary Olefin-Pd(0) Complex. *Angew. Chem. Int. Ed.* **1997**, *36*, 2108–2110. (b) Bai, D.-C.; Yu, F.-L.; Wang, W.-Y.; Chen, D.; Li, H.; Liu, Q.-R.; Ding, C.-H.; Chen, B.; Hou, X.-L. Palladium/N-Heterocyclic Carbene Catalysed Regio and Diastereoselective Reaction of Ketones with Allyl Reagents via Inner-Sphere Mechanism. *Nat. Comm*. **2016**, *7*, 1–11. (c) Sha, S. C.; Jiang, H.; Mao, J.; Bellomo, A.; Jeong, S. A.; Walsh, P. J. Nickel-Catalyzed Allylic Alkylation with Diarylmethane Pronucleophiles: Reaction Development and Mechanistic Insights. *Angew. Chem. Int. Ed.* **2016**, *55*, 1070–1074.

(25) Jarugumilli, G. K.; Zhu, C.; Cook, S. P. Re-Evaluating the Nucleophilicity of Zinc Enolates in Alkylation Reactions. *Eur. J. Org. Chem.* **2012**, *4*, 1712–1715.

(26) (a) Tasker, S. Z.; Standley, E. A.; Jamison, T. F. Recent Advances in Homogeneous Nickel Catalysis. *Nature* **2014**, *509*, 299–309. (b) Ananikov, P. V. Nickel: The "Spirited Horse" of Transition Metal Catalysis. *ACS Catal*. **2015**, *5*, 1964–1971.

(27) Chernyshev, V. M.; Ananikov, V. P. Nickel and Palladium Catalysis: Stronger Demand than Ever. *ACS Catal.* **2022**, *12*, 1180–1200.

(28) (a) Mackenzie, P. B.; Whelan, J.; Bosnich, B. Asymmetric Synthesis. Mechanism of Asymmetric Catalytic Allylation. *J. Am. Chem. Soc.* **1985**, *107*, 2046–2054. (b) Osakada, K.; Chiba, T.; Nakamura, Y.;

Yamamoto, T.; Yamamoto, A. Steric Effect of Substituents in Allylic Groups in Oxidative Addition of Allylic Phenyl Sulphides to a Palladium (0) Complex. C–S Bond Cleavage Triggered by Attack of Pd on the Terminal Carbon of the C–C Double Bond. *J. Chem. Soc., Chem. Commun.* **1986**, *21*, 1589–1591. (c) Kurosawa, H.; Kajimaru, H.; Ogoshi, S.; Yoneda, H.; Miki, K.; Kasai, N.; Murai, S.; Ikeda, I. Novel Syn Oxidative Addition of Allylic Halides to Olefin Complexes of Palladium (0) and Platinum (0). *J. Am. Chem. Soc.* **1992**, *114*, 8417–8424.

(29) (a) Trost, B. M.; Verhoeven, T. R. Allylic Alkylation. Palladium-Catalyzed Substitutions of Allylic Carboxylates. Stereo-and Regiochemistry. *J. Am. Chem. Soc.* **1980**, *102*, 4730–4743. (b) Trost, B. M.; Ariza, X. Enantioselective Allylations of Azlactones with Unsymmetrical Acyclic Allyl Esters. *J. Am. Chem. Soc.* **1999**, *121*, 10727–10737.

(30) (a) Gómez-Gallego, M.; Sierra, M. A. Kinetic Isotope Effects in the Study of Organometallic Reaction Mechanisms. *Chem. Rev*. **2011**, *111*, 4857. (b) Simmons, E. M.; Hartwig, J. F. On the Interpretation of Deuterium Kinetic Isotope Effects in C—H Bond Functionalizations by Transition-Metal Complexes. *Angew. Chem. Int. Ed*. **2012**, *51*, 3066–3072.

(31) Alexanian, E. J.; Hartwig, J. F. Mechanistic Study of *β*-Hydrogen Elimination from Organoplatinum (II) Enolate Complexes. *J. Am. Chem. Soc.* **2008**, *130*, 15627–15635.

(32) Jones, W. D. Isotope Effects in C–H Bond Activation Reactions by Transition Metals. *Acc. Chem. Res.* **2003**, *36*, 140–146.

(33) (a) Brookhart, M.; Green, M. L. Carbon—Hydrogen-Transition Metal Bonds. *J. Organomet. Chem.* **1983**, *250*, 395–408. (b) Ryabov, A. D.; Sakodinskaya, I. K.; Yatsimirsky, A. K. Kinetics and Mechanism of Ortho-Palladation of Ring-Substituted *N*,*N*-Dimethylbenzylamines. *J. Chem. Soc., Dalton Trans.* **1985**, *12*, 2629–2638. (c) Ryabov, A. D. *Chem. Rev.* **1990**, *2*, 403–424. (d) Crabtree, R. H. Transition Metal Complexation of σ Bonds. *Angew. Chem. Int. Ed*. **1993**, *32*, 789–805. (e) Brookhart, M.; Green, M. L.; Parkin, G. Agostic Interactions in Transition Metal Compounds. *Proc. Nat. Acad. Sci. U.S.A.* **2007**, *104*, 6908–6914.

(34) (a) Solin, N.; Szabó, K. J. Mechanism of the η^3–η^1–η^3 Isomerization in Allylpalladium Complexes: Solvent Coordination, Ligand, and Substituent Effects. *Organometallics* **2001**, *20*, 5464–5471. (b) Trost, B. M.; Bunt, R. C. On the Effect of the Nature of Ion Pairs as Nucleophiles in a Metal-Catalyzed Substitution Reaction. *J. Am. Chem. Soc.* **1998**, *120*, 70–79. (c) Sakaki, S.; Satoh, H.; Shono, H.; Ujino, Y. Ab Initio MO Study of the Geometry, $\eta^3 \rightleftarrows \eta^1$ Conversion, and Reductive Elimination of a Palladium (II) η^3-Allyl Hydride Complex and Its Platinum (II) Analogue. *Organometallics* **1996**, *15*, 1713-1720.

(35) (a) Lin, B.-L.; Liu, L.; Fu, Y.; Luo, S.-W.; Chen, Q.; Guo, Q.-X. Comparing Nickel-and Palladium-Catalyzed Heck Reactions. *Organometallics* **2004**, *23*, 2114–2123. (b) Menezes da Silva, V. H.; Braga, A. A.; Cundari, T. R. *N*-Heterocyclic Carbene Based Nickel and Palladium Complexes: A DFT Comparison of the Mizoroki–Heck Catalytic Cycles. *Organometallics* **2016**, *35*, 3170–3181.

(36) (a) Andersson, P. G.; Schab, S. Mechanism of the Palladium-Catalyzed Elimination of Acetic Acid from Allylic Acetates. *Organometallics* **1995**, *14*, 1–2. (b) Takacs, J. M.; Lawson, E. C.; Clement, F. On the Nature of the Catalytic Palladium-Mediated Elimination of Allylic Carbonates and Acetates to Form 1,3-Dienes. *J. Am. Chem. Soc.* **1997**, *119*, 5956–5957.

(37) Biswas, B.; Sugimoto, M.; Sakaki, S. Theoretical Study of the Structure, Bonding Nature, and Reductive Elimination Reaction of Pd $(XH_3)(\eta^3\text{-}C_3H_5)(PH_3)$(X = C, Si, Ge, Sn). Hypervalent Behavior of Group 14 Elements. *Organometallics* **1999**, *18*, 4015–4026.

(38) For reviews and perspectives, see: (a) Zweig, J. E.; Kim, D. E.; Newhouse, T. R. Methods Utilizing First-Row Transition Metals in Natural Product Total Synthesis. *Chem. Rev.* **2017**, *117*, 11680–11752. (b) Holland, P. L. Reaction: Opportunities for Sustainable Catalysts. *Chem* **2017**, *2*, 443–444. (c) Hayler, J. D.; Leahy, D. K.; Simmons, E. M. A Pharmaceutical Industry Perspective on Sustainable Metal Catalysis. *Organometallics* **2018**, *38*, 36–46. (d) Haibach, M. C.; Ickes, A. R.; Wilders, A. M.; Shekhar, S. Recent Advances in Nonprecious Metal Catalysis. *Org. Process Res. Dev*. **2020**, *24*, 2428–2444. (e) Rana, S.; Biswas, J. P.; Paul, S.; Paik, A.; Maiti, D. Organic Synthesis with the Most Abundant Transition Metal – Iron: From Rust to Multitasking Catalysts. *Chem. Soc. Rev.* **2021**, *50*, 243–472.

A Comprehensive Mechanistic Analysis of Palladium- and Nickel-Catalyzed α,β-Dehydrogenation of Carbonyls via Organozinc Intermediates

Alexandra K. Bodnar, Suzanne M. Szewczyk, Yang Sun, Yifeng Chen, Anson X. Huang, and Timothy R. Newhouse*

Department of Chemistry, Yale University

225 Prospect St., New Haven, Connecticut 06520-8107

*E-mail: timothy.newhouse@yale.edu

Table of Contents

General Experimental

All reactions were carried out under an inert nitrogen atmosphere with dry solvents under anhydrous conditions unless otherwise stated. All reactions were capped with a rubber septum, or Teflon-coated silicon microwave cap unless otherwise stated. Stainless steel cannula or syringe was used to transfer solvent, and air- and moisture sensitive liquid reagents. Reactions were monitored by thin-layer chromatography (TLC) carried out on 0.25 mm Merck silica gel plates (60F-254) using UV light as the visualizing agent and potassium permanganate, an acidic solution of *p*-anisaldehyde, phosphomolybdic acid, or I_2 on SiO_2 as developing agents. Flash column chromatography employed SiliaFlash® P60 (40-60 μm, 230-400 mesh) silica gel purchased from SiliCycle, Inc.

Materials: All reaction solvents were purified using a Seca solvent purification system by Glass contour or the anhydrous solvents were purchased from Sigma Aldrich and used under nitrogen. *N*,*N*-diisopropylamine and 2,2,6,6-tetramethylpiperidine were distilled over CaH_2. [Ni(dme)Cl_2] and [Ni(dme)Br_2] were purchased from Strem and stored in a desiccator. Zn(TMP)$_2$ (0.5 M in toluene), *n*-BuLi (2.5 M in hexanes), *s*-BuLi (1.4 M in cyclohexane) and $ZnCl_2$ (0.5M in THF) were purchased from Sigma Aldrich. Hydrocinnamoyl chloride (**SI-3**) was purchased from Sigma Aldrich and used as received. Phenylpropiolic acid (**SI-10**) was purchased from Alfa Aesar and used as received. All other reagents were used as received without further purification, unless otherwise stated.

Instrumentation: All new compounds were characterized by means of ^{1}H NMR, ^{13}C NMR, ^{19}F NMR, FT-IR (thin film), and GCMS or HRMS. Copies of the ^{1}H- and ^{13}C-NMR spectra can be found at the end of each experimental procedure. NMR spectra were recorded using a Varian 400 MHz NMR spectrometer, Varian 500 MHz NMR spectrometer, or a Varian 600 MHz NMR spectrometer. All ^{1}H-NMR data are reported in δ units, parts per million (ppm), and were calibrated relative to the signals for residual chloroform (7.26 ppm) in deuterochloroform ($CDCl_3$). All ^{13}C-NMR data are reported in ppm relative to $CDCl_3$ (77.16 ppm) and were obtained with ^{1}H decoupling unless otherwise stated. The following abbreviations or combinations thereof were used to explain the multiplicities: s = singlet, d = doublet, t = triplet, q = quartet, quint = quintet, hept = heptet, br = broad, m = multiplet, dd = doublet of doublets, td = triplet of doublets, ddd =

doublet of doublet of doublets, ddt = doublet of doublet of triplets. All IR spectra were taken on an FT-IR/Raman Thermo Nicolet 6700. Gas chromatography mass spectra (GCMS) were recorded on an Agilent Technologies 6890N Network Gas Chromatograph System with an Agilent Technologies 5973N Mass Selective Detector. High resolution mass spectra (HRMS) were recorded on a Waters Xevo high resolution mass spectrometer using Qtof (quadrupole-time of flight). Optical rotation data was obtained using a Perkin-Elmer 341 polarimeter.

General Experimental Procedures for *α,β*-Dehydrogenation

Preparation of [Pd(allyl)Cl]$_2$ and allyl acetate stock solution (0.2 mmol scale):

To a flame-dried microwave vial equipped with a magnetic stir bar was added [Pd(allyl)Cl]$_2$ (7.32 mg, 0.02 mmol, 2 mol%). The reaction vessel was evacuated and backfilled with N_2 (this process was repeated three times). To the reaction vessel was added anhydrous THF (2.5 mL) and allyl acetate (0.13 mL, 1.2 mmol, 1.2 equiv), and the solution was stirred for at least 10 min before use and used within 1 hour. For a 0.2 mmol scale reaction, 0.5 mL of this stock solution is used.

Preparation of [Ni(dme)Br$_2$)] and diethyl allyl phosphate stock solution (0.2 mmol scale):

To a flame-dried microwave vial equipped with a magnetic stir bar was added [Ni(dme)Br$_2$] (30.9 mg, 0.10 mmol, 10 mol%). The reaction vessel was evacuated and backfilled with N_2 (this process was repeated three times). To the reaction vessel was added anhydrous THF (2.5 mL) and diethyl allyl phosphate (0.21 mL, 1.2 mmol, 1.2 equiv) and the solution was stirred for at least 10 min before use and used within 1 hour. For a 0.2 mmol scale reaction, 0.5 mL of this stock solution is used.

Addition of dehydrogenation substrates:

Liquid substrates were added dropwise via a microliter syringe to the reaction. Viscous oils or solid substrates were weighed into a flame-dried microwave vial equipped with magnetic stir bar. The reaction vessel was evacuated and backfilled with N_2 (this process was repeated three times). To the reaction vessel was added anhydrous THF (0.5 mL), then the solution was added dropwise via syringe. The transfers were quantitated by rinsing with additional THF (0.5 mL).

General Procedure A for *α,β*-Dehydrogenation with LiTMP (0.2 mmol scale):

To a solution of 2,2,6,6-tetramethylpiperidine (TMPH) (41 μL, 0.24 mmol, 1.2 equiv) in THF (1 mL, 0.24 M) was added *n*-BuLi (2.5 M in hexanes, 0.096 mL, 0.24 mmol, 1.2 equiv) at –40 °C and the resulting solution was stirred at –40 °C for 1 h. The substrate (0.20 mmol, 1.0 equiv) was added dropwise into the resulting solution, warmed to 0 °C and stirred for 30 min at 0 °C. $ZnCl_2$ (0.5 M in THF, 0.8mL, 0.4 mmol, 2.0 equiv) was next added and the mixture was stirred

for 30 min at 0 °C. Then 0.5 mL of the catalyst and oxidant stock solution was added at 0 °C. The reaction was warmed to ambient temperature. The reaction was quenched by the addition of sat. aq. NH_4Cl (2.0 mL). Yield was determined by ^1H NMR using 1,3,5-trimethoxybenzene as internal standard.

General Procedure B for *α,β*-Dehydrogenation with LiCyan (0.2 mmol scale):

To a –40 °C solution of CyanH (62.0 mg, 0.24 mmol, 1.2 equiv) in THF (1.0 mL, 0.24 M) was added *n*-BuLi (2.5 M in hexanes, 0.096 mL, 0.24 mmol, 1.2 equiv). The reaction quickly became opaque and was stirred for 1 hour at –40 °C forming a pale-yellow mixture. If the mixture stays translucent and does not become opaque, then the LiCyan has not formed properly. The substrate (0.20 mmol, 1.0 equiv) was added dropwise into the reaction mixture, warmed to 0 °C, and stirred for 30 min. $ZnCl_2$ (0.5 M in THF, 0.8 mL, 0.4 mmol, 2.0 equiv) was added and the mixture was stirred for 30 min at 0 °C. Subsequently, 0.5 mL of the catalyst and oxidant stock solution was added at 0 °C. The reaction was warmed to ambient temperature. The reaction was quenched by the addition of sat. aq. NH_4Cl (2.0 mL). Yield was determined by ^1H NMR using 1,3,5-trimethoxybenzene as internal standard. A scalable procedure for this chemistry has been published in *Organic Syntheses*.[1]

General Procedure C for *α,β*-Dehydrogenation with $Zn(TMP)_2$ (0.2 mmol scale):

To a solution of substrate (0.20 mmol, 1.0 equiv) in THF (1.0 mL, 0.20 M) was added $Zn(TMP)_2$ (0.5 M in toluene, 0.48 mL, 0.24 mmol, 1.2 equiv) and the resulting solution was stirred for 1 hour at room temperature. Then 0.5 mL of the stock solution of catalyst and oxidant was added, and the resulting mixture was stirred at ambient temperature. The reaction was quenched by the addition of sat. aq. NH_4Cl (2.0 mL). Yield was determined by ^1H NMR using 1,3,5-trimethoxybenzene as internal standard.

Experimental Procedures and Characterization Data for KIE Studies

KIE Studies of Nitrile Substrates

Synthesis of Deuterated Substrates

3-Phenylpropanenitrile-3,3-d_2 (1c-ßd$_2$):

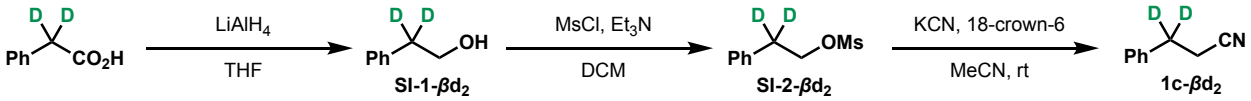

To a suspension of $LiAlH_4$ powder (5.10 g, 134 mmol, 2.0 equiv) in THF (100 mL, 1.3 M) at 0 °C was added 2-phenylacetic-2,2-d_2 acid[2] (9.2 g, 67 mmol, 1.0 equiv in 30 mL THF) over 5 minutes. The resulting suspension was warmed to room temperature and stirred for 5 hours. After cooling to 0 °C, water (5.0 mL), 10% aq. NaOH (10 mL), and water (15 mL) were added dropwise sequentially into the mixture. The resulting precipitate was removed by filtration and washed with Et_2O (200 mL). The filtrate was concentrated under reduced pressure by rotary evaporation to afford crude alcohol **SI-1-ß*d*$_2$** which was used without further purification.

MsCl (7.8 mL, 0.10 mol, 1.5 equiv) and Et_3N (18.6 mL, 134 mmol, 2.0 equiv) were sequentially added dropwise to a solution of **SI-1-ß*d*$_2$** in CH_2Cl_2 (60 mL, 1.1 M) at 0 °C. The resulting mixture was warmed to room temperature and stirred for 5 hours. The mixture was quenched by the addition of sat. aq. NH_4Cl (100 mL), and the organic phase was separated. The aqueous phase was extracted with CH_2Cl_2 (3 × 50 mL) and the combined organic layers were washed with brine (200 mL), dried over anhydrous Na_2SO_4, filtered, and concentrated under reduced pressure by rotary evaporation. Purification by flash column chromatography on silica gel (hexanes/EtOAc = 2:1) afforded 2-phenylethyl-2,2-d_2 methanesulfonate (**SI-2-ß*d*$_2$**) as a yellow oil (8.18 g, 60%). The characterization data matches previous literature reports.[3] **R_f** = 0.29 (hexanes/EtOAc = 10:1); **^{1}H NMR** (400 MHz, $CDCl_3$): δ 7.35–7.31 (m, 2H), 7.28–7.21 (m, 3H), 4.40 (s, 2H), 2.82 (s, 3H); **^{13}C{^{1}H} NMR** (101 MHz, $CDCl_3$): δ 136.3, 129.0 128.8, 127.1, 70.4, 37.3, 35.0 (quint, $J_{C\text{-}D}$ = 19.5 Hz); **IR** (cm^{-1}): 3028, 1497, 1348, 1169, 946, 735, 698; **ESI-HRMS** (m/z): $[M+H]^+$ calc'd for $C_9H_{11}D_2O_3S^+$: 203.0705; found: 203.0716.

To a solution of 2-phenylethyl-2,2-d_2 methanesulfonate **SI-2-ß*d*$_2$** (2.0 g, 10. mmol, 1.0 equiv) in MeCN (50 mL, 0.20 M) were sequentially added 18-crown-6 (6.6 g, 25 mmol, 2.5 equiv),

and KCN (1.6 g, 25 mmol, 2.5 equiv). The resulting suspension was stirred at room temperature for 12 hours. The mixture was quenched by the addition of water (50 mL), diluted with Et_2O (50 mL), and the organic phase was separated. The aqueous phase was extracted with Et_2O (3 × 30 mL) and the combined organic layers were washed with brine (100 mL), dried over anhydrous Na_2SO_4, filtered, and concentrated under reduced pressure by rotary evaporation. Purification by flash column chromatography on silica gel (hexanes/EtOAc = 10:1) afforded the title compound **1c-ß*d*$_2$** as a colorless oil (1.09 g, 82%, 96% D, unoptimized). The characterization data matches previous literature reports.[3] **R_f** = 0.19 (hexanes/EtOAc = 19:1); **^{1}H NMR** (400 MHz, $CDCl_3$): δ 7.38–7.33 (m, 2H), 7.31–7.27 (m, 1H), 7.26–7.24 (m, 2H), 2.61 (s, 2H); **^{13}C{^{1}H} NMR** (101 MHz, $CDCl_3$): δ 138.0, 128.9, 128.3, 127.3, 119.2, 31.0 (quint, $J_{C\text{-}D}$ = 20.0 Hz), 19.3; **IR** (cm^{-1}): 3031, 2246, 1496, 1448, 1426, 1026, 736. **LRMS** (m/z): $[M+H]^+$ calc'd for $C_9H_8D_2N^+$: 134.09 found: 134.09.

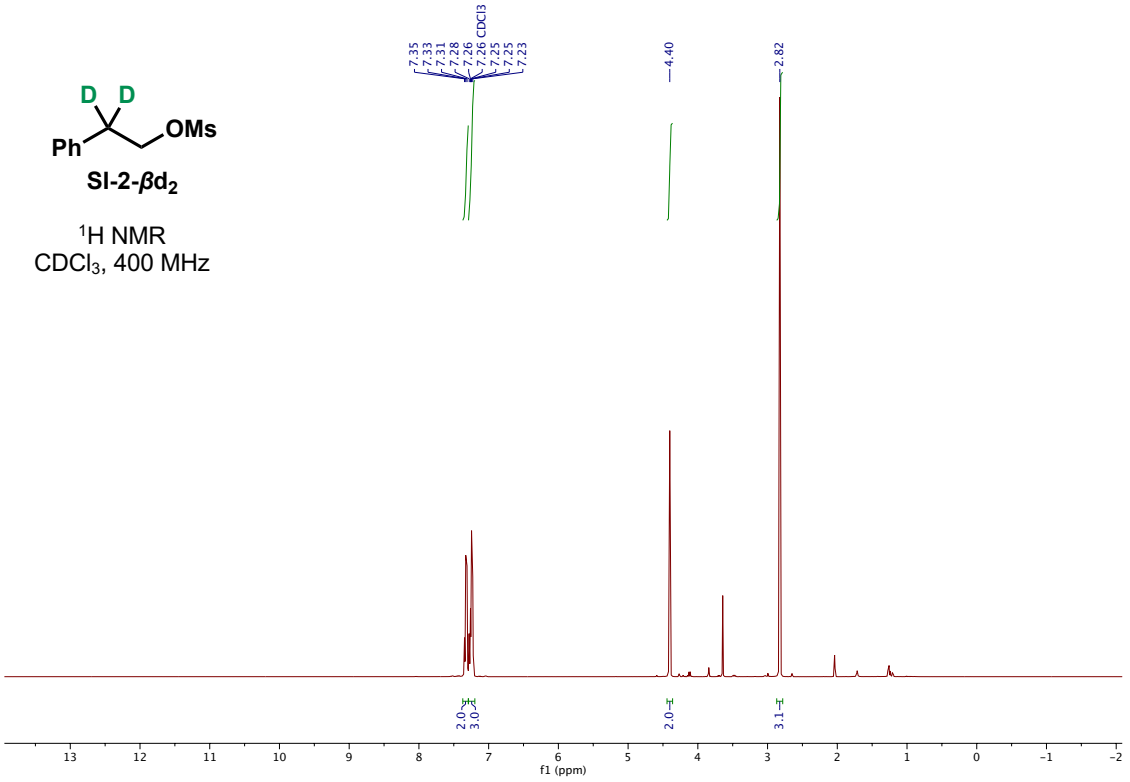

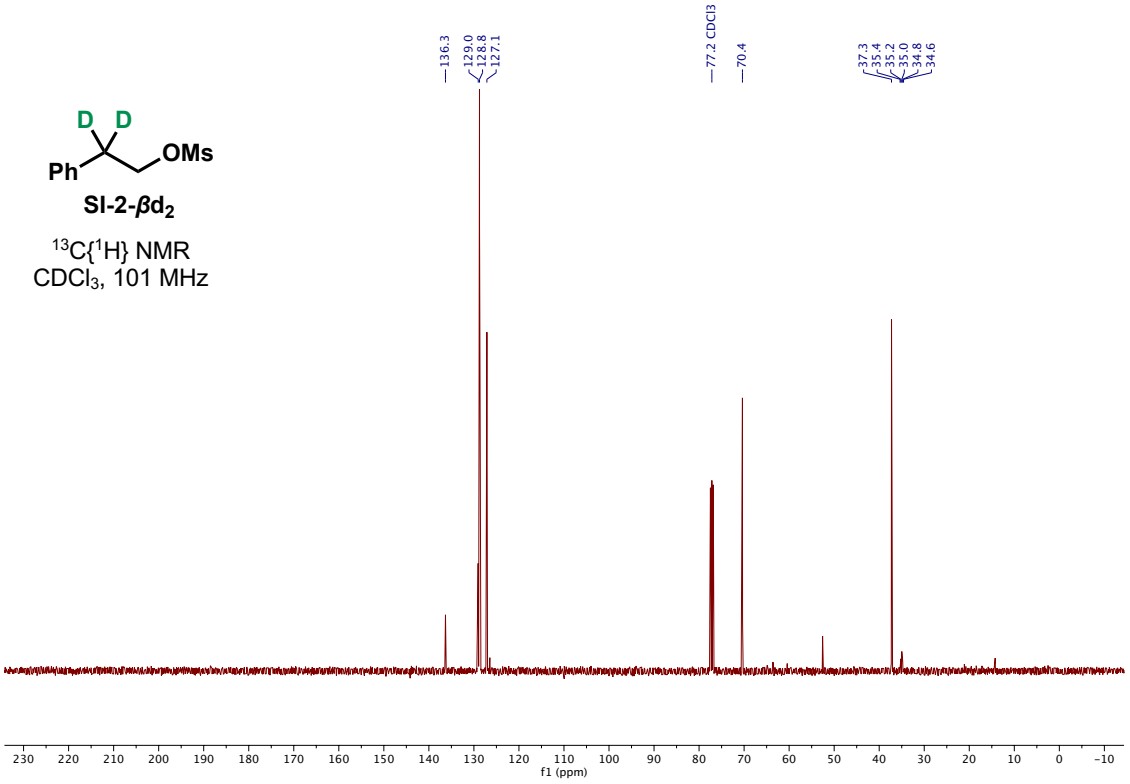

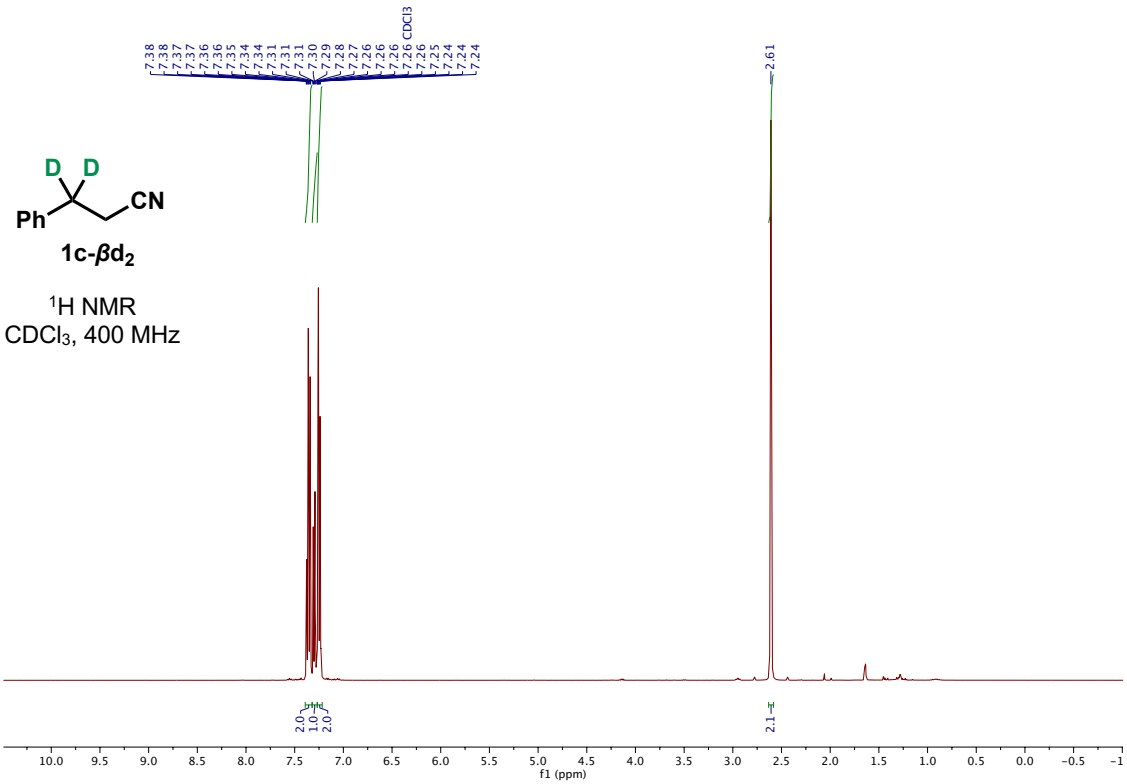

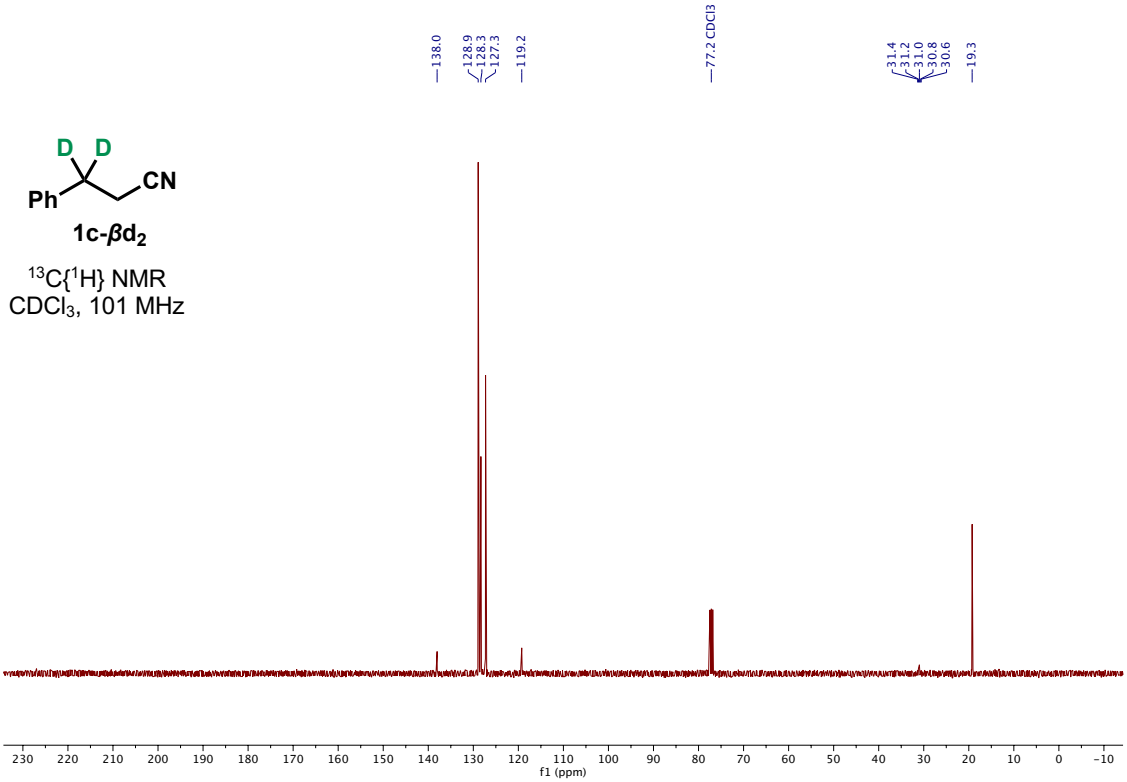

(*R*)-3-Phenylpropanenitrile-3-d_1 (1c-ßd_1):

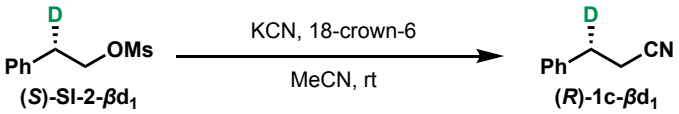

To a solution of (*S*)-2-phenylethyl-2-*d* methanesulfonate[4] (0.54 g, 2.7 mmol, 1.0 equiv) in MeCN (13 mL, 0.20 M) were sequentially added 18-crown-6 (1.77 g, 6.7 mmol, 2.5 equiv), and KCN (0.44 g, 6.7 mmol, 2.5 equiv). The resulting suspension was stirred at room temperature for 24 hours. The mixture was quenched by the addition of water (30 mL), diluted with Et_2O (30 mL), and the organic phase was separated. The aqueous phase was extracted with Et_2O (3 × 20 mL) and the combined organic layers were washed with brine (100 mL), dried over anhydrous Na_2SO_4, filtered, and concentrated under reduced pressure by rotary evaporation. Purification by flash column chromatography on silica gel (hexanes/EtOAc = 10:1) afforded **1c-ßd_1** as a colorless oil (291 mg, 82%). The characterization data matches previous literature reports.[5] $\mathbf{R_f}$ = 0.18 (hexanes/EtOAc = 19:1); $[\alpha]_D^{23}$ = –1.5 (*c*, 1.0, $CHCl_3$); **^{1}H NMR** (400 MHz, $CDCl_3$): δ 7.35 (t, *J* = 7.6 Hz, 2H), 7.29 (d, *J* = 7.2 Hz, 1H), 7.24 (d, *J* = 6.8 Hz, 2H), 2.93 (at, *J* = 7.2 Hz, 1H), 2.60 (d, *J* = 7.2 Hz, 2H); **^{13}C{^{1}H} NMR** (101 MHz, $CDCl_3$): δ 138.0, 128.9, 128.3, 127.2, 119.2, 31.2 (t, J_{C-D} = 20.0 Hz), 19.3; **IR** (cm^{-1}): 3027, 2246, 1495, 1451, 1425, 1077, 742, 697. **LRMS** (m/z): $[M+H]^+$ calc'd for $C_9H_9DN^+$: 133.09 found: 133.09.

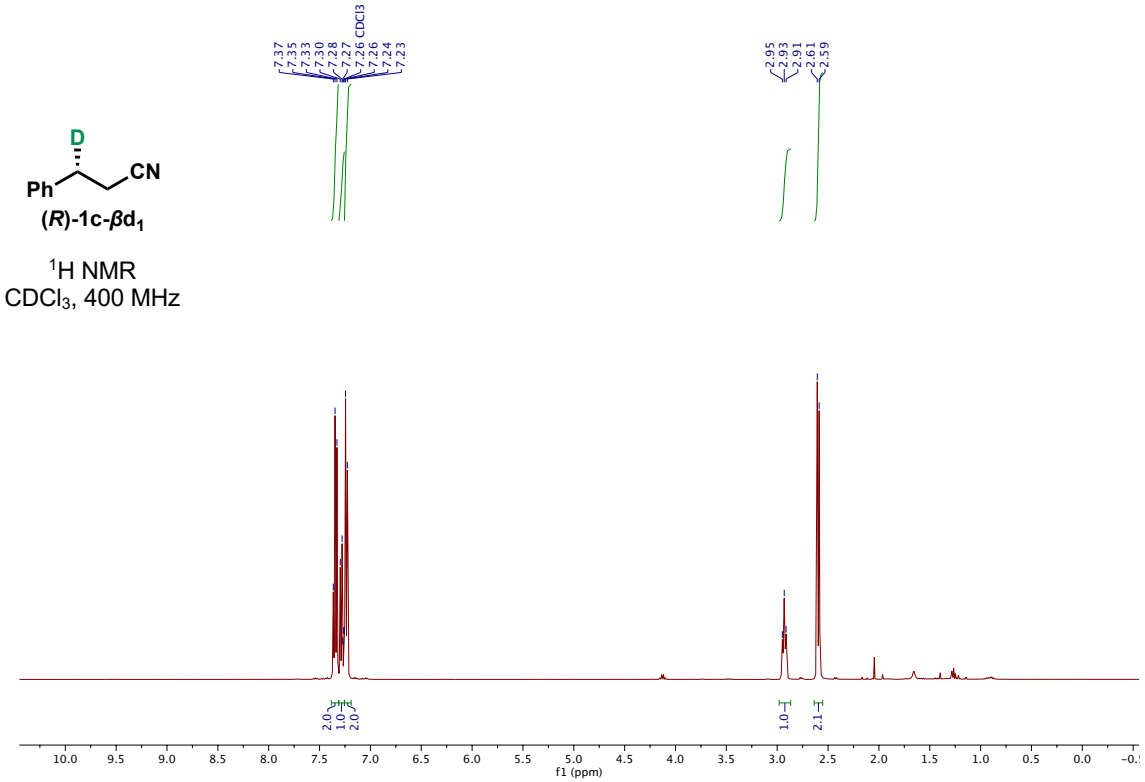

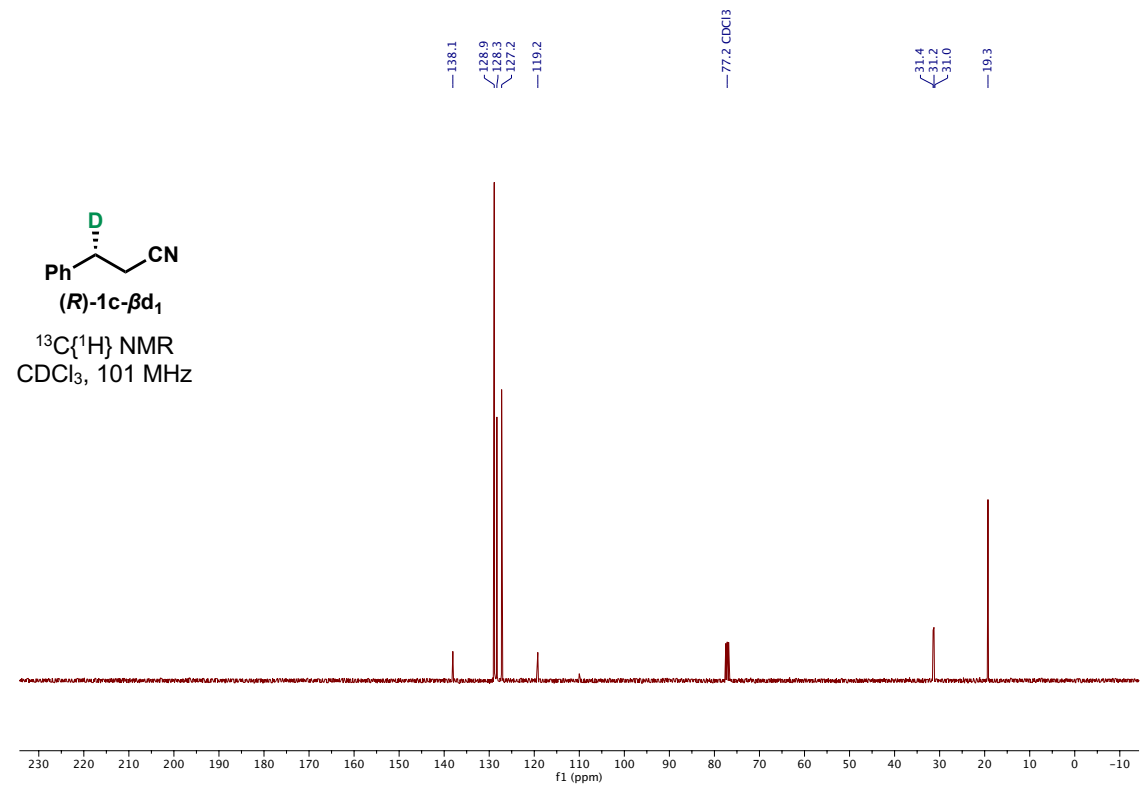

Scheme S1: Parallel KIE Experiment with Nitrile 1c and 1c-ßd_2

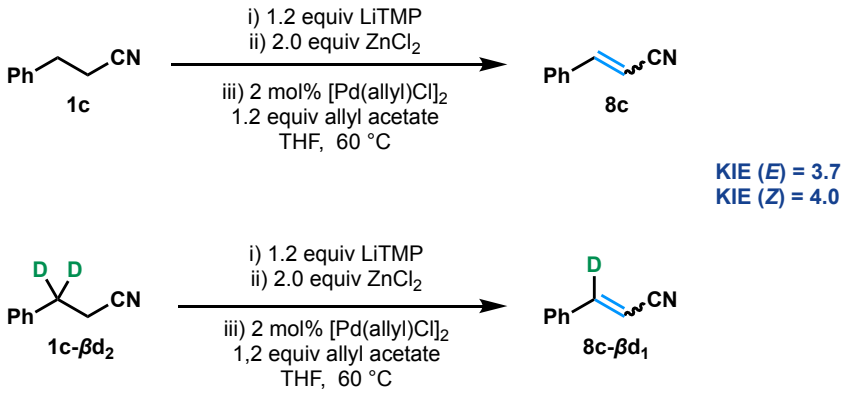

Reaction of 1c: Prepared according to **General Procedure A** on 0.30 mmol scale with 5.0 mol% $[Pd(allyl)Cl]_2$. The final reaction mixture was placed into a pre-heated 60 °C oil bath. The reaction was quenched after 10 minutes by the addition of sat. aq. NH_4Cl (2.0 mL).

Reaction of 1c-ßd$_2$: Prepared according to **General Procedure A** on 0.30 mmol scale with 5.0 mol% $[Pd(allyl)Cl]_2$. The final reaction mixture was placed into a pre-heated 60 °C oil bath. The reaction was stopped after 10 minutes by the addition of sat. aq. NH_4Cl (2.0 mL).

The two reaction mixtures were combined and diluted with additional sat. aq. NH_4Cl (15 mL) and Et_2O (10 mL), and the organic phase was separated. The aqueous phase was extracted with Et_2O (3 × 10 mL) and the combined organic layers were washed with brine (20 mL), dried over anhydrous Na_2SO_4, filtered, and concentrated under reduced pressure by rotary evaporation. The ^{1}H-NMR yields were obtained using dibromomethane (21 µL, 0.3 mmol) as an internal standard. The conversion for both runs of **1c** and **1c-ßd$_2$** was less than 25%. The KIE value for the *trans* alkene was 3.7 and 4.0 for the *cis* alkene.

Scheme S2: Intramolecular Competition Experiment with Nitrile 1c-ßd$_1$

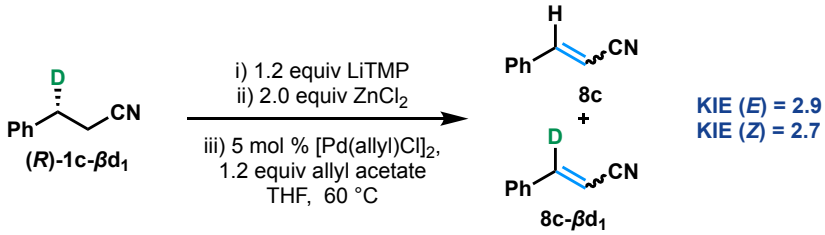

Prepared according to **General Procedure A** on 0.30 mmol scale of **1c-ßd$_1$** with 5.0 mol% [Pd(allyl)Cl]$_2$. The final reaction mixture was placed into a preheated 60 °C oil bath. The reaction was stopped after 10 minutes by the addition of sat. aq. NH_4Cl (2.0 mL). The resulting mixture was poured into sat. aq. NH_4Cl (10 mL), diluted with 10 mL Et_2O, and the organic phase was separated. The aqueous phase was extracted with Et_2O (3 × 10 mL) and the combined organic layers were washed with brine (20 mL), dried over anhydrous Na_2SO_4, filtered, and concentrated under reduced pressure by rotary evaporation. The ^{1}H NMR was obtained using dibromomethane (21 µL, 0.3 mmol) as internal standard. The conversion of **1c-ßd$_1$** was 17%. The KIE value for the *trans* alkene was 2.9 and 2.7 for the *cis* alkene.

Scheme S3: Oxidative Addition Competition Experiment: Dehydrogenation of Nitrile 1c using Ox 2 and Ox 1

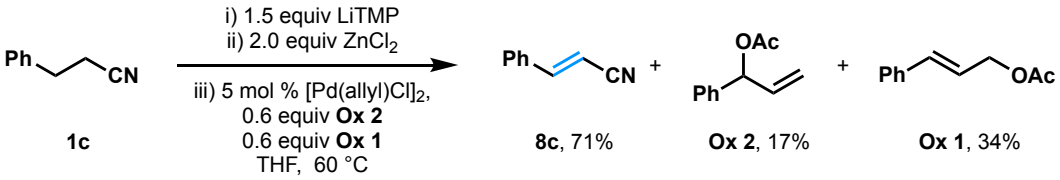

To a –40 °C solution of 2,2,6,6-tetramethylpiperidine (0.13 mL, 0.77 mmol, 1.5 equiv) in THF (1.5 mL, 0.5 M) was added *n*-BuLi (2.5 M in hexanes, 0.30 mL, 0.75 mmol, 1.5 equiv) and the resulting solution was stirred for 1 h. Nitrile **1c** (66 mg, 0.5 mmol) was added dropwise into the reaction mixture, which was moved into an ice-water bath and stirred for 30 min. $ZnCl_2$ (0.5 M in THF, 2.0 mL, 1.0 mmol, 2.0 equiv) was added and the mixture was stirred for 30 min. The stock solution of [Pd(allyl)Cl]$_2$ (4.6 mg, 0.013 mmol, 0.05 equiv) and 1-phenylallyl acetate (**Ox 2**) (53 mg, 0.30 mmol, 1.2 equiv) in THF (0.25 mL) and stock solution of [Pd(allyl)Cl]$_2$ (4.6 mg, 0.013 mmol, 0.05 equiv) and cinnamyl acetate (**Ox 1**) (53 mg, 0.30 mmol, 1.2 equiv) in THF (0.25 mL) were sequentially added. The reaction mixture was placed into a preheated 60 °C oil bath and stirred for 3 hours. The resulting mixture was cooled to room temperature and poured into sat. aq. NH_4Cl (20 mL), diluted with Et_2O (10 mL), and the organic phase was separated. The aqueous phase was extracted with Et_2O (3 × 10 mL) and the combined organic layers were washed with brine (20 mL), dried over anhydrous Na_2SO_4, filtered, and concentrated under reduced pressure by rotary evaporation. A ^{1}H-NMR yield was obtained using $MeNO_2$ (27 µL, 0.5 mmol) as an internal standard. The ^{1}H NMR revealed that the alkene product **8c** was produced in 71% yield, while 0.17

equiv of 1-phenylallyl acetate **(Ox 2)** and 0.34 equiv of cinnamyl acetate **(Ox 1)** remained; the ratio of **Ox 2** to **Ox 1** consumed was 2:1.

Scheme S4: Parallel dehydrogenation experiment with nitrile 1b as substrate using Ox 1 or Ox 2

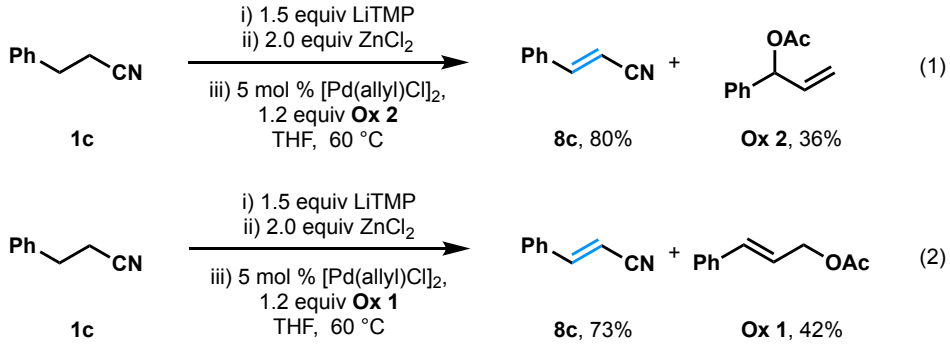

Equation 1: To a –40 °C solution of 2,2,6,6-tetramethylpiperidine (0.13 mL, 0.77 mmol, 1.5 equiv) in THF (1.5 mL, 0.5 M) was added *n*-BuLi (2.5 M in hexanes, 0.30 mL, 0.75 mmol, 1.5 equiv) and the resulting solution was stirred for 1 h. Nitrile **1c** (66 mg, 0.5 mmol) was added dropwise into the reaction mixture, which was then moved into an ice-water bath and stirred for 30 min. $ZnCl_2$ (0.5 M in THF, 2.0 mL, 1.0 mmol, 2.0 equiv) was added and the mixture was stirred for 30 min. The stock solution of $[Pd(allyl)Cl]_2$ (9.1 mg, 0.025 mmol, 0.05 equiv) and 1-phenylallyl acetate **(Ox 2)** (0.11 g, 0.60 mmol, 1.2 equiv) in THF (0.5 mL) was added. The reaction mixture was placed into a preheated 60 °C oil bath and stirred for 3 hours. The resulting mixture was cooled to room temperature and poured into sat. aq. NH_4Cl (20 mL), diluted with Et_2O (10 mL), and the organic phase was separated. The aqueous phase was extracted with Et_2O (3 × 10 mL) and the combined organic layers were washed with brine (20 mL), dried over anhydrous Na_2SO_4, filtered, and concentrated under reduced pressure by rotary evaporation. A ^{1}H-NMR yield was obtained using $MeNO_2$ (27 μL, 0.5 mmol) as an internal standard. The ^{1}H-NMR yield of **8c** was 80%; 0.36 equiv 1-phenylallyl acetate **(Ox 2)** remained, which corresponded to 0.84 equiv of the 1.2 equiv of **Ox 2** consumed.

A similar reaction was executed with cinnamyl acetate **(Ox 1)** (0.11 g, 0.60 mmol, 1.2 equiv) as the oxidant. The ^{1}H-NMR yield of **8c** was 73%; 0.42 equiv cinnamyl acetate **(Ox 1)** remained, which corresponded to 0.78 equiv of the 1.2 equiv of **Ox 1** consumed.

KIE Studies of Amide Substrates

Synthesis of Ester and Amide Substrates

N,N-Dibenzyl-3-phenylpropanamide (1a)

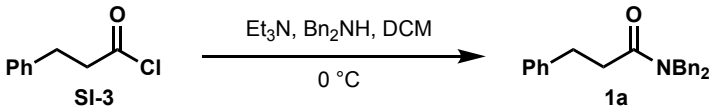

To a solution of acyl chloride **SI-3** (1.8 g, 10.7 mmol, 1.0 equiv) in CH_2Cl_2 (54 mL, 0.2 M) was added anhydrous Et_3N (4.5 mL, 32.1 mmol, 3.0 equiv) and dibenzylamine (1.3 mL, 11.8 mmol, 1.1 equiv) dropwise at 0 °C in an ice-water bath. After stirring for 5 min at 0 °C, the mixture was warmed to room temperature and stirred overnight. Sat. aq. NH_4Cl was added (50 mL), and the organic phase was separated. The aqueous phase was extracted with CH_2Cl_2 (3 x 20 mL), and the combined organic layers were washed with brine, dried over anhydrous Na_2SO_4, filtered, and concentrated under reduced pressure by rotary evaporation. Purification by flash column chromatography on silica gel (hexanes/EtOAc = 10:1 to 5:1) afforded the title product **1a** as a white solid in 80% yield (2.63 g). **^{1}H NMR** (400 MHz, $CDCl_3$) δ 7.38 – 7.23 (m, 8H), 7.23 – 7.15 (m, 5H), 7.11 – 7.05 (m, 2H), 4.61 (s, 2H), 4.38 (s, 2H), 3.06 (t, J = 7.7 Hz, 2H), 2.74 (t, J = 7.7 Hz, 2H); **^{13}C{^{1}H} NMR** (101 MHz, $CDCl_3$) δ 172.9, 141.3, 137.4, 136.5, 129.1, 128.7, 128.7, 128.6, 128.5, 127.7, 127.5, 126.5, 126.3, 50.0, 48.5, 35.1, 31.8. The characterization data matches previous literature reports.[6]

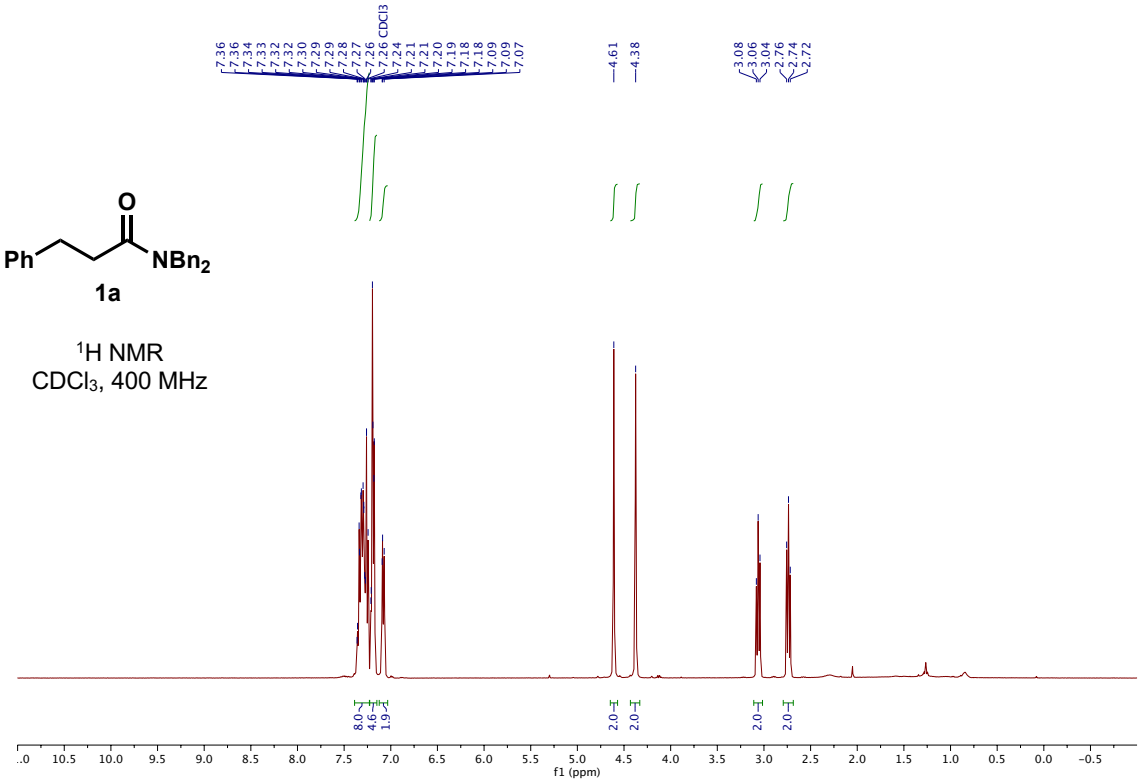

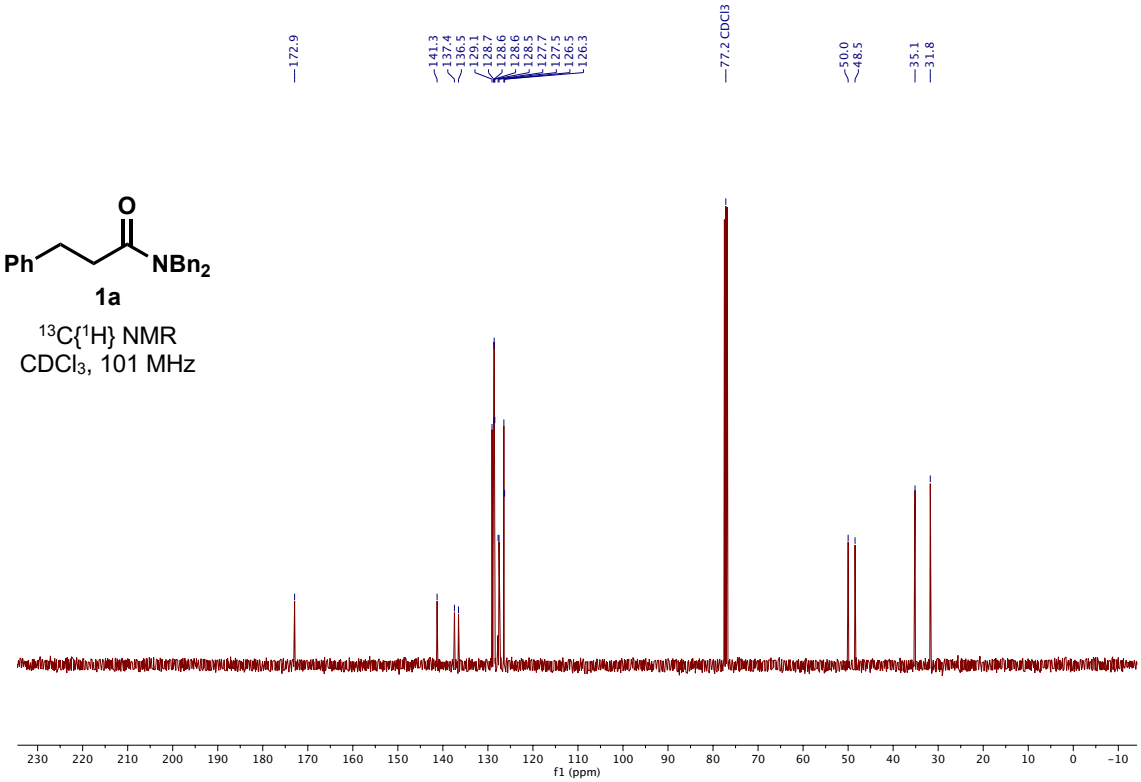

***N,N*-Dibenzyl-3-phenylpropanamide-3,3-d$_2$ (1a-ßd$_2$)**:

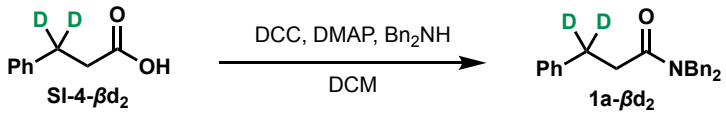

To a solution of DCC (2.9 g, 14.2 mmol, 1.1 equiv) and DMAP (159 mg, 1.3 mmol, 0.1 equiv) in CH_2Cl_2 (65 mL, 0.2 M) was added dibenzylamine (2.7 mL, 14.1 mmol, 1.1 equiv) followed by 3-phenylpropanoic-3,3-*d*$_2$ acid (1.95 g, 12.9 mmol, 1.0 equiv). The reaction was stirred at ambient temperature for 24h. The mixture was filtered through a silica plug and eluted with EtOAc. The eluent was concentrated under reduced pressure by rotary evaporation. Purification by flash column chromatography on silica gel (10:1-5:1 hexanes:EtOAc) afforded the title product **1a-ßd$_2$** as an off white solid (3.71 g, 87%). **R$_f$**: 0.26 (40% Et_2O/hexanes); **^{1}H NMR** (400 MHz, $CDCl_3$): δ 7.36 – 7.25 (m, 8H), 7.21 – 7.18 (m, 5H), 7.09 – 7.07 (m, 2H), 4.61 (s, 2H), 4.38 (s, 2H), 2.72 (s, 2H); **^{13}C{^{1}H} NMR** (151 MHz, $CDCl_3$): δ 172.9, 141.2, 137.5, 136.6, 129.1, 128.7, 128.63, 128.60, 128.4, 127.7, 127.5, 126.4, 126.3, 50.0, 48.4, 35.0, 31.1 (quint, J_{C-D} = 19.6 Hz); **IR** (cm^{-1}): 3026, 1631, 1443, 1208, 958, 702; **ESI-HRMS** (m/z): $[M+H]^+$ calc'd for $C_{23}H_{22}D_2NO^+$: 332.1983; found: 332.1972. **m.p.** 105 °C

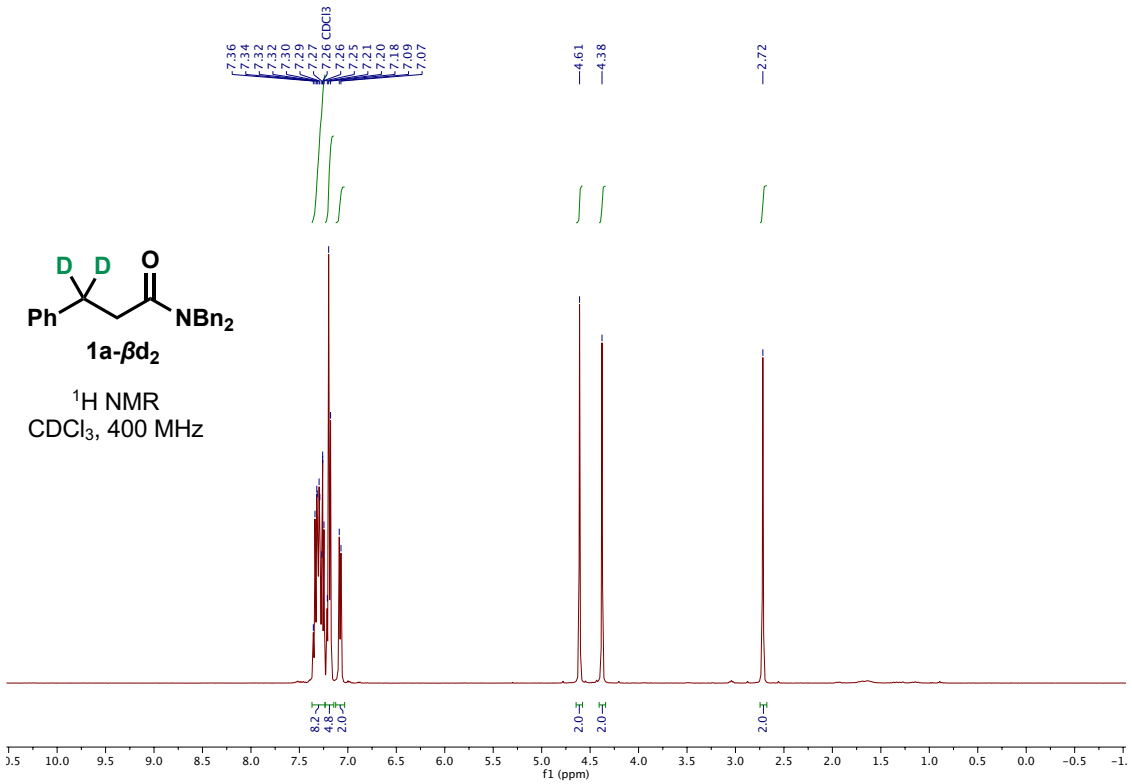

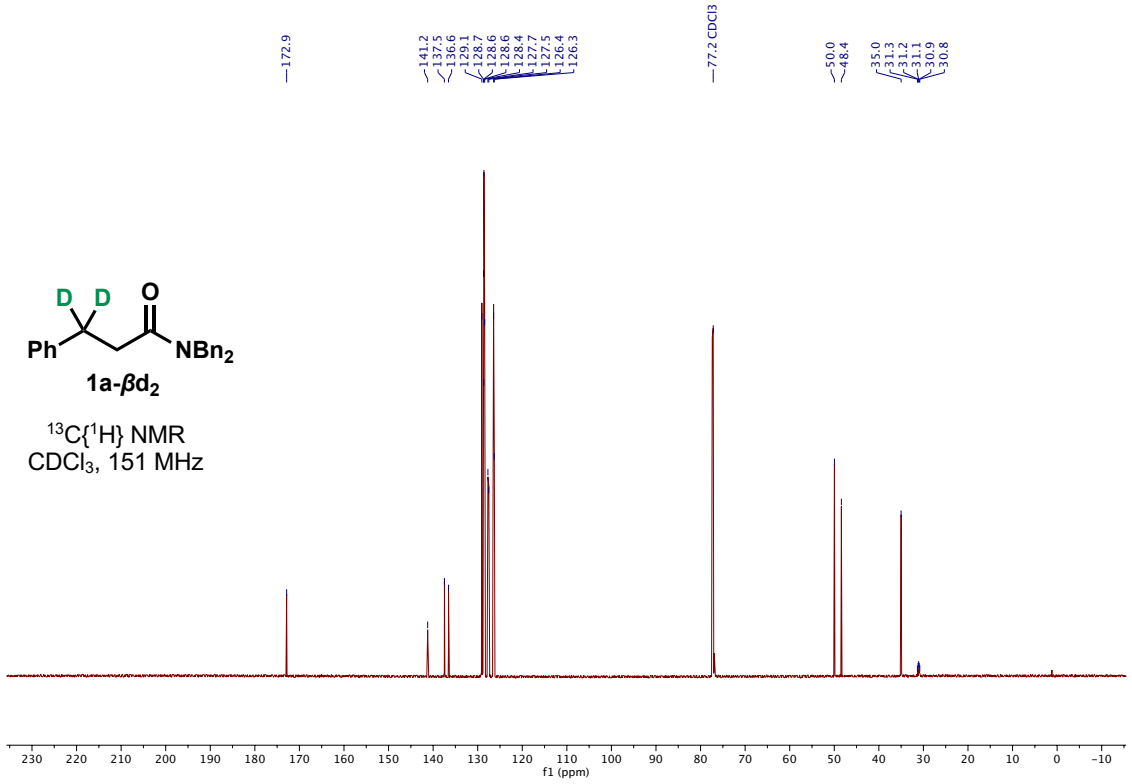

***N,N*-Dibenzyl-3-phenylpropanamide-3-*d* (1a-ßd$_1$):**

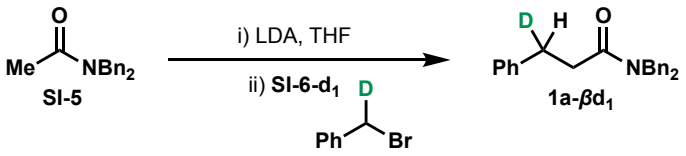

To a solution of diisopropylamine (1.05 mL, 7.5 mmol, 1.5 equiv) in THF (20 mL, 0.25 M) at 0 °C was added *n*-BuLi (2.5 M in hexanes, 2.7 mL, 6.5 mmol, 1.3 equiv). The reaction was stirred for 30 min then cooled to –78 °C. *N,N*-dibenzylacetamide (1.197 g, 5.0 mmol, 1.0 equiv) was added and the solution was warmed to 0 °C and stirred for 30 min. The reaction was re-cooled to –78 °C and (bromomethyl-*d*)benzene (0.60 mL, 5.0 mmol, 1 equiv) was added. The reaction was transferred to 0 °C ice-water bath and allowed to warm to room temperature over 7h. The reaction was quenched with the addition of sat. aq. NH_4Cl (20 mL) and the organic phase was separated. The aqueous phase was extracted with EtOAc (3 x 20 mL) and the combined organic extracts were washed with brine (50 mL), dried over anhydrous Na_2SO_4, filtered, and concentrated under reduced pressure by rotary evaporation. Purification by flash column chromatography on silica gel (6%–9% EtOAc/hexanes) afforded **1a-ßd$_1$** (564 mg, 34%) over two steps as a white solid. **R$_f$**: 0.26 (40% Et_2O/hexanes); **^{1}H NMR** (400 MHz, $CDCl_3$): δ 7.36 – 7.25 (m, 8H), 7.21 – 7.18 (m, 5H), 7.09 – 7.07 (m, 2H), 4.61 (s, 2H), 4.38 (s, 2H), 3.04 (t, J = 7.6 Hz, 1H), 2.73 (d, J = 7.6 Hz, 2H); **^{13}C{^{1}H} NMR** (101 MHz, $CDCl_3$): δ 172.9, 141.3, 137.5, 136.6, 129.1, 128.7, 128.64, 128.61, 128.4, 127.7, 127.5, 126.4, 126.3, 50.0, 48.4, 35.1, 31.4 (t, $J_{C–D}$ = 19.6 Hz); **IR** (cm^{-1}): 3026, 2916, 1631, 1207, 697; **ESI-HRMS (m/z)**: $[M+H]^+$ calc'd for $C_{23}H_{23}DNO^+$: 331.1921; found: 331.1915. **m.p.** 94 °C

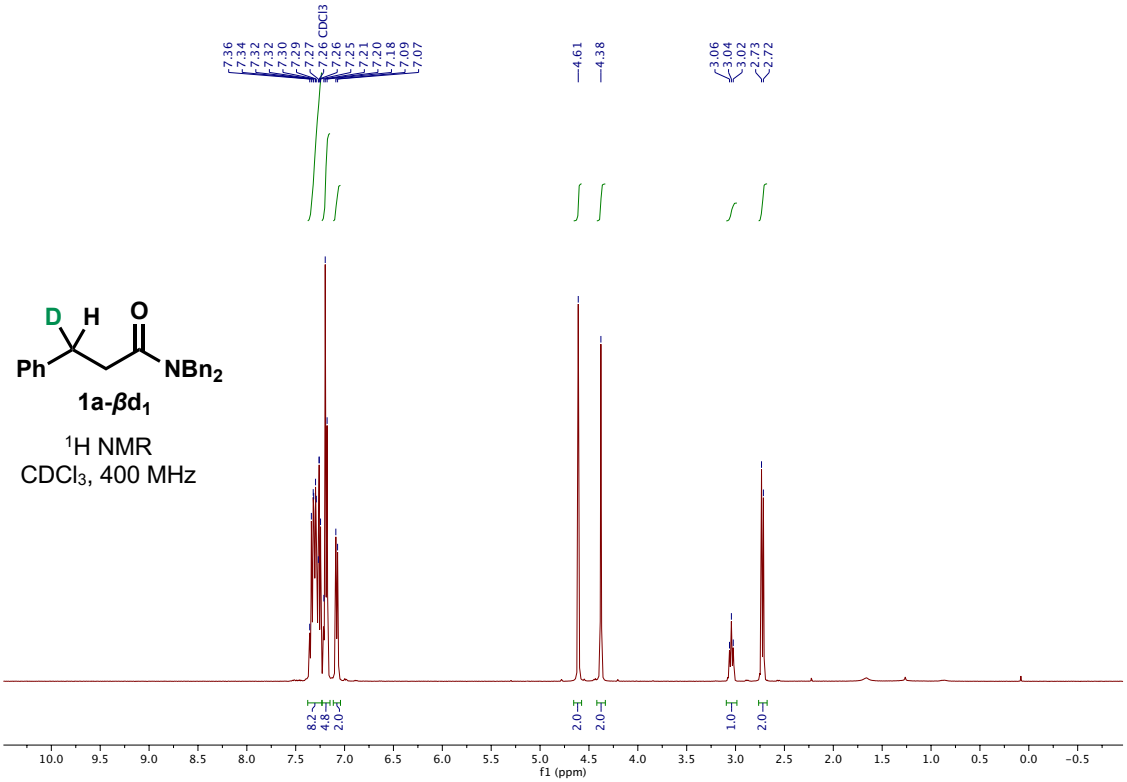

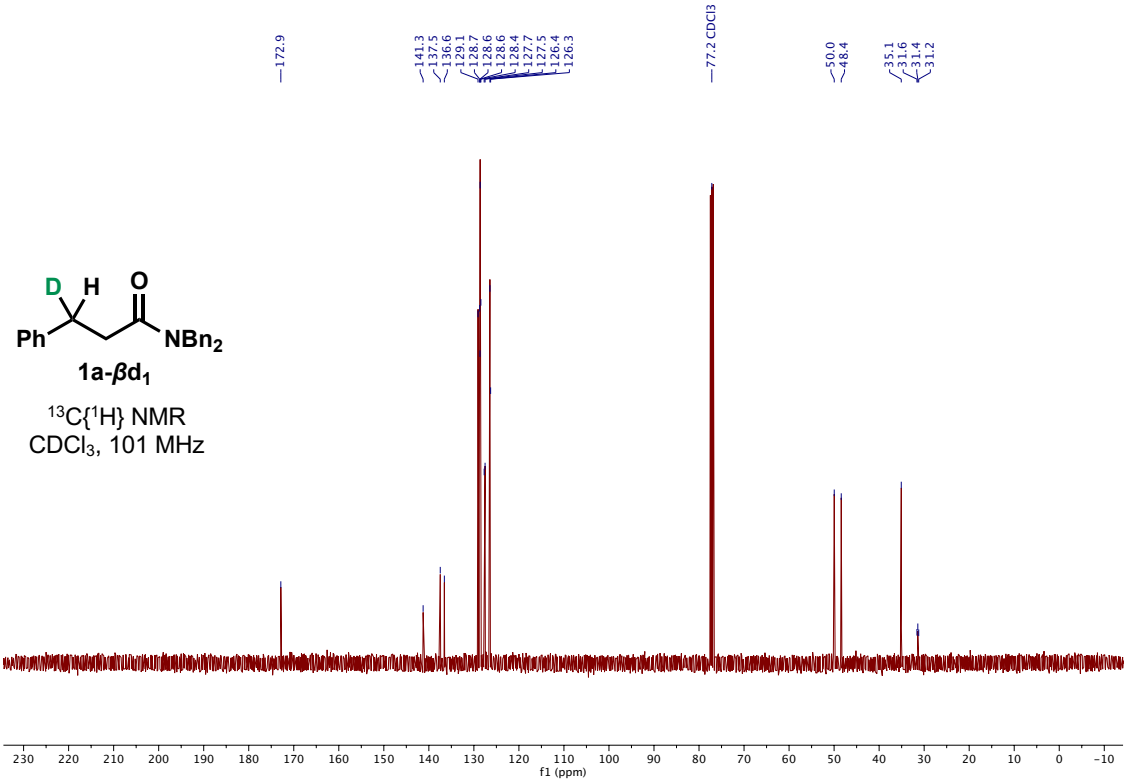

***tert*-butyl 2-benzyl-3-phenylpropanoate (SI-8)**:

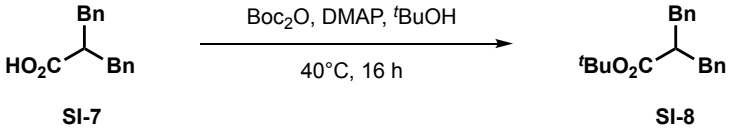

SI-7 **SI-8**

To a solution of 2-benzyl-3-phenylpropanoic acid (**SI-7**) (240 mg, 1.0 mmol, 1.0 equiv) in tert-butanol (2 mL, 0.5 M) was added DMAP (36.7 mg, 0.3 mmol, 0.3 equiv) and Boc_2O (436.6 mg, 2.0 mmol, 2.0 equiv). After stirring for 30 min at 23 °C, the mixture was placed into a preheated 40 °C oil bath and stirred for 4 h. After the mixture was cooled down to room temperature, water (5 mL) was added, the mixture was diluted with Et_2O (2 mL), and the organic phase was separated. The aqueous phase was extracted with Et_2O (3 x 5 mL) and the combined organic layers were washed with brine, dried over anhydrous Na_2SO_4, filtered, and concentrated under reduced pressure by rotary evaporation. Purification by flash column chromatography on silica gel (10% Et_2O in hexanes) afforded **SI-8** (154 mg, 52% yield) as a colorless oil. $\mathbf{R_f}$ = 0.56 (15% Et_2O in hexanes); **^{1}H NMR** (600 MHz, $CDCl_3$): δ 7.29 – 7.26 (m, 4H), 7.21 – 7.19 (m, 6H), 2.95 – 2.86 (m, 3H), 2.78 (dd, J = 12.8, 5.2 Hz, 2H), 1.20 (s, 9H);**^{13}C{^{1}H} NMR** (151 MHz, $CDCl_3$) δ 174.3, 139.5, 129.2, 128.4, 126.4, 80.4, 50.3, 38.7, 28.0. The characterization data matches those previously reported in the literature.[7]

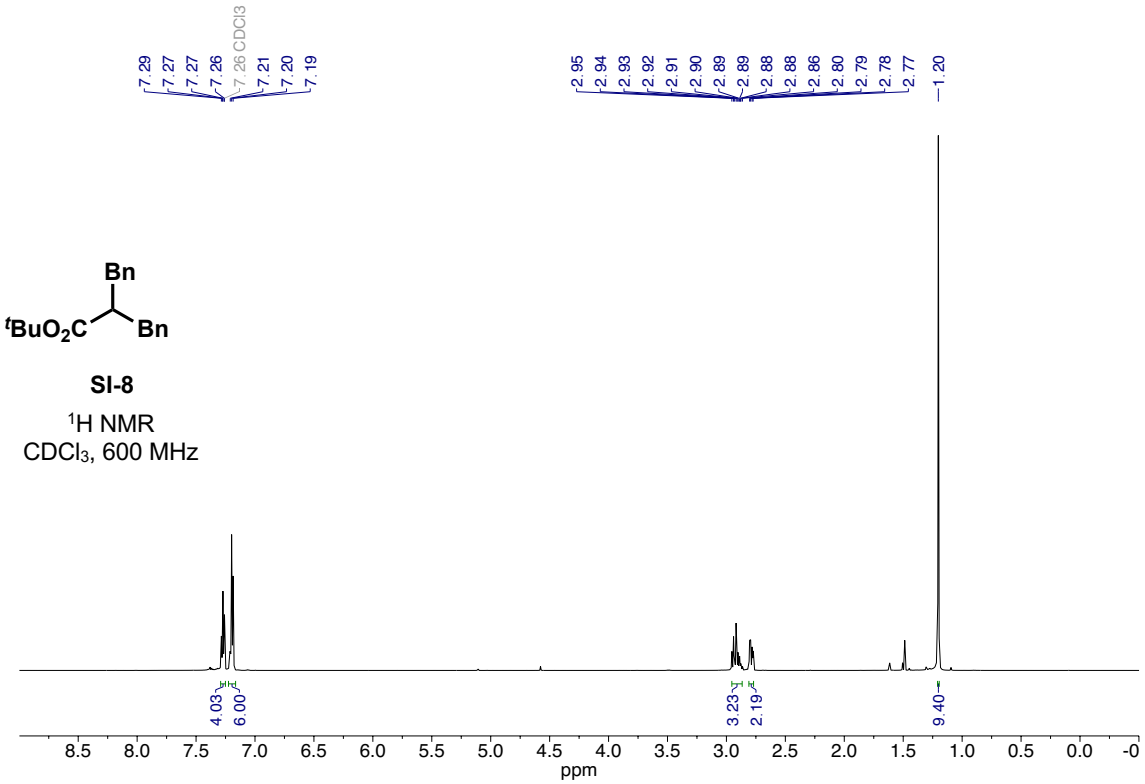

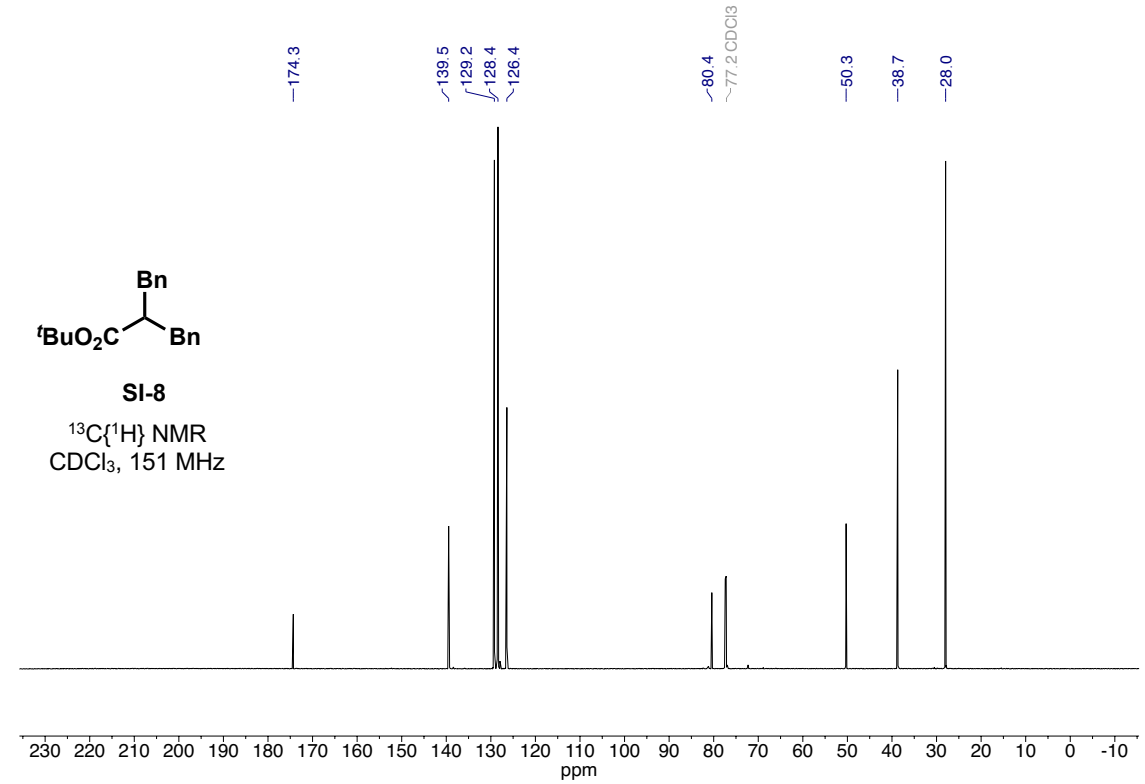

***tert*-butyl 2-benzyl-3-phenylpropanoate-3,3-d_2 (1e-ßd$_2$)**:

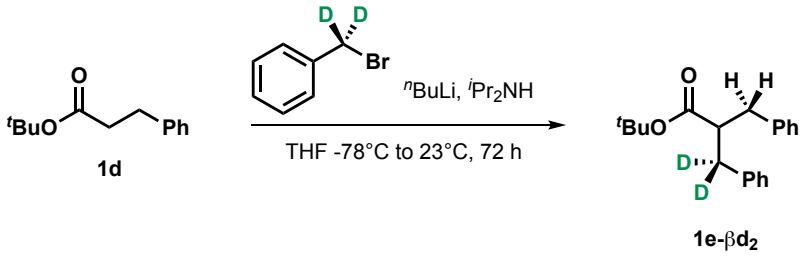

The title compound was synthesized according to a modified literature procedure.[8] Purification by flash column chromatography on silica gel (10% Et_2O in hexanes) afforded the title compound (75 mg, 50% yield) as a colorless oil. $\mathbf{R_f}$ = 0.66 (15% Et_2O in hexanes); **^{1}H NMR** (600 MHz, $CDCl_3$): δ 7.27 – 7.29 (m, 4H), 7.22 – 7.19 (m, 6H), 2.97 – 2.86 (m, 2H), 2.79 (dd, *J* = 13.1, 5.6 Hz, 1H), 1.21 (s, 9H); **^{13}C{^{1}H} NMR** (151 MHz, $CDCl_3$) δ 174.3, 139.5, 139.4, 130.7, 129.2, 129.2, 128.4, 128.1, 126.4, 80.4, 50.2, 38.7, 38.3, 38.1, 38.0, 37.9, 37.8, 28.0. **IR** (cm^{-1}): 3027, 2977, 1722, 1605, 1449, 1366, 1146, 846, 736, 696. **GC-MS (m/z)**: [M] calc'd for $C_{20}H_{22}D_2O_2$: 298.2, found: 298.2.

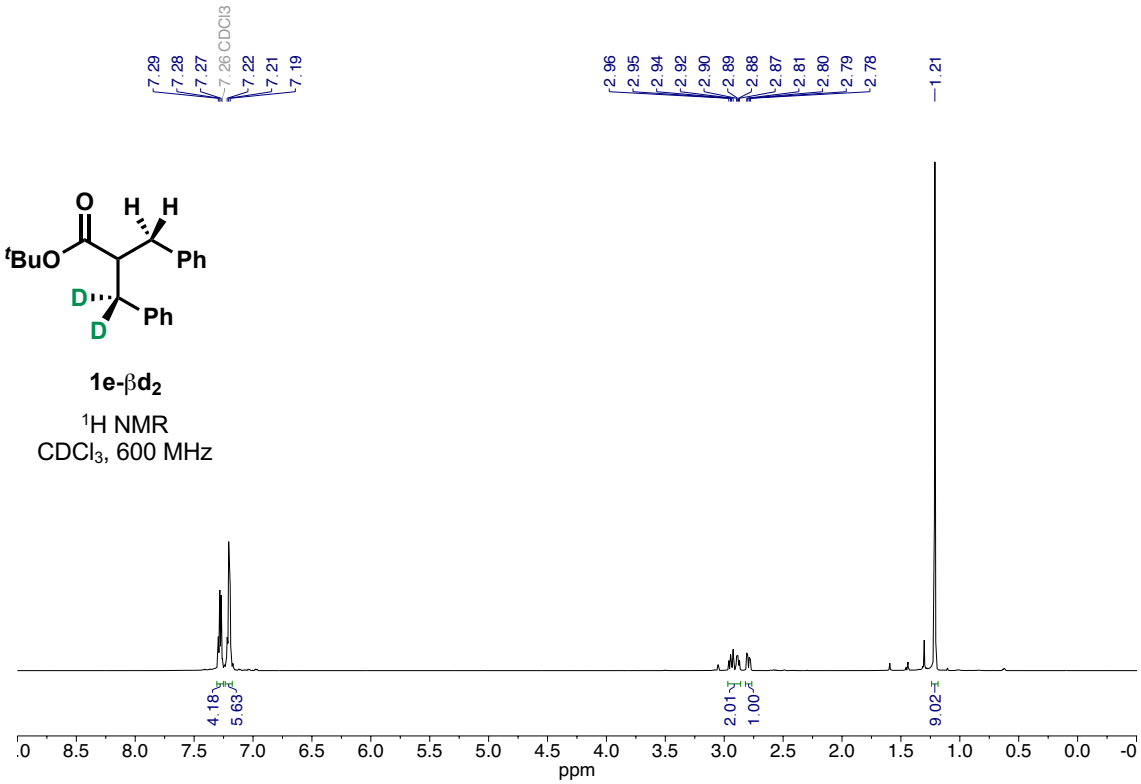

1e-βd$_2$

^{1}H NMR
$CDCl_3$, 600 MHz

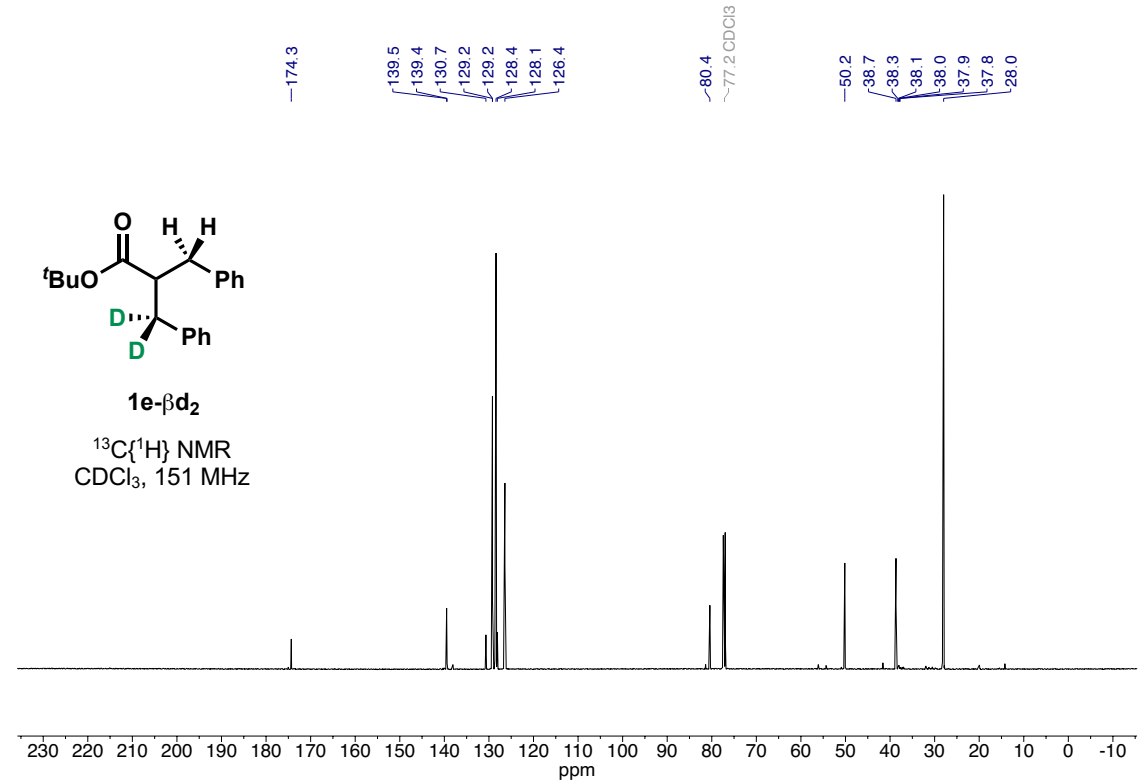

1e-βd$_2$

$^{13}C\{^1H\}$ NMR
$CDCl_3$, 151 MHz

Characterization Date for *α,β*-Unsaturated Esters and Amides

***N,N*-Dibenzylcinnamamide (8a)**:

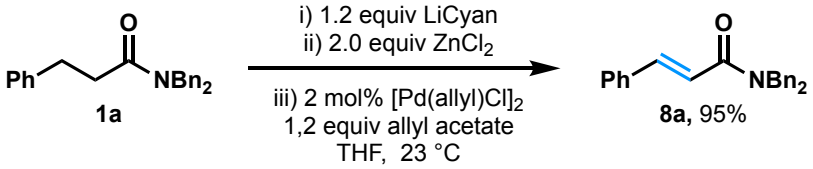

Prepared according to **General Procedure B** on a 0.20 mmol scale of **1a** with 2.0 mol% $[Pd(allyl)Cl]_2$. The reaction was stirred at room temperature for 1 hour, then quenched by the addition of sat. aq. NH_4Cl (2.0 mL) and diluted with EtOAc (1.0 mL). The organic layer was separated, and the aqueous phase was extracted with EtOAc (3 × 1.0 mL), and the combined organic layers were washed with brine (2.0 mL), dried over anhydrous Na_2SO_4, filtered, and concentrated under reduced pressure by rotary evaporation. Purification by flash column chromatography on silica gel (1:8-1:4 EtOAc:hexanes) afforded **8a** as a white solid (62.2 mg, 95%). $\mathbf{R_f}$: 0.21 (15% EtOAc/hexanes); $^{\mathbf{1}}\mathbf{H}$ **NMR** (400 MHz, $CDCl_3$): δ 7.87 (d, J = 15.6 Hz, 1H), 7.48 – 7.46 (m, 2H), 7.43 – 7.30 (m, 10H), 7.30 – 7.21 (m, 3H), 6.92 (d, J = 15.6 Hz, 1H), 4.73 (s, 2H), 4.62 (s, 2H); $^{\mathbf{13}}\mathbf{C}\{^{\mathbf{1}}\mathbf{H}\}$ **NMR** (101 MHz, $CDCl_3$) δ 167.3, 144.0, 137.5, 136.8, 135.3, 129.8, 129.1, 128.9, 128.8, 128.5, 128.0, 127.9, 127.6, 126.7, 117.3, 50.2, 48.9; **IR** (cm^{-1}): 3028, 2926, 1641, 1592, 1425, 1197, 695; **ESI-HRMS (m/z)**: $[M+H]^+$ calc'd for $C_{23}H_{22}NO^+$: 328.1696; found: 328.1701. The characterization data matches those previously reported in the literature.[9]

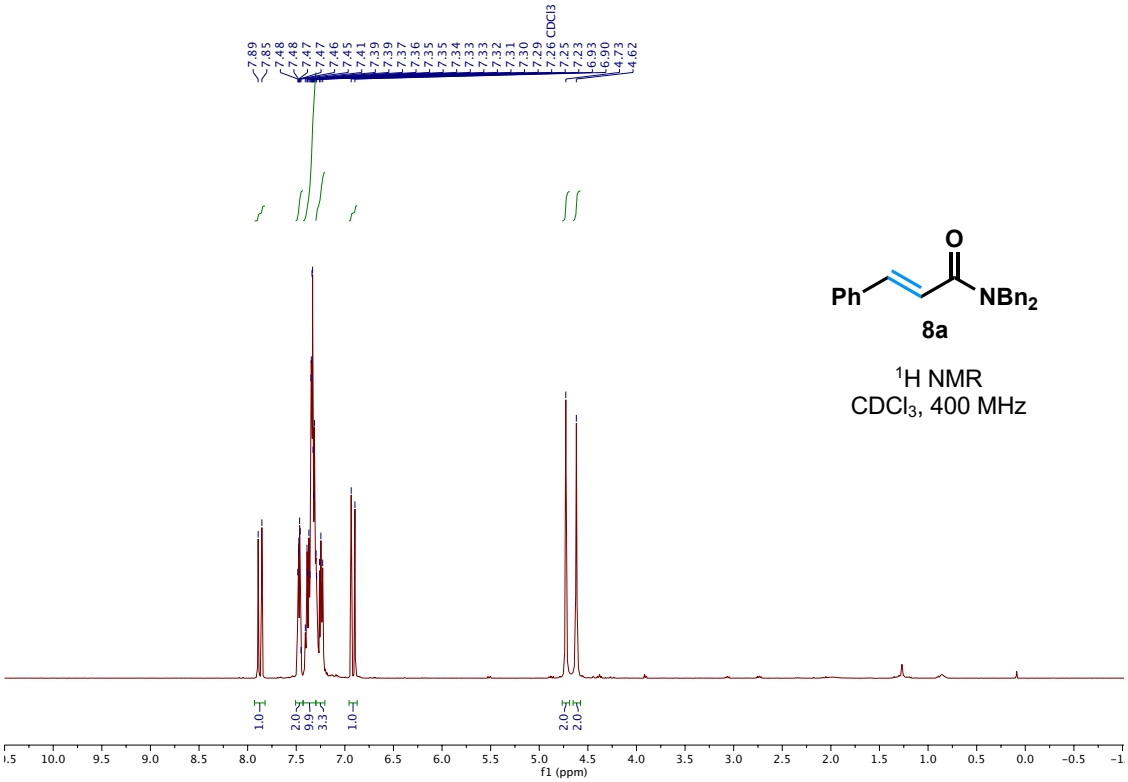

8a

^{1}H NMR
$CDCl_3$, 400 MHz

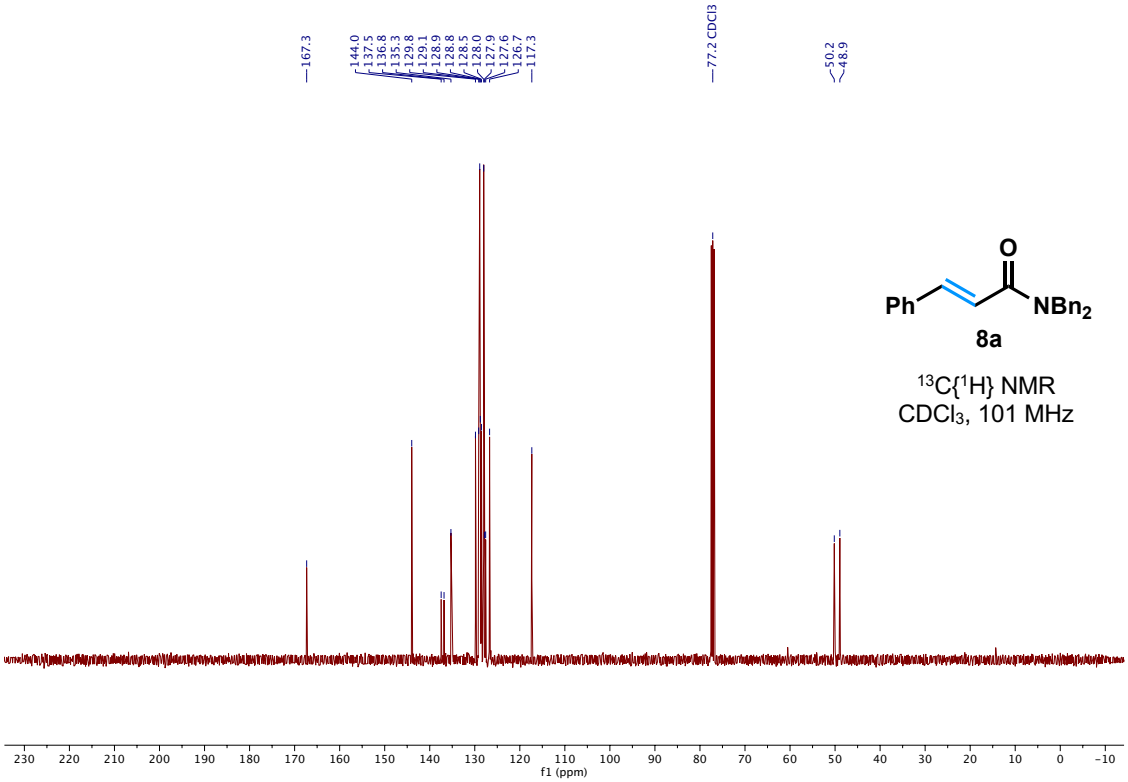

8a

$^{13}C\{^{1}H\}$ NMR
$CDCl_3$, 101 MHz

***N,N*-Dibenzylcinnamamide-3-*d* (8a-ßd$_1$)**:

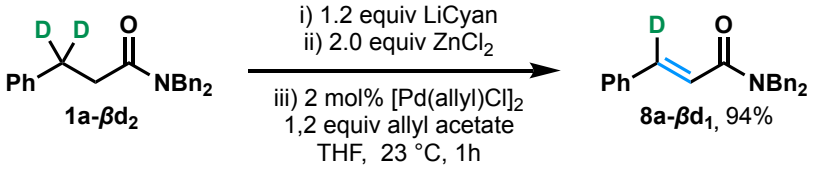

Prepared according to **General Procedure B** on a 0.20 mmol scale of **1a-ß*d*$_2$** with 2.0 mol% [Pd(allyl)Cl]$_2$. The reaction was stirred at room temperature for 1 hour, then quenched by the addition of sat. aq. NH_4Cl (2.0 mL) and diluted with EtOAc (2.0 mL). The organic layer was separated, and the aqueous phase was extracted with EtOAc (3 × 2.0 mL) and the combined organic layers were washed with brine (5.0 mL), dried over anhydrous Na_2SO_4, filtered, and concentrated under reduced pressure by rotary evaporation. Purification by flash column chromatography on silica gel (10% - 20% hexanes/EtOAc) afforded the title product **8a-ßd$_1$** as an off-white solid (120 mg, 94%). **R$_f$**: 0.26 (40% Et_2O/hexanes); **^{1}H NMR** (400 MHz, $CDCl_3$): δ 7.48 – 7.45 (m, 2H), 7.40 – 7.29 (m, 11H), 7.24 – 7.22 (m, 2H), 6.90 (s, 1H), 4.72 (s, 2H), 4.61 (s, 2H); **^{13}C{^{1}H} NMR** (151 MHz, $CDCl_3$): δ 167.3, 143.6 (t, J_{C-D} = 23.9 Hz), 137.4, 136.8, 135.2, 129.8, 129.1, 128.9, 128.7, 128.5, 128.0, 127.8, 127.5, 126.7, 117.2, 50.1, 48.9; **IR** (cm^{-1}): 2925, 1629, 1589, 1200, 696. **ESI-HRMS (m/z)**: $[M+H]^+$ calc'd for $C_{23}H_{21}DNO^+$: 329.1759; found: 329.1761. **m.p.** 134–136 °C

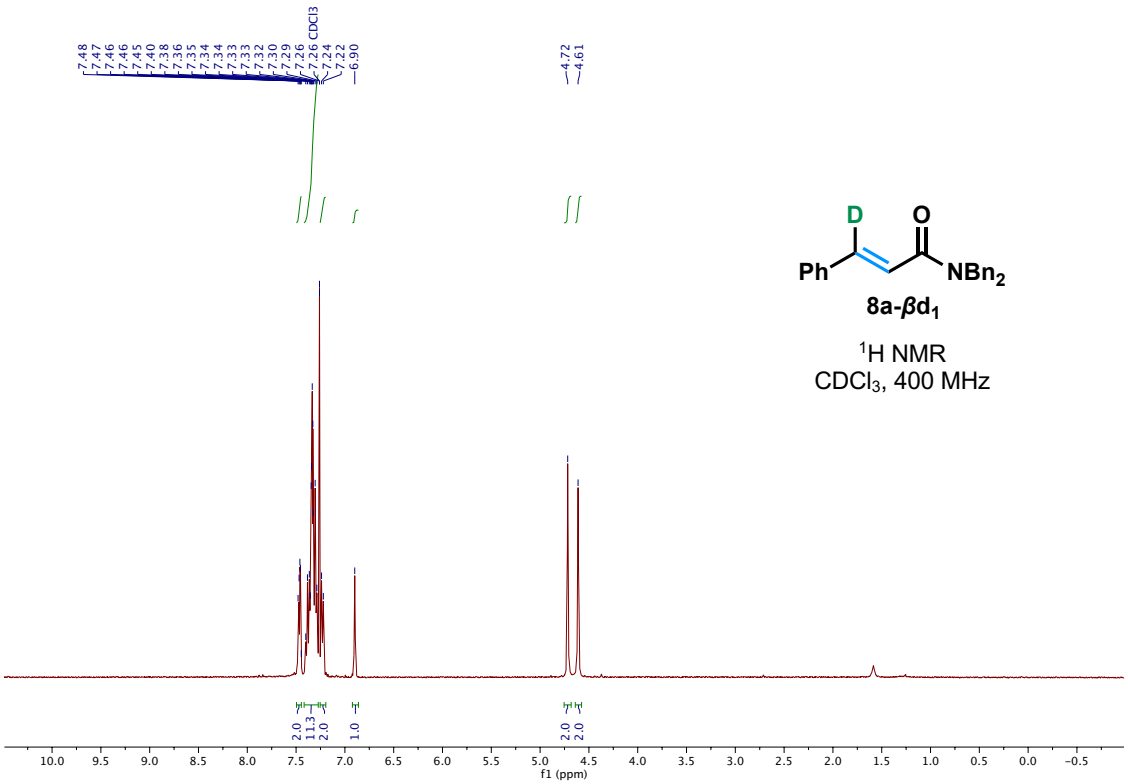

8a-βd$_1$

^{1}H NMR
$CDCl_3$, 400 MHz

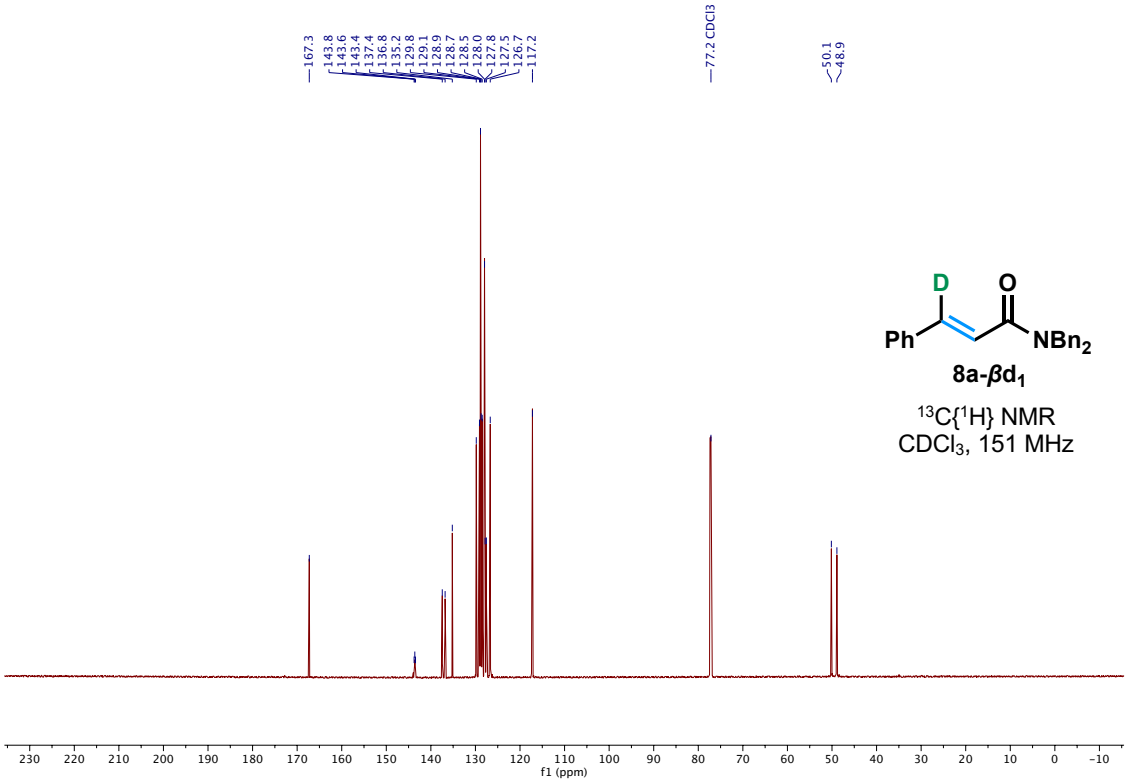

8a-βd$_1$

$^{13}C\{^{1}H\}$ NMR
$CDCl_3$, 151 MHz

***tert*-butyl (*E*)-2-benzyl-3-phenylacrylate (SI-9)**

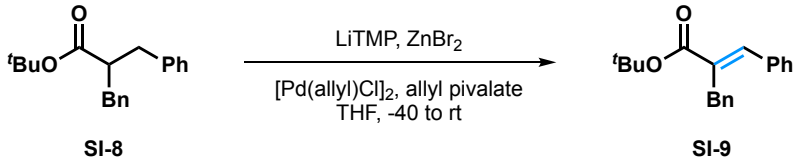

SI-8 **SI-9**

Prepared according to **General Procedure A** on a 0.20 mmol scale of **SI-8** using $ZnBr_2$ (90 mg, 0.4 mmol, 2.0 equiv) and 5.0 mol% $[Pd(allyl)Cl]_2$. The reaction was stirred at room temperature for 90 minutes, then quenched by the addition of sat. aq. NH_4Cl (2.0 mL) and diluted with Et_2O (2.0 mL). The organic layer was separated, and the aqueous phase was extracted with Et_2O (3 × 2.0 mL) and the combined organic layers were washed with brine (5.0 mL), dried over anhydrous Na_2SO_4, filtered, and concentrated under reduced pressure by rotary evaporation. Purification by flash column chromatography on silica gel (10% Et_2O in hexanes) afforded the title product **SI-9** as a colorless oil (29.4 mg, 50%). $\mathbf{R_f}$: 0.58 (15% Et_2O in hexanes); **^{1}H NMR** (600 MHz, $CDCl_3$): δ 7.84 (s, 1H), 7.39 – 7.33 (m, 4H), 7.33 – 7.26 (m, 3H), 7.19 (m, 3H), 3.90 (s, 2H), 1.39 (s, 9H); **^{13}C{^{1}H} NMR** (151 MHz, $CDCl_3$): δ 167.5, 140.1, 139.8, 135.9, 132.9, 129.2, 128.7, 128.6, 128.6, 128.1, 126.1, 80.9, 33.5, 28.1. The characterization data matches previous literature reports.[10]

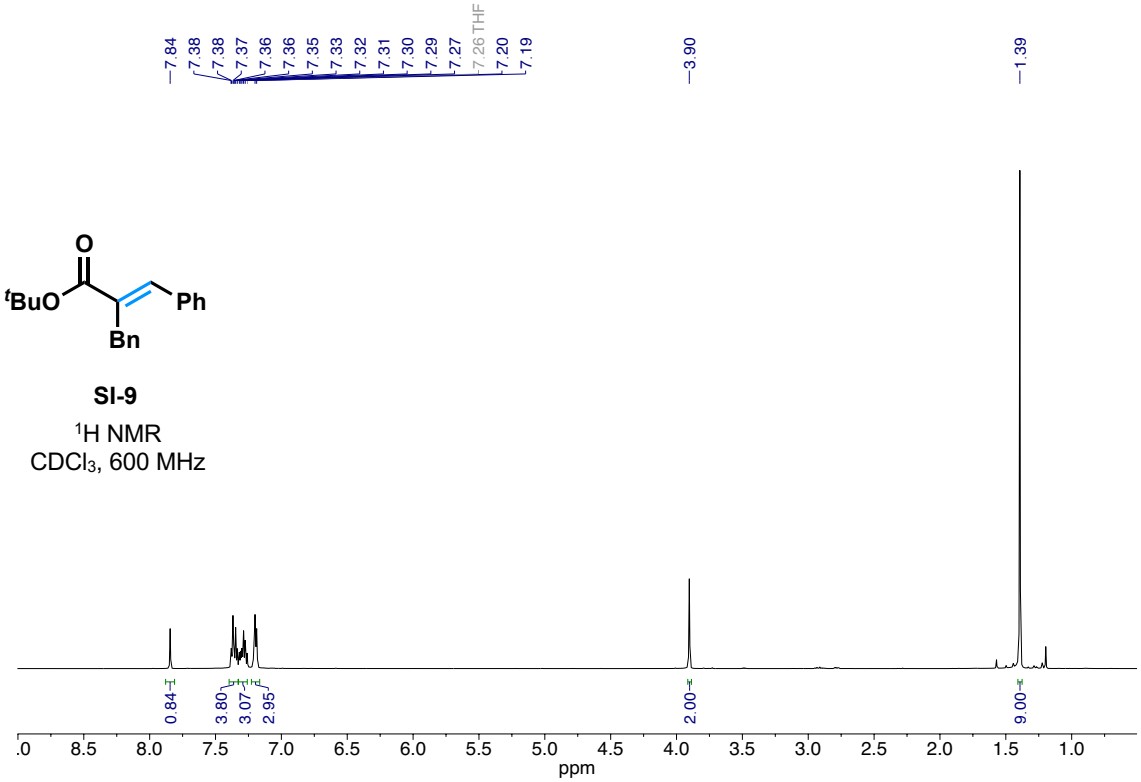

SI-9

^{1}H NMR

$CDCl_3$, 600 MHz

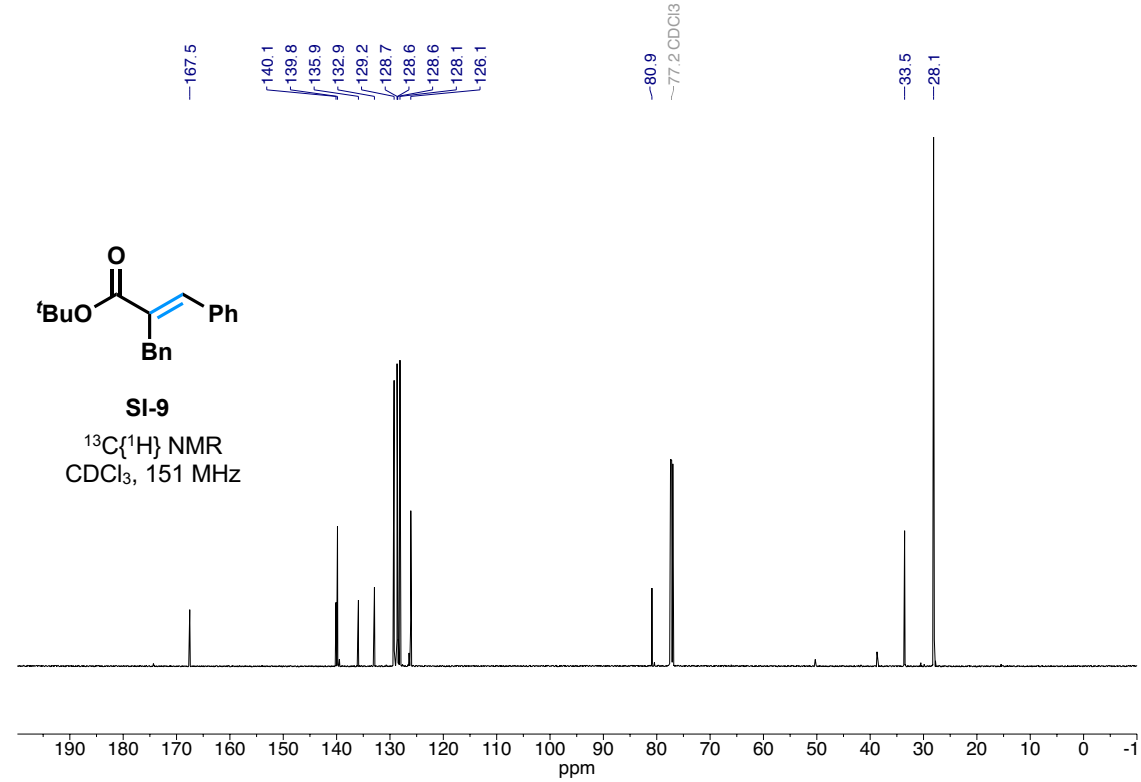

SI-9

^{13}C{^{1}H} NMR

$CDCl_3$, 151 MHz

Scheme S5: Intermolecular Parallel KIE Experiment with Amide 1a and 1a-ßd_2

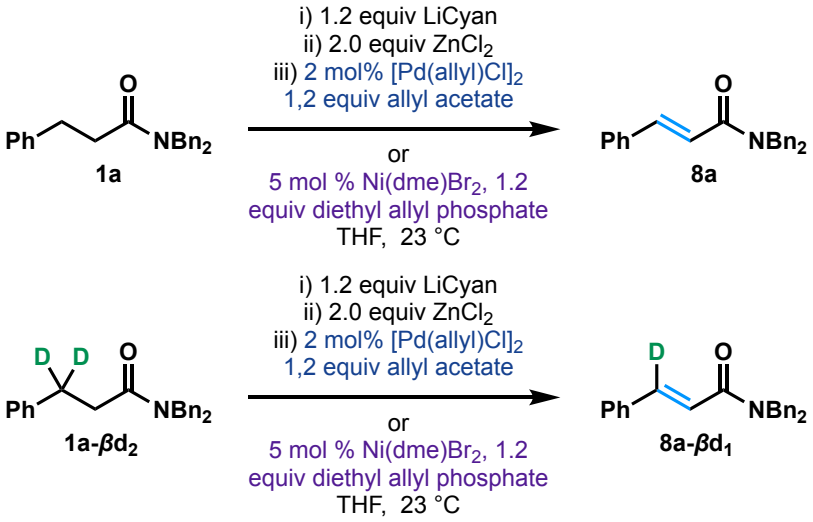

To a –40 °C solution of CyanH (62 mg, 0.24 mmol, 1.2 equiv) in THF (2.0 mL, 0.1 M) was added *n*-BuLi (2.5 M in hexanes, 0.096 mL, 0.24 mmol, 1.2 equiv). The reaction quickly became opaque and was stirred for 1 hour, forming a pale-yellow mixture. Amide **1a** (66 mg, 0.20 mmol, 1.0 equiv) or **1a-ß*d*$_2$** (66 mg, 0.20 mmol, 1.0 equiv) and 1,3,5-trimethoxybenzene (11.2 mg, 0.067 mmol, 0.67 equiv) in THF (1.0 mL) were added, and the reaction was stirred for 30 min at 0 °C. $ZnCl_2$ (0.5 M in THF, 0.80 mL, 0.40 mmol, 2.0 equiv) was added and stirred for 30 min at 0 °C. A solution of $[Pd(allyl)Cl]_2$ (0.73 mg, 0.0020 mmol, 0.010 equiv) and allyl acetate (26 µL, 0.24 mmol, 1.2 equiv) in THF (0.5 mL) or a solution of $[Ni(dme)Br_2]$ (3.1 mg, 0.010 mmol, 0.050 equiv) and diethyl allyl phosphate (41 µL, 0.24 mmol, 1.2 equiv) in THF (0.5 mL) was next added. The reaction mixture was warmed to ambient temperature. 0.5 mL aliquots were removed sequentially which were separately quenched with sat. aq. NH_4Cl (1.0 mL) and diluted with EtOAc (1.0 mL). The organic layer was separated, and the aqueous layer was extracted with EtOAc (3 x 1.0 mL), washed with brine (5.0 mL), dried over anhydrous Na_2SO_4, filtered, and concentrated under reduced pressure by rotary evaporation. The yield was determined by ^{1}H NMR using 1,3,5-trimethoxybenzene as internal standard.

Figure S1. Pd-catalyzed intermolecular parallel KIE experiment with 1a and 1a-ßd$_2$

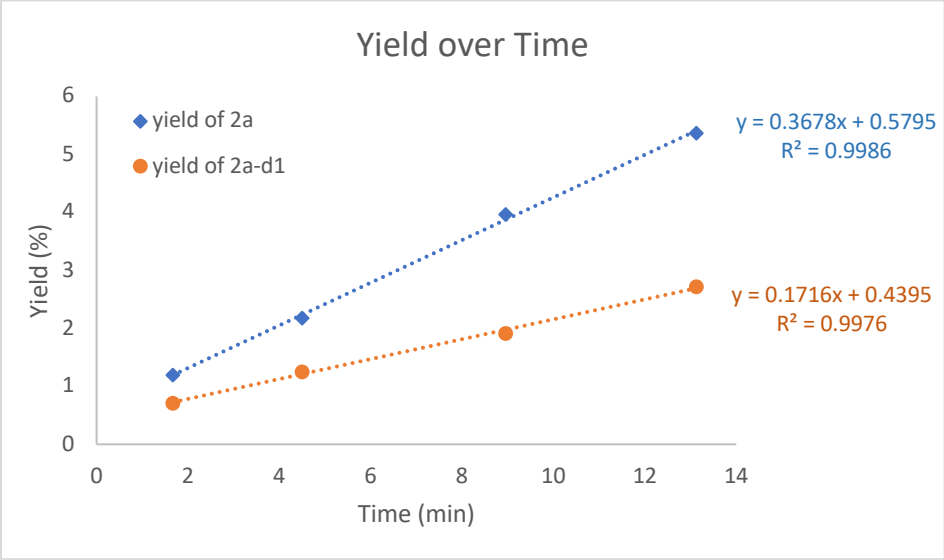

Kinetic isotope effect (KIE) = 0.3678/0.1716 = 2.1

Figure S2. Ni-catalyzed intermolecular parallel KIE experiment with 1a and 1a-ßd$_2$

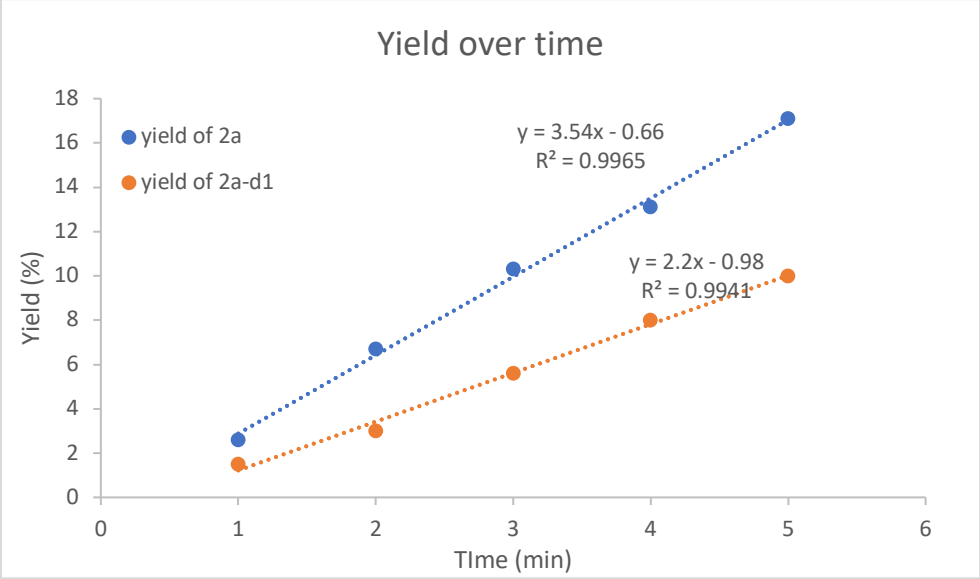

Kinetic isotope effect (KIE) = 3.54/2.2 = 1.6

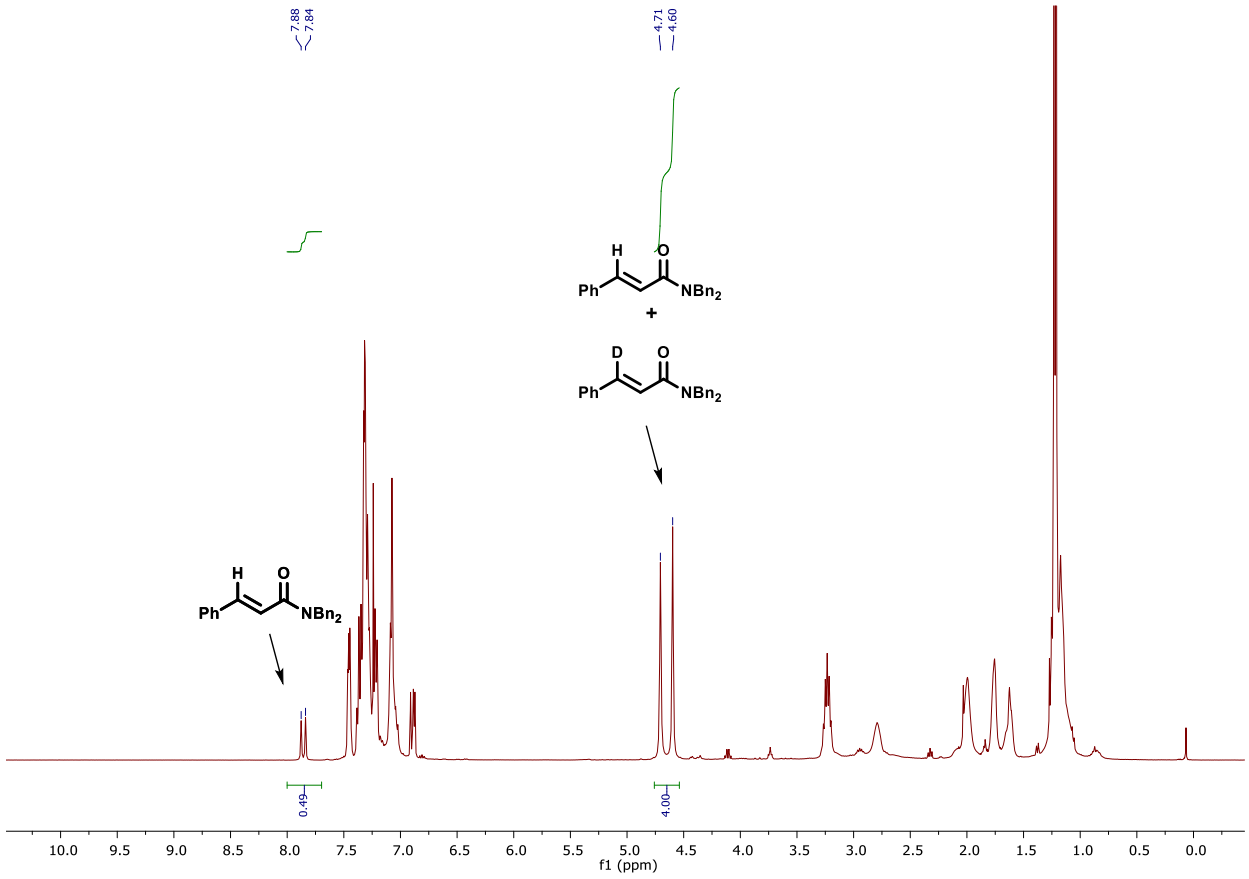

^{1}H NMR of the crude material following an aqueous workup from the intramolecular competition experiment using amide **1a-ßd$_1$** and Pd

Scheme S6: Intramolecular Competition Experiment with Amide 1a-ßd$_1$ and Ni

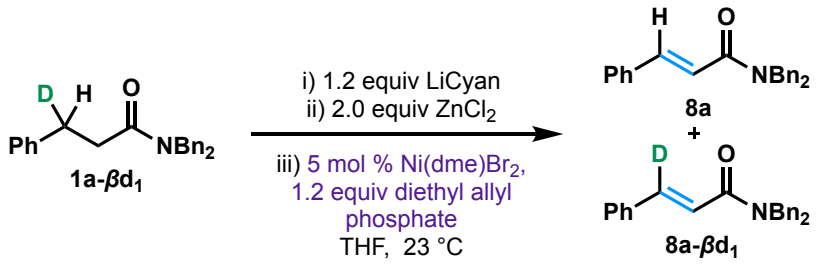

The reaction was prepared according to **General Procedure B** on a 0.2 mmol scale using amide **1a-ßd$_1$** as substrate and 5.0 mol % [Ni(dme)Br$_2$]. The reaction was warmed to ambient temperature. 0.5 mL aliquots were removed sequentially which were separately quenched with sat. aq. NH_4Cl (1.0 mL) and diluted with EtOAc (1.0 mL). Yield was determined by ^{1}H NMR using 1,3,5-trimethoxybenzene as internal standard.

Figure S3. Ni-catalyzed intramolecular competition experiment with 1a-ßd$_1$

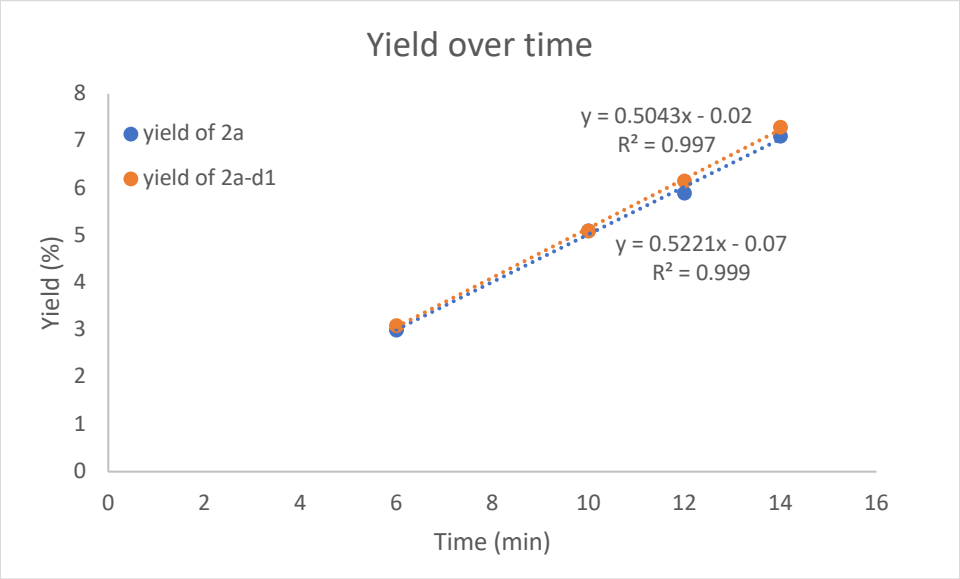

Kinetic isotope effect (KIE) = 0.5221/0.5043 = 1.0

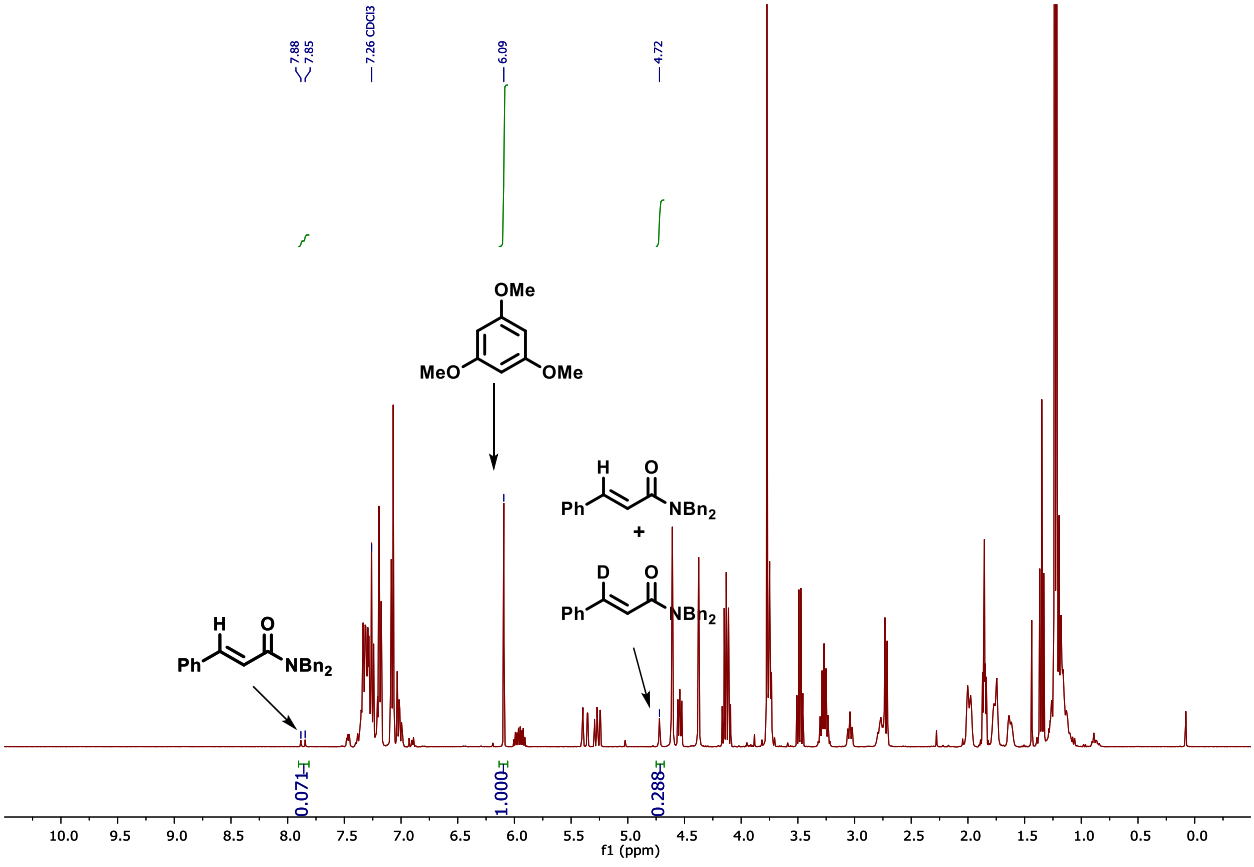

^{1}H NMR of the crude material following aqueous workup from the intramolecular competition experiment using amide **1a-ßd$_1$** and Ni after 14 min

Scheme S7: Intramolecular Competition Experiment with ester 1e-ßd_2 and Pd

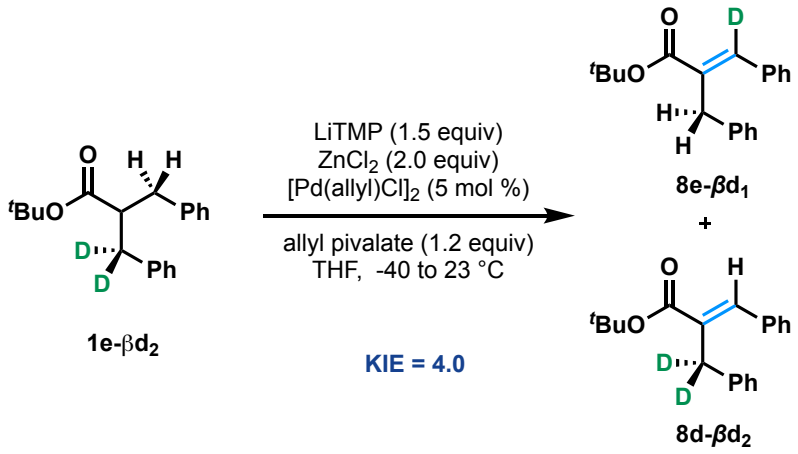

The reaction was prepared according to **General Procedure A** on a 0.1 mmol scale using ester **1e-*ß*d$_2$** as substrate, 1.5 equivalents of LiTMP and 5.0 mol % [Pd(allyl)Cl]$_2$. The reaction mixture was warmed to ambient temperature and quenched after 30 minutes with sat. aq. NH_4Cl (1.0 mL) and diluted with Et_2O (1.0 mL). The organic layer was separated, and the aqueous layer was extracted with Et_2O (3 x 1.0 mL), washed with brine (5.0 mL), dried over anhydrous Na_2SO_4, filtered, and concentrated under reduced pressure by rotary evaporation. The product ratio was determined by direct integration using the peaks of **8e-*ß*d$_2$** and **8e-*ß*d$_1$**. Dibromomethane was used as internal standard. The KIE = 4.0.

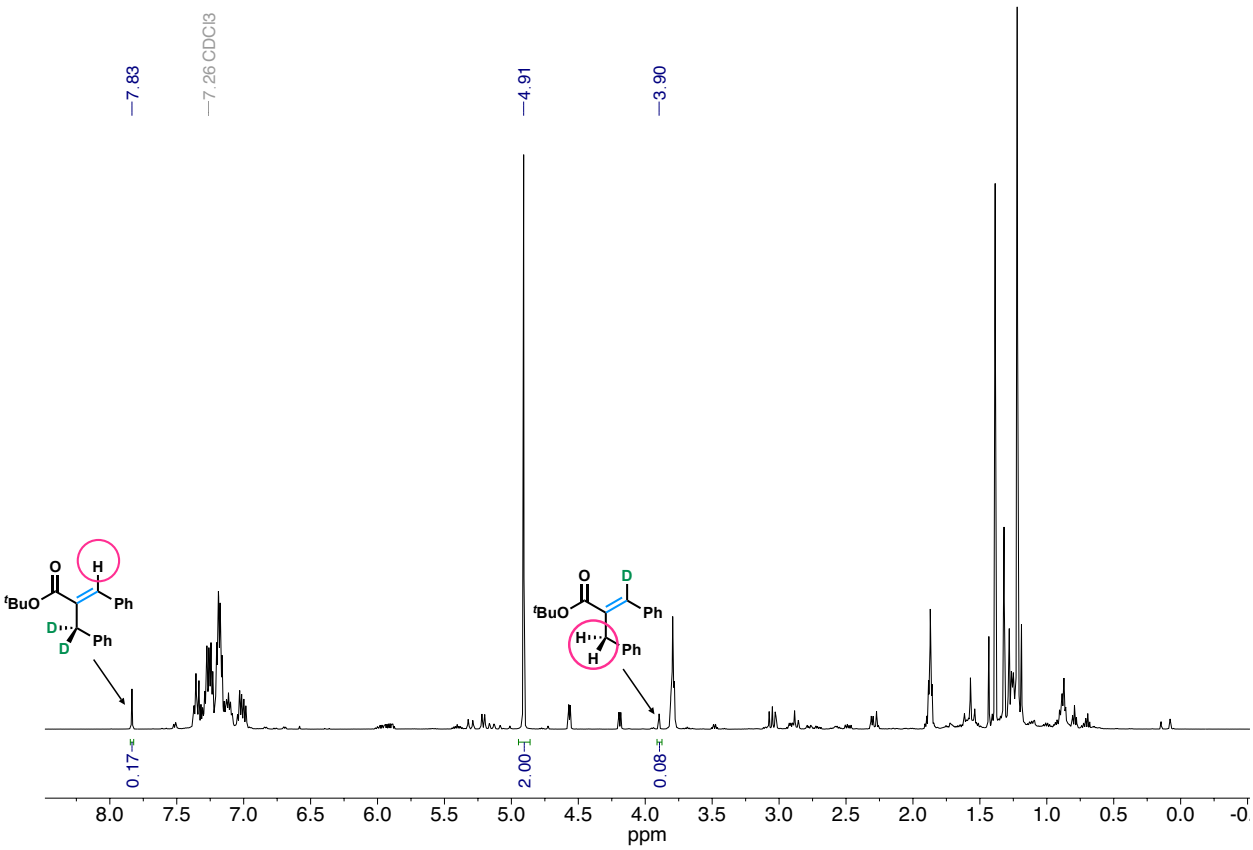

^{1}H NMR of the crude material following aqueous workup from the intramolecular competition experiment using ester **1e-*β*d$_2$** and Pd after 30 min using dibromomethane as an internal standard.

Experimental Procedures and Characterization Data for Base Studies

Scheme S8: D_2O Quench Directly after Deprotonation of 1a

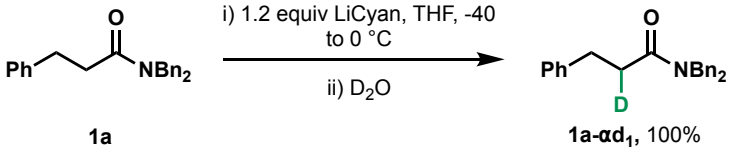

1a **1a-αd$_1$**, 100%

To a –40 °C solution of amide **1a** (33 mg, 0.10 mmol, 1.0 equiv) in THF (1 mL), *s*-BuLi or *n*-BuLi was added (0.12 mmol, 1.2 equiv). The reaction turned yellow immediately and was stirred for 1h before being quenched with D_2O (2.0 mL) and diluted with EtOAc (1.0 mL). The organic layer was separated, and the aqueous layer was extracted with EtOAc (3 x 1.0 mL). The organic layers were combined, washed with brine (5.0 mL), dried over anhydrous Na_2SO_4, filtered, and concentrated under reduced pressure by rotary evaporation. The yield was determined by ^1H NMR using 1,3,5-trimethoxybenzene as internal standard.

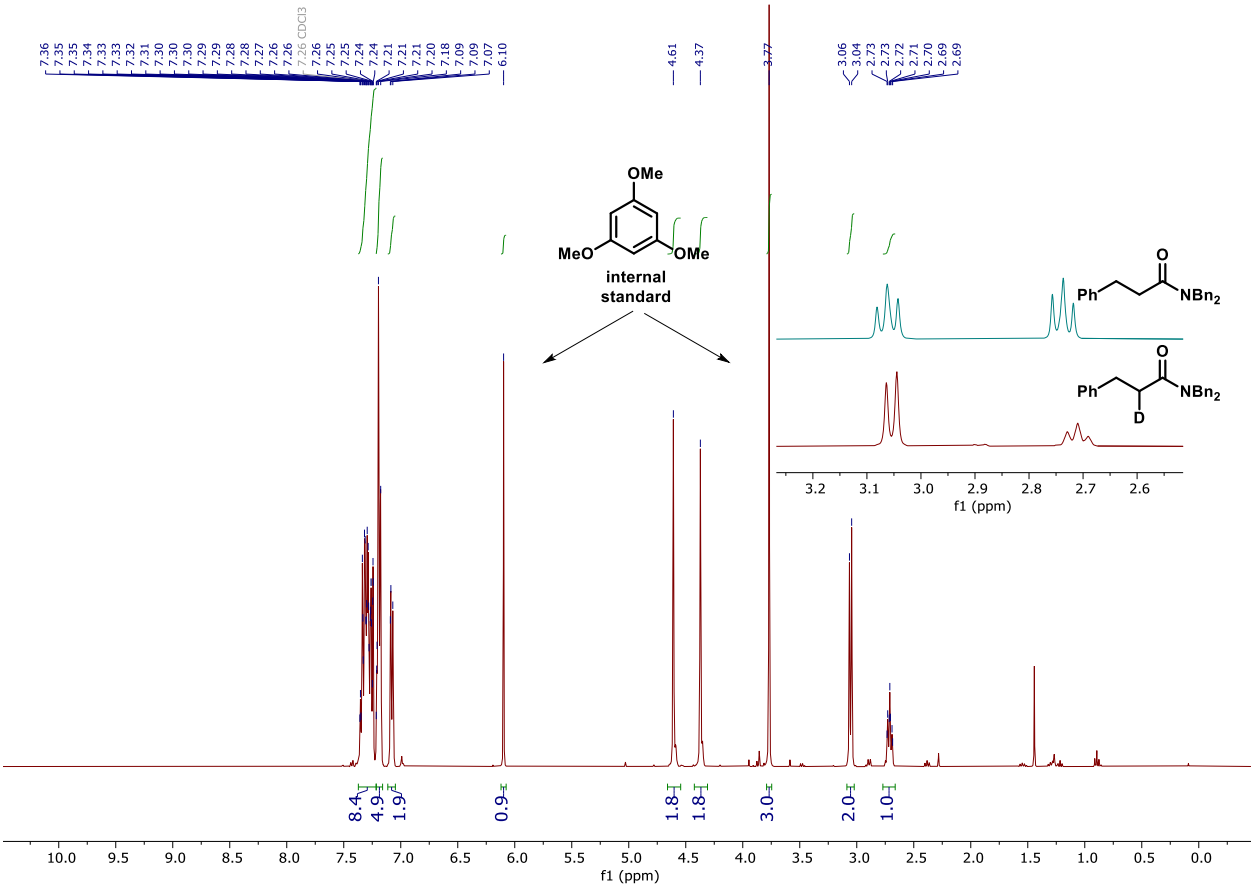

^{1}H NMR of the crude reaction mixture following a D_2O quench, aqueous workup, and comparison to amide **1a**

Table S1. Comparison of alkyl- and *N*-type-lithium bases.

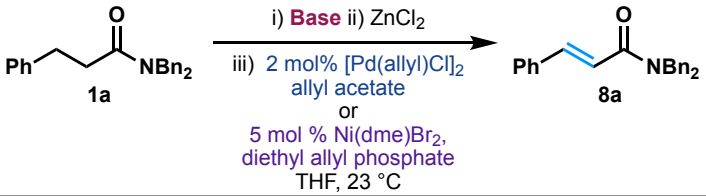

Entry	Base	Yield Pd[a]	Yield Ni[a]
1	^{s}BuLi	16% (42)	6% (32)
2	^{s}BuLi + CyanH	91% (95)	90% (94)
3	^{n}BuLi	2% (17)	57% (71)
4	^{n}BuLi + CyanH	95% (99)	86% (98)
5	^{n}BuLi + TMPH	81% (87)	65% (76)

[a]Conversion and yield were determined by ^{1}H-NMR spectroscopy using 1,3,5-trimethoxybenzene as internal standard.

Reactions with *s*-BuLi or *n*-BuLi:

To a –40 °C solution of amide **1a** (33 mg, 0.10 mmol, 1.0 equiv), *s*-BuLi or *n*-BuLi was added (0.12 mmol, 1.2 equiv). The reaction quickly turned yellow and was stirred for 1h. $ZnCl_2$ (0.5 M in THF, 0.4 mL, 0.2 mmol, 2.0 equiv) was added and the reaction was stirred for 30 min at 0 °C. A solution of $[Pd(allyl)Cl]_2$ (0.73 mg, 0.002 mmol, 0.02 equiv) and allyl acetate (13 µL, 0.12 mmol, 1.2 equiv) in THF (0.5 mL) or $[Ni(dme)Br_2]$ (3.1 mg, 0.010 mmol, 0.050 equiv) and diethyl allyl phosphate (41 µL, 0.24 mmol, 1.2 equiv) in THF (0.5 mL) was next added at 0 °C. The reaction mixture was warmed to ambient temperature. The reaction was stirred for 30 min then quenched with sat. aq. NH_4Cl (1.0 mL) and diluted with EtOAc (1.0 mL). The organic layer was separated, and the aqueous layer was extracted with EtOAc (3 x 1.0 mL). The organic layers were combined, washed with brine (5.0 mL), dried over anhydrous Na_2SO_4, filtered, and concentrated under reduced pressure by rotary evaporation. The yield was determined by ^{1}H NMR using 1,3,5-trimethoxybenzene as internal standard.

Reactions with the combination of CyanH and *s*-BuLi or *n*-BuLi:

Prepared according to **General Procedure B** using either *s*-BuLi or *n*-BuLi as the alkyl lithium**.**

Figure S4: A Time Track Experiment - Comparison of LiCyan and LiTMP over time in the Pd- and Ni-catalyzed Dehydrogenation of 1a

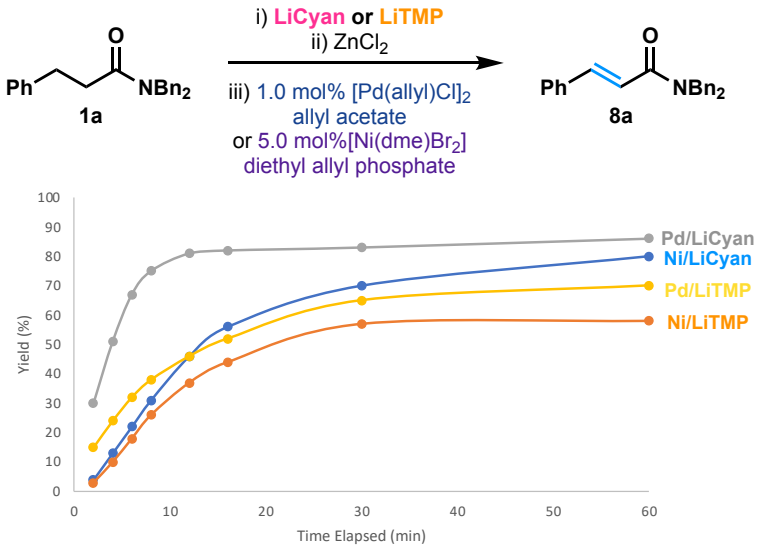

Reactions with LiTMP were prepared according to **General Procedure A** on a 0.2 mmol scale using 1.0 mol % $[Pd(allyl)Cl]_2$ or 5 mol % $Ni(dme)Br_2$. Reactions with LiCyan were prepared according to **General Procedure B** on a 0.2 mmol scale using 1.0 mol % $[Pd(allyl)Cl]_2$ or 5 mol % $Ni(dme)Br_2$. 1,3,5-trimethoxybenzene (11.2 mg, 0.067 mmol, 0.67 equiv) was added to each reaction via the amide/THF solution. All reactions were run in parallel. The reaction mixtures were warmed to ambient temperature. 0.5 mL aliquots were removed after 2, 4, 6, 8, 12, 16, 30, and 60 minutes, which were separately quenched with sat. aq. NH_4Cl (1.0 mL) and diluted with EtOAc (1.0 mL). The organic layer was separated, and the aqueous layer was extracted with EtOAc (3 x 1.0 mL). The organic layers were combined, washed with brine (5.0 mL), dried over anhydrous Na_2SO_4, filtered, and concentrated under reduced pressure by rotary evaporation. Yields were determined by ^1H NMR using 1,3,5-trimethoxybenzene as internal standard.

^{1}H-NMR Studies on the Coordination of CyanH and Cyan imine to [Pd(allyl)Cl]$_2$ in d$_8$-THF

The CyanH + [Pd(allyl)Cl]$_2$ and Cyan imine + [Pd(allyl)Cl]$_2$ NMR samples were prepared by addition of CyanH (25.9 mg, 1.0 equiv, 0.1 mmol) or Cyan imine (25.7 mg, 1.0 equiv, 0.1 mmol) to [Pd(allyl)Cl]$_2$ (18.3 mg, 0.50 equiv, 0.05 mmol) in 0.60 mL THF-d_8.

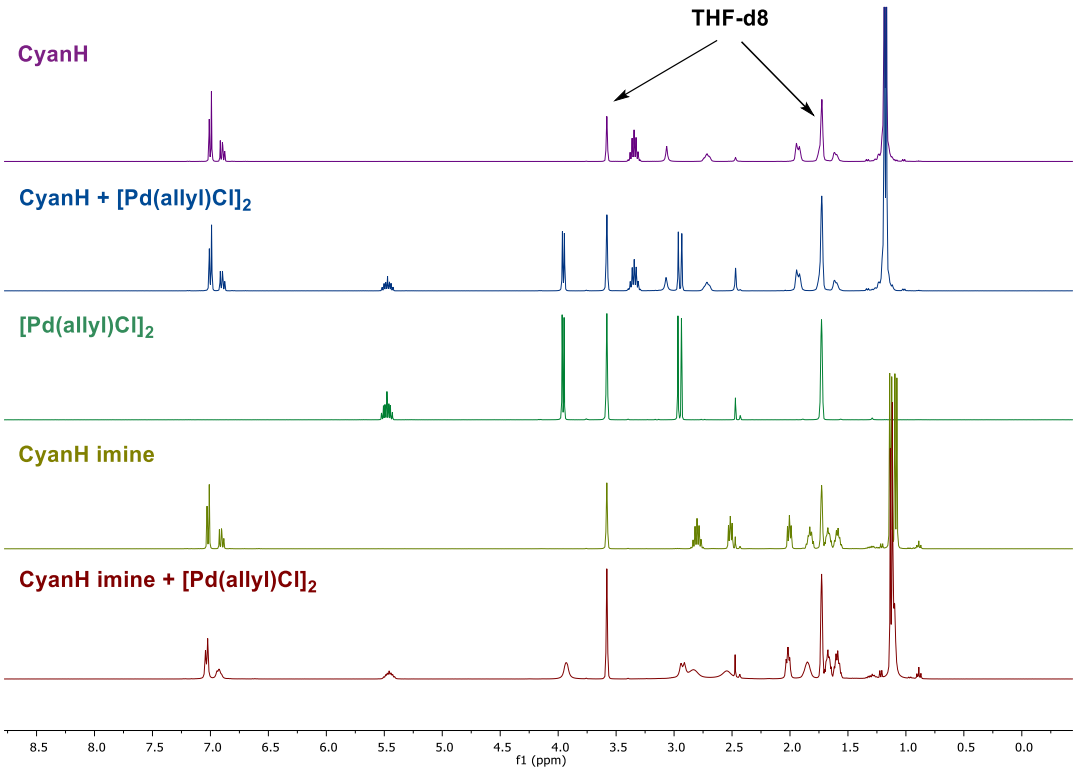

$^{13}C\{^{1}H\}$-NMR of Cyan imine + $[Pd(allyl)Cl]_2$

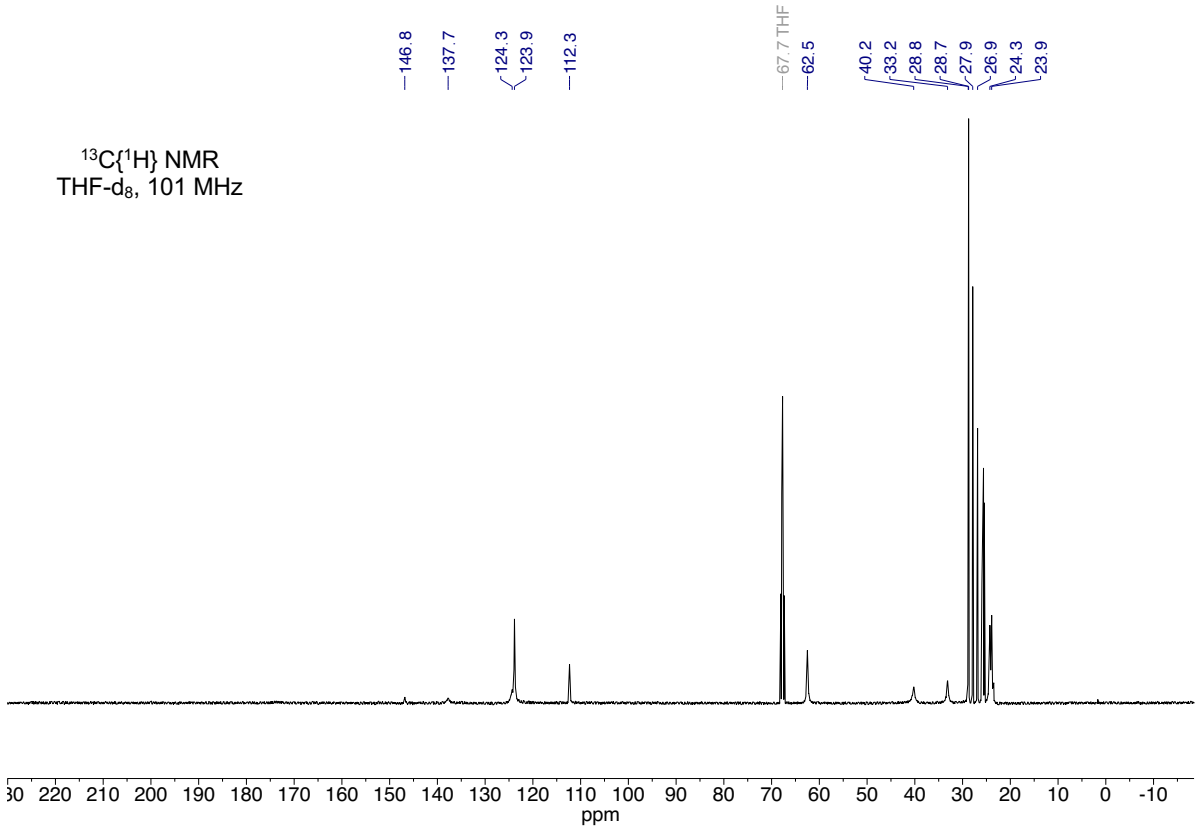

Scheme S9: Dehydrogenation of LiCyan with Stoichiometric [Pd(allyl)Cl]$_2$, Catalytic [Pd(allyl)Cl]$_2$, or Catalytic [Ni(dme)Br$_2$]

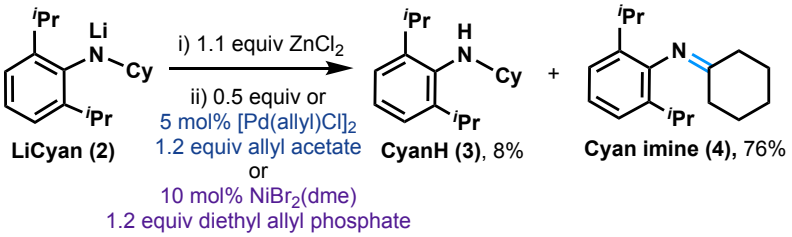

Stoichiometric [Pd(allyl)Cl]$_2$: To a –40 °C solution of CyanH (**3**) (51.9 mg, 0.20 mmol, 1.0 equiv) in THF (1.0 mL, 0.1 M) was added *n*-BuLi (2.5 M in hexanes, 80 µL, 0.20 mmol, 1.0 equiv). and the resulting solution was stirred for 1 hour until the solution was opaque and pale-yellow. $ZnCl_2$ (0.5 M in THF, 0.44mL, 0.022 mmol, 1.1 equiv) was added and stirred for 30 min more at 0 °C. $[Pd(allyl)Cl]_2$ (36.5 mg, 0.10 mmol, 0.50 equiv) was added and the reaction darkened immediately. The reaction was stirred for 30 min at ambient temperature then quenched with sat. aq. NH_4Cl (2.0 mL). Yield was determined by ^{1}H NMR using 1,3,5-trimethoxybenzene as internal standard.

Catalytic [Pd(allyl)Cl]$_2$ or [Ni(dme)Br$_2$]: To a –40 °C solution of CyanH (**3**) (51.9 mg, 0.20 mmol, 1.0 equiv) in THF (1.0 mL, 0.1 M) was added *n*-BuLi (2.5 M in hexanes, 80 µL, 0.20 mmol, 1.0 equiv). and the resulting solution was stirred for 1 hour until the solution was opaque and pale-yellow. $ZnCl_2$ (0.5 M in THF, 0.44mL, 0.022 mmol, 1.1 equiv) was added and stirred for 30 min more at 0 °C. The $[Pd(allyl)Cl]_2$ (3.6 mg, 0.010 mmol, 0.050 equiv) and allyl acetate (26 µL, 0.24mmol, 1.2 equiv) stock solution or $[Ni(dme)Br_2]$ (6.2 mg, 0.020 mmol, 0.10 equiv) and diethyl allyl acetate (42 µL, 0.24mmol, 1.2 equiv) was added. The reaction was stirred for 30 min at ambient temperature before quenching with sat. aq. NH_4Cl (2.0 mL). Yield was determined by ^{1}H NMR using 1,3,5-trimethoxybenzene as internal standard.

***N*-(2,6-Diisopropylphenyl)cyclohexanimine (Cyan imine, 4)**

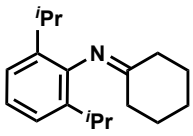

To a –40 °C solution of CyanH (**3**) (51.9 mg, 0.20 mmol, 1.0 equiv) in THF (1.0 mL, 0.1 M) was added *n*-BuLi (2.5 M in hexanes, 80 µL, 0.20 mmol, 1.0 equiv). and the resulting solution was stirred for 1 hour until the solution was opaque and pale-yellow. $ZnCl_2$ (0.5 M in THF, 0.44mL, 0.022 mmol, 1.1 equiv) was added and stirred for 30

min more at 0 °C. $[Pd(allyl)Cl]_2$ (36.5 mg, 0.10 mmol, 0.50 equiv) was added and the reaction darkened immediately. The reaction was stirred for 1 hour at ambient temperature then quenched with sat. aq. NH_4Cl (2.0 mL) and diluted with EtOAc (2.0 mL). The organic layer was separated, and the aqueous layer was extracted with EtOAc (3 x 1.0 mL). The organic layers were combined, washed with brine (5.0 mL), dried over anhydrous Na_2SO_4, filtered, and concentrated under reduced pressure by rotary evaporation. The resulting solid was then recrystallized from hexanes at –78 °C, affording the title compound **4** as an off-white solid (45 mg, 88%). **^{1}H NMR** (400 MHz, $CDCl_3$) δ 7.12 – 7.05 (m, 2H), 7.03 (dd, J = 8.8, 6.2 Hz, 1H), 2.81 (hept, J = 6.9 Hz, 2H), 2.56 (t, J = 6.4 Hz, 2H), 2.02 (t, J = 6.4 Hz, 2H), 1.92 – 1.81 (m, 2H), 1.73 – 1.62 (m, 2H), 1.60 (m, 2H), 1.14 (dd, J = 6.9, 2.2 Hz, 12H); **^{13}C{^{1}H} NMR** (101 MHz, $CDCl_3$) δ 174.0, 145.5, 137.0, 123.3, 122.9, 38.9, 32.0, 27.9, 27.7, 26.7, 25.9, 23.6, 23.4. The characterization data matches previous literature reports.[11]

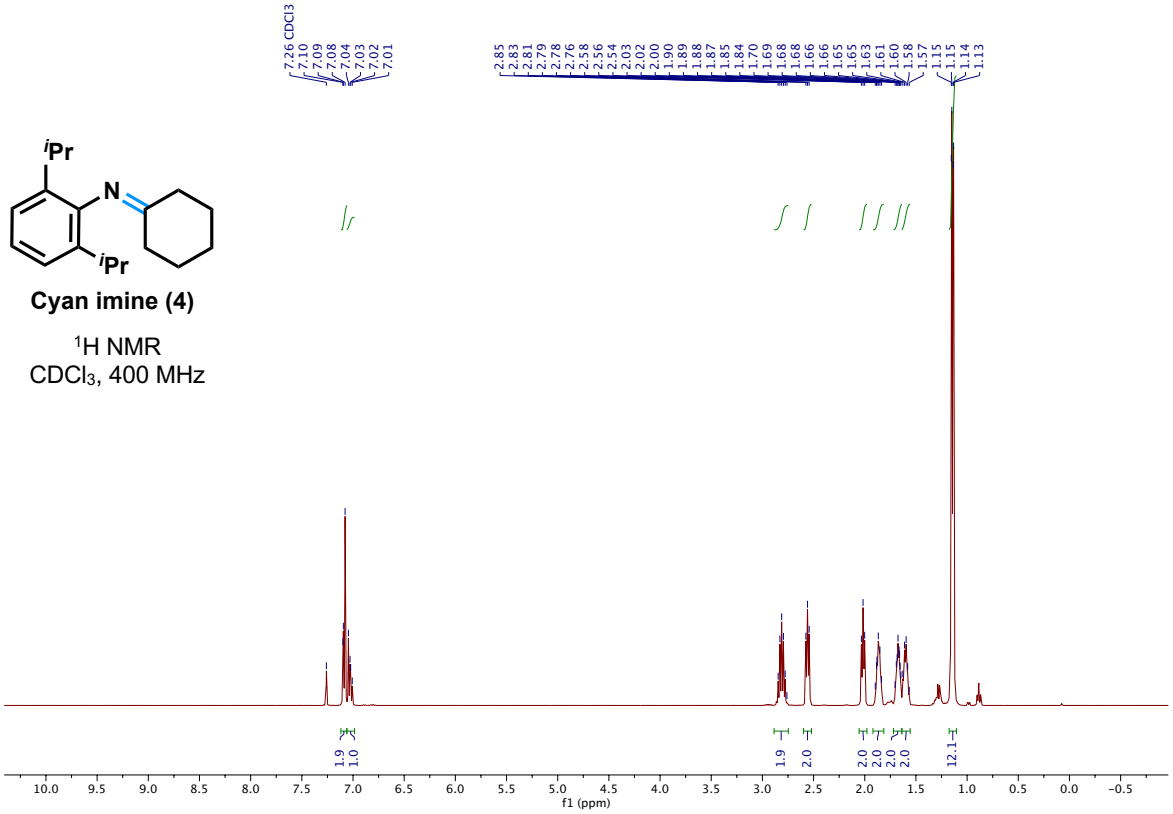

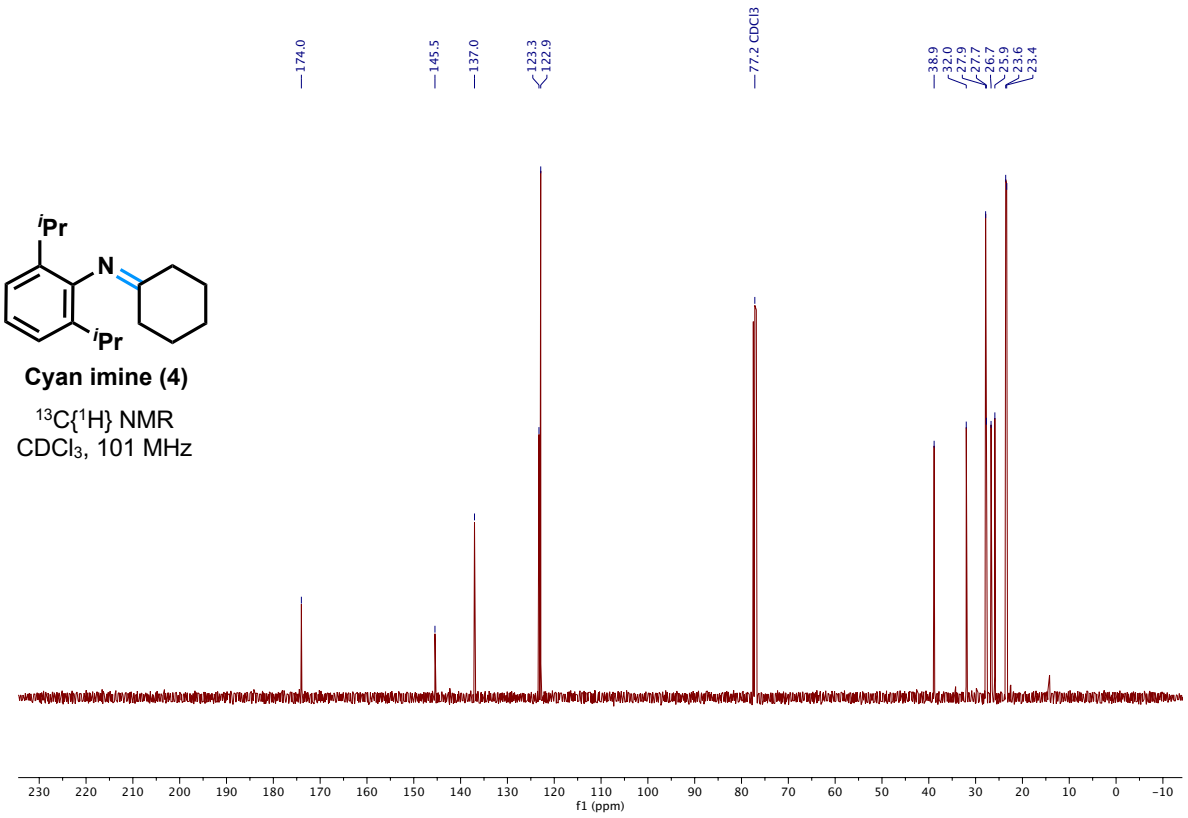

Scheme S10: CyanH, Cyan Imine, and LiCyan as Ligands in Pd- and Ni-Catalyzed Dehydrogenation of 1a

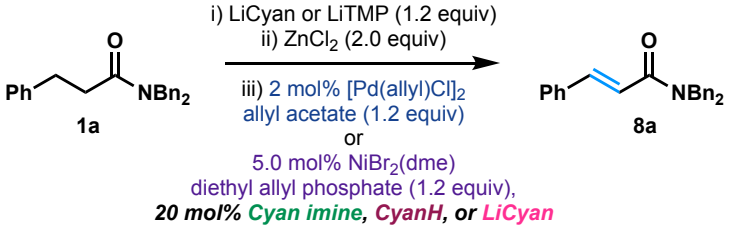

To a –40 °C solution of TMPH (41 µL, 0.24 mmol, 1.2 equiv) in THF (2.0 mL, 0.1 M) was added *n*-BuLi (2.5 M in hexanes, 0.096 mL, 0.24 mmol, 1.2 equiv). The reaction was stirred for 1h forming a light-yellow mixture. Amide **1a** (66 mg, 0.20 mmol, 1.0 equiv) and 1,3,5-trimethoxybenzene (11.2 mg, 0.067 mmol, 0.67 equiv) in THF (0.5 mL) were added and the reaction was stirred for 30 min at 0 °C. $ZnCl_2$ (54.5 mg, 0.40 mmol, 2.0 equiv) in THF (1 mL) was added and stirred for 30 min at 0 °C.

CyanH (**3**) (10.4 mg, 0.040 mmol, 0.20 equiv), Cyan imine (**4**) (10.3 mg, 0.04 mmol, 0.2 equiv), or LiCyan (**2**) (0.040 mmol, 0.20 equiv) in THF (0.1mL) was added to a solution of $[Pd(allyl)Cl]_2$ (1.4 mg, 0.004 mmol, 0.02 equiv) and allyl acetate (26 µL, 0.24 mmol, 1.2 equiv) in THF (0.5 mL) or $Ni(dme)Br_2$ (3.1 mg, 0.010 mmol, 0.050 equiv) and diethyl allylphosphate (41 µL, 0.24 mmol, 1.2 equiv) in THF (0.5 mL) and stirred for 15 minutes. The catalyst solution was then added to the reaction, which was warmed to ambient temperature. 0.5 mL aliquots were removed sequentially which were separately quenched with sat. aq. NH_4Cl (1.0 mL) and diluted with EtOAc (1.0 mL). Yield was determined by ^1H NMR using 1,3,5-trimethoxybenzene as internal standard.

Experimental Procedures and Results for Unsaturated Product Inhibition Studies

Preparation of (*Z*)-*N*,*N*-dibenzyl-3-phenylacrylamide (8a-*Z*):

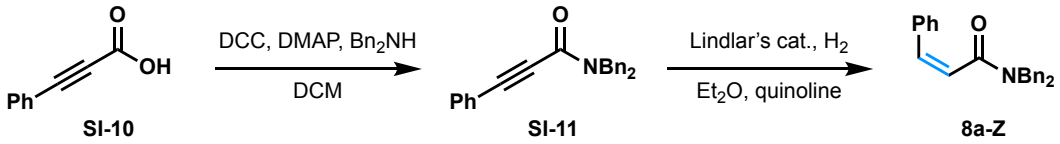

To a solution of DCC (1.56 g, 7.6 mmol, 1.1 equiv) and DMAP (85.4 mg, 0.7 mmol, 0.1 equiv) in CH_2Cl_2 (34 mL, 0.2 M) was added **SI-10** (1.0 g, 7.1 mmol, 1.0 equiv) followed by dibenzylamine (1.5 mL, 7.8 mmol, 1.1 equiv). The reaction was stirred at ambient temperature for 24h. The mixture was filtered through a silica plug and eluted with EtOAc. The eluent was concentrated under reduced pressure by rotary evaporation. Purification by flash column chromatography on silica gel (1:7 EtOAc/hexanes) afforded **SI-11** (703 mg, 32%) as a white solid. **R_f**: 0.48 (1:4 EtOAc:hexanes); **^{1}H NMR** (400 MHz, CDCl3): δ 7.52 – 7.50 (m, 2H), 7.43 – 7.30 (m, 11 H), 7.28 – 7.27 (m, 1 H), 7.26 – 7.25 (m, 1 H), 4.76 (s, 2H), 4.57 (s, 2H); **^{13}C{^{1}H} NMR** (151 MHz, $CDCl_3$): δ155.2, 136.4, 136.2, 132.6, 130.3, 129.1, 128.9, 128.7, 128.6, 128.1, 127.9, 127.8, 120.5, 91.0, 81.8, 51.6, 46.5; **IR** (cm^{-1}): 3027, 2937, 2214, 1624, 1420, 1190, 687; **ESI-HRMS (m/z)**: $[M+H]^+$ calc'd for $C_{23}H_{20}NO^+$: 326.1545; found: 326.1545. The characterization data matches previous literature reports.[12]

To a solution of **SI-11** (304 mg, 0.92 mmol, 1.0 equiv) in Et_2O (34 mL, 0.027 M) was added quinoline (153 µL, 0.47 mmol, 1.4 equiv) followed by Lindlar's catalyst (219 mg, 10 mol% Pd). A hydrogen balloon was attached to the flask and the flask was put under vacuum until the solvent began to bubble, then the hydrogen balloon was opened to the flask. This process was repeated 3 times, then the reaction was carefully monitored by TLC analysis for the consumption of starting material. After 30 min the hydrogen balloon was removed and N_2 was bubbled into the reaction for 5 min. The mixture was passed through a silica plug and eluted with Et_2O. The eluent was concentrated under reduced pressure by rotary evaporation. Purification by flash column chromatography on silica gel (6-10% EtOAc/hexanes) afforded **8a-*Z*** (293 mg, 97%) as a white solid. **R_f**: 0.36 (1:12 EtOAc:hexanes); **^{1}H NMR** (400 MHz, $CDCl_3$): δ 7.38 – 7.27 (m, 10H), 7.25 – 7.21 (m, 3H), 7.07 – 7.05 (m, 2H), 6.67 (d, J = 12.8 Hz, 1H), 6.17 (d, J = 12.8 Hz, 1H), 4.59 (s, 2H), 4.38 (s, 2H); **^{13}C{^{1}H} NMR** (151 MHz, $CDCl_3$): δ 169.3, 136.6, 136.3, 135.4, 134.1, 129.2,

129.0, 128.70, 128.66, 128.63, 127.8, 127.7, 127.3, 123.2, 50.6, 46.8; **IR** (cm^{-1}): 3026, 1605, 1423, 1218, 1080, 690; **ESI-HRMS (m/z)**: $[M+H]^+$ calc'd for $C_{23}H_{22}NO^+$: 328.1701; found: 328.1701. The characterization data matches previous literature reports.[13]

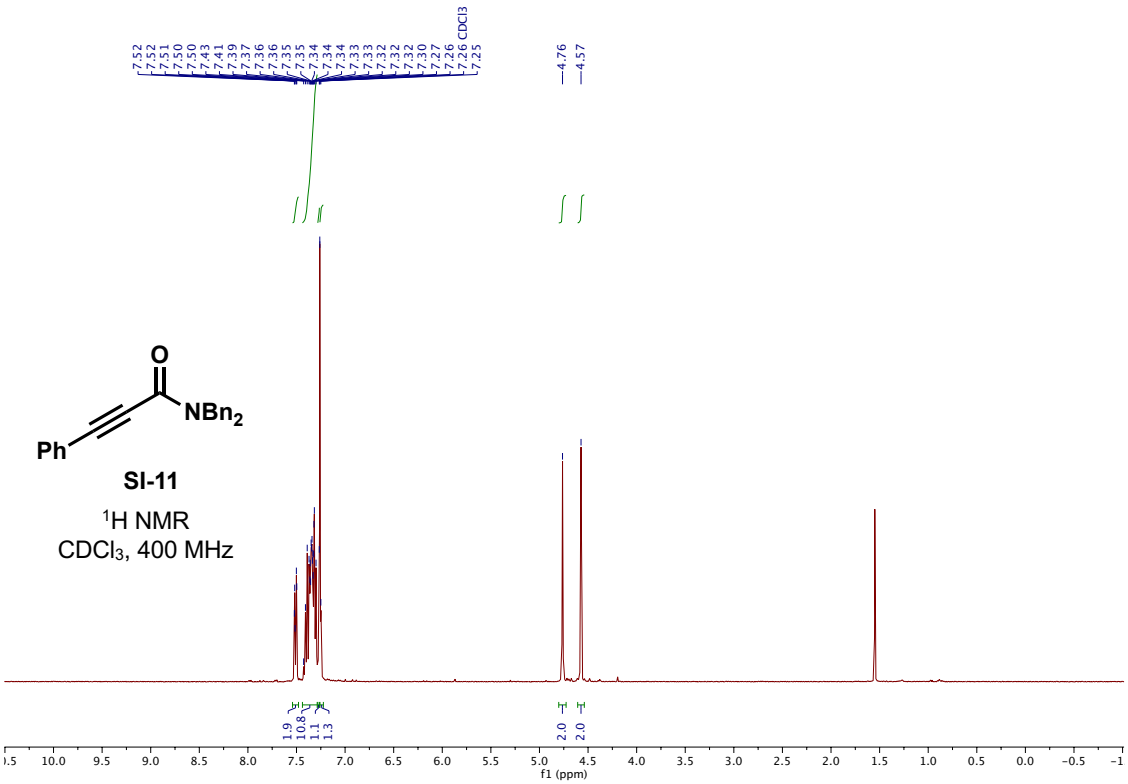

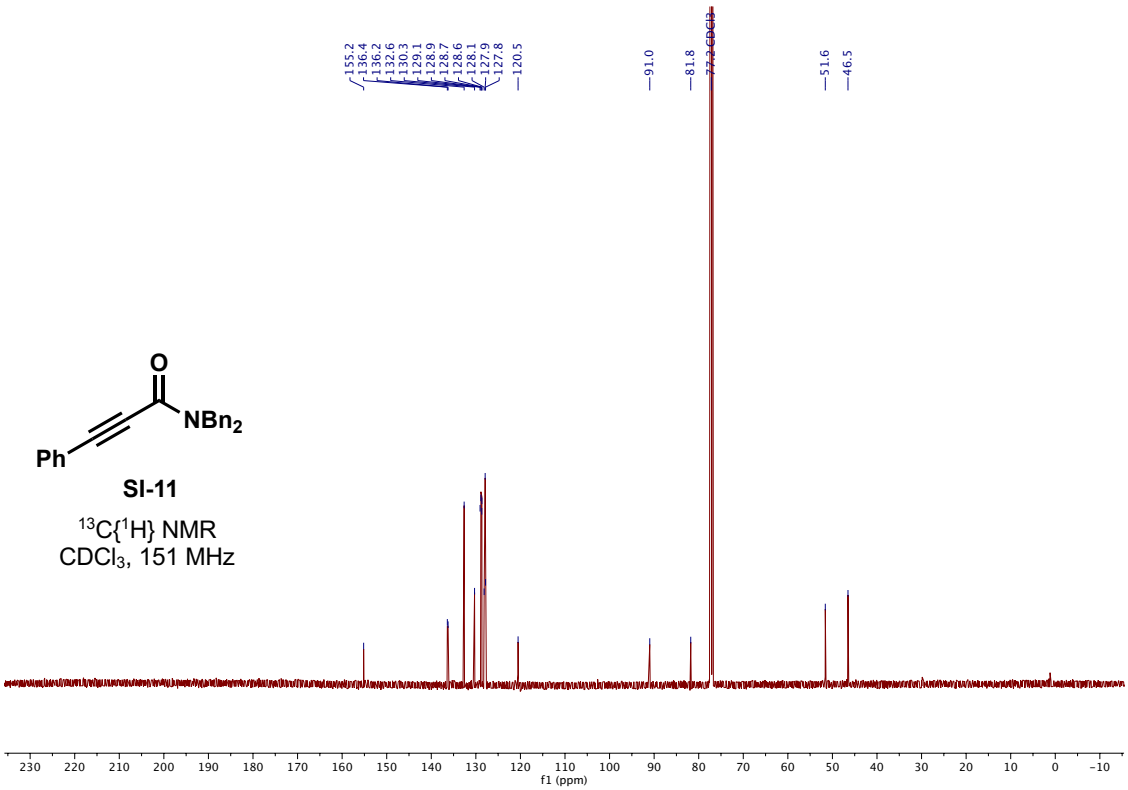

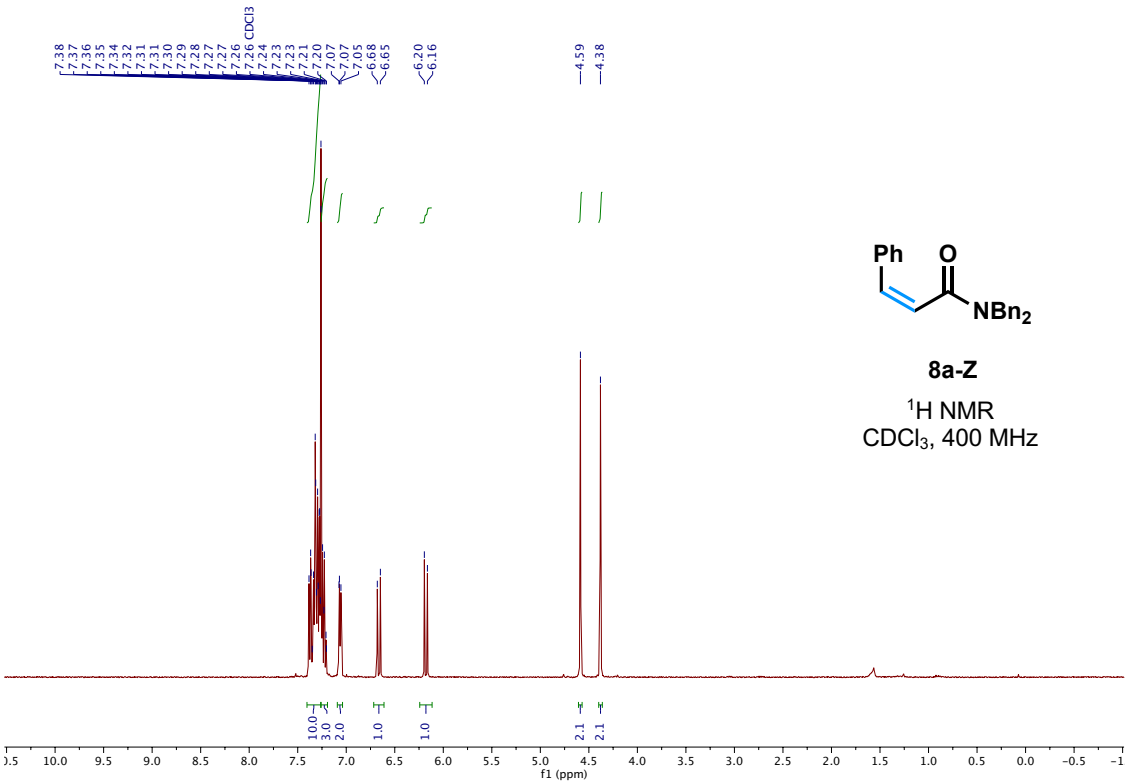

8a-Z

^{1}H NMR
$CDCl_3$, 400 MHz

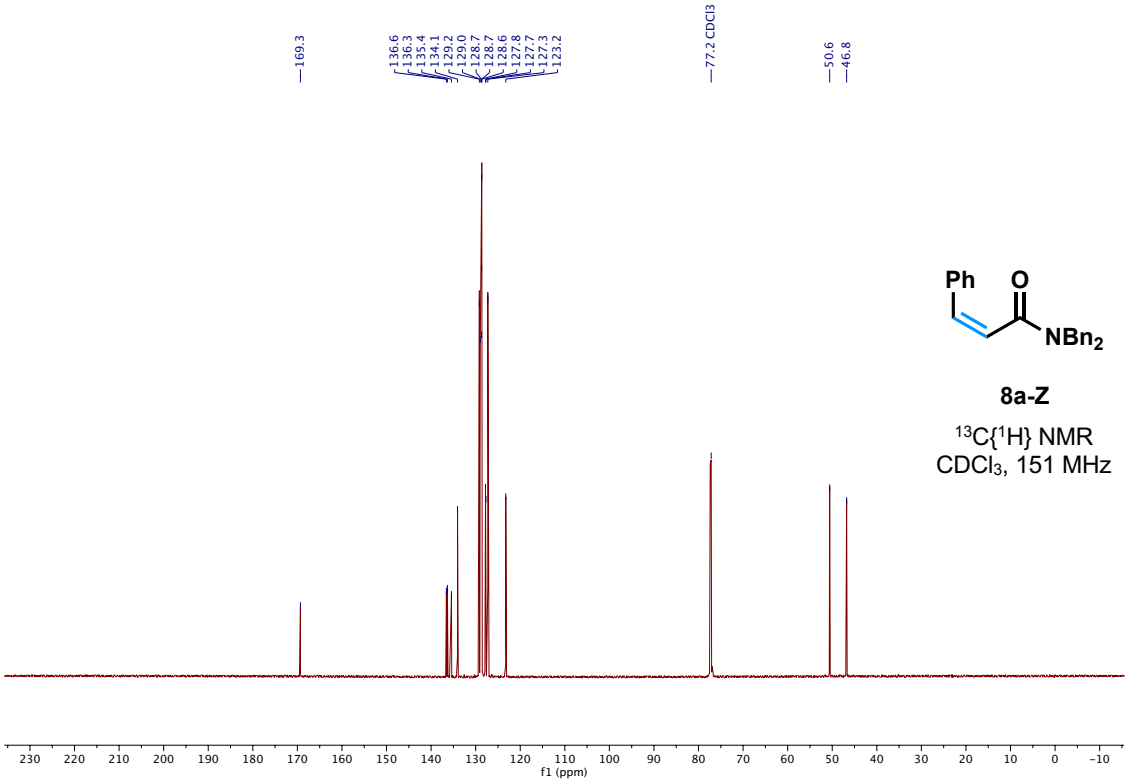

8a-Z

$^{13}C\{^{1}H\}$ NMR
$CDCl_3$, 151 MHz

Dehydrogenation with the Addition of Unsaturated Products

To a –40 °C solution of CyanH (31 mg, 0.12 mmol, 1.2 equiv) in THF (1.0 mL, 0.10 M) was added *n*-BuLi (2.5 M in hexanes, 48 µL, 0.12 mmol, 1.2 equiv). The reaction quickly became opaque and was stirred for 1h forming a pale-yellow mixture. Amide **1a** (33 mg, 0.10 mmol, 1.0 equiv) was added and the reaction was stirred for 30 min at 0 °C. $ZnCl_2$ (0.5 M in THF, 0.40 mL, 0.20 mmol, 2.0 equiv) was added and stirred for 30 min more at 0 °C. Alkene **8a-*Z*** (16 mg, 0.050 mmol, 0.50 equiv) or alkene **8a-ß*d*$_1$** was added (16 mg, 0.050 mmol, 0.50 equiv) in THF (0.5 mL) followed by a solution of $[Pd(allyl)Cl]_2$ (0.73 mg, 0.0020 mmol, 0.020 equiv) and allyl acetate (13 µL, 0.12 mmol, 1.2 equiv) in THF (0.5 mL) or a solution of $[Ni(dme)Br_2]$ (3.1 mg, 0.010 mmol, 0.050 equiv) and diethyl allyl phosphate (41 µL, 0.24 mmol, 1.2 equiv) in THF (0.5 mL) was next added. The reaction mixture was warmed to ambient temperature. After stirring for 1h, the reaction was quenched with sat. aq. NH_4Cl (1.0 mL) and diluted with EtOAc (1.0 mL). The yields were determined by ^1H NMR using 1,3,5-trimethoxybenzene as internal standard.

Figure S5. Addition of unsaturated products inhibits dehydrogenation.

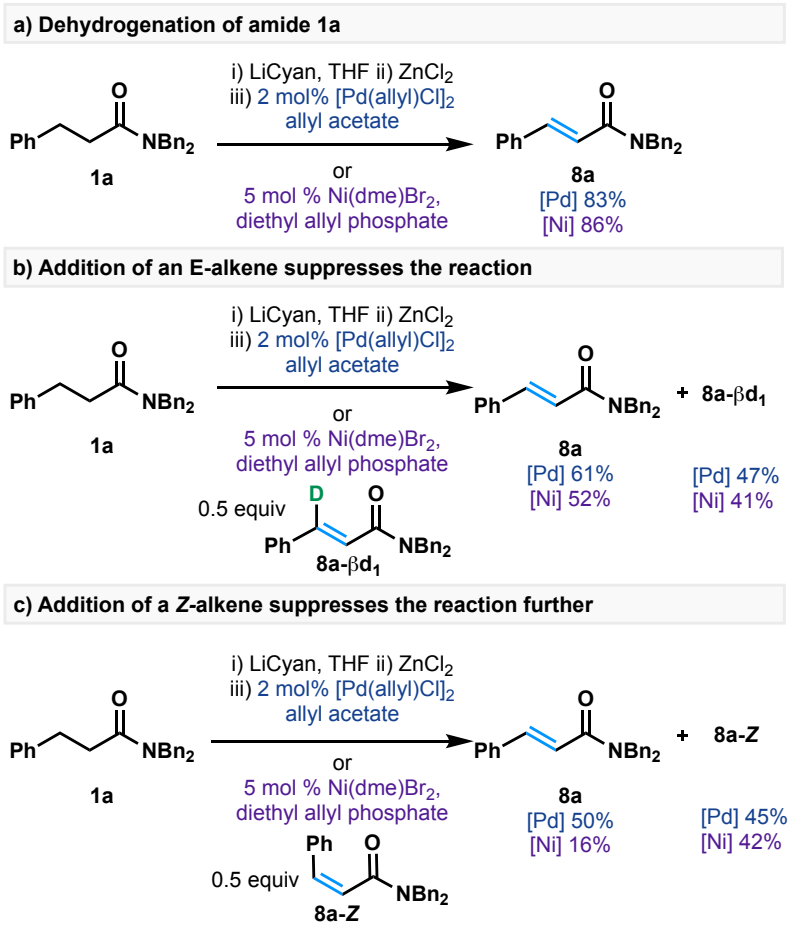

Dehydrogenation of acyclic amides yields exclusively *E*-alkene products (Figure SI-5a). β-deuterated **8a-βd$_1$** (0.5 equiv.) was added under standard dehydrogenation conditions (Figure SI-5b), which resulted in a depreciated yield of **8a** and significant recovery of **8a-βd$_1$** for both Ni- and Pd-catalyzed reactions. In the second experiment, *cis*-alkene **8a-*Z*** was added under standard dehydrogenation conditions (Figure SI-5c) and the yield of **8a** was suppressed even further for both Ni- and Pd-catalyzed reactions. These experiments indicate that product inhibition occurs at a greater extent for Ni than Pd, and that *Z*-alkenes lead to more significant inhibition.

Scheme S11: Dehydrogenation with Increasing Amounts of Cinnamonitrile 8c

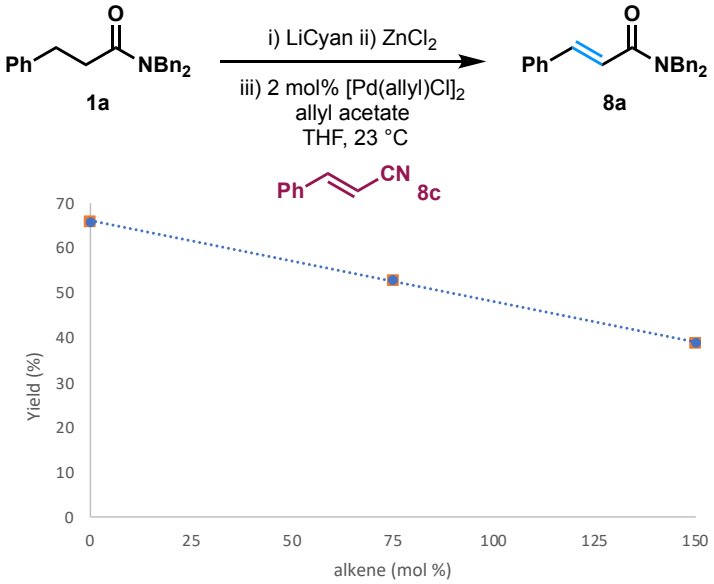

To a –40 °C solution of CyanH (31 mg, 0.12 mmol, 1.2 equiv) in THF (1.0 mL, 0.1 M) was added *n*-BuLi (2.5 M in hexanes, 48 µL, 0.12 mmol, 1.2 equiv). The reaction quickly became opaque and was stirred for 1h forming a pale-yellow mixture. Amide **1a** (36 mg, 0.1 mmol, 1.0 equiv) was added and the reaction was stirred for 30 min at 0 °C. $ZnCl_2$ (0.5 M in THF, 0.4 mL, 0.2 mmol, 2.0 equiv) was added and stirred for 30 min more at 0 °C. Varying amounts of cinnamyl nitrile (**8c**) were added to parallel reactions (0.0, 0.75, 1.5 equiv). A solution of $[Pd(allyl)Cl]_2$ (0.73 mg, 0.002 mmol, 0.02 equiv) and allyl acetate (13 µL, 0.12 mmol, 1.2 equiv) in THF (0.5 mL) was added. The reaction mixture was warmed to ambient temperature. After stirring for 10 min the reactions were quenched with sat. aq. NH_4Cl (1.0 mL) and diluted with EtOAc (1.0 mL). The yields were determined by ^1H NMR using 1,3,5-trimethoxybenzene as internal standard.

Table S2. Unsaturated nitriles inhibit dehydrogenation.

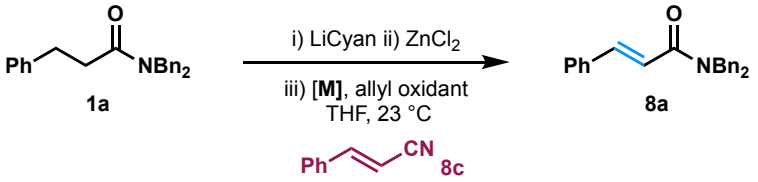

Entry	Amount of 8c (equiv)	Yield Pd[a,b]	Yield Ni[a,c]
1	0	66%	86%
2	0.75	53%	0%
3	1.5	39%	0%

[a] Yields and conversions were determined by ^{1}H-NMR spectroscopy using 1,3,5-trimethoxybenzene as an internal standard. [b] 2 mol% $[Pd(allyl)Cl]_2$ and 1.2 equiv allyl acetate were used. [c] 5 mol% $Ni(dme)Br_2$ and 1.2 equiv diethyl allyl phosphate were used.

Inhibition Studies. We hypothesized that other reaction components that coordinate to the metal center, such as electron-deficient alkenes, would decrease the rate of dehydrogenation. We conducted a series of experiments that show that alkene products are inhibitors (Figure SI-5). To determine the extent of product inhibition, an experiment was performed in which variable amounts of cinnamyl nitrile **8c** were added to Ni- and Pd-catalyzed dehydrogenation reactions (Table SI-2). For the Pd-catalyzed reaction, an inverse linear relationship was observed between the yield of **8a** and the amount of **8c** added to the reaction.

For the Ni-catalyzed reaction, severe inhibition was observed, with the product not observed when 0.8 or 1.5 equivalents of cinnamyl nitrile were added. Similar results are observed in the presence of other electron-deficient olefins, as shown in Figure SI-5. These results suggest that Ni is more prone to product inhibition than Pd, which is consistent with the earlier observations that rate suppression is observed to a greater extent with Ni than Pd with the addition of Cyan imine (**4**), presence of peripheral basic functionality on the substrate, or added salts (Table SI-7). Coordination could result in decreased rates due to blocking an open site for β-hydride elimination or suppressing oxidative addition through stabilization of Ni(0). Additionally, no allylation product was detected from these experiments.

Experimental Procedures, Results, and Characterization Data for *α*-Allylation Product 9a

Scheme S12: Reactions with *N*-(tert-butyl)-2,6-diisopropylaniline (SI-12) as base

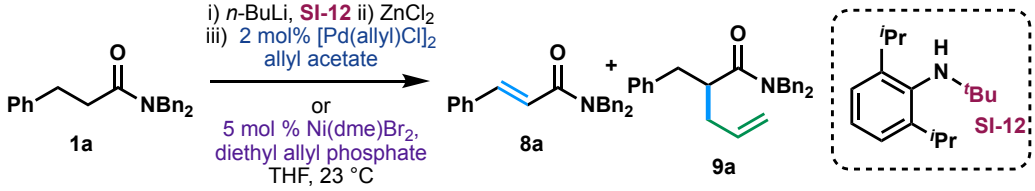

This reaction was run according to **General Procedure B**, using *N*-(tert-butyl)-2,6-diisopropylaniline (**SI-12**) (56 mg, 0.24 mmol, 1.2 equiv) instead of CyanH (**3**). The reaction was performed on a 0.2 mmol scale. The reaction mixture was warmed to ambient temperature and stirred for 1h. The reaction was quenched with sat. aq. NH_4Cl (1.0 mL) and diluted with EtOAc (1.0 mL). Yield was determined by ^1H NMR using 1,3,5-trimethoxybenzene as internal standard.

Scheme S13: Reactions with *N*-(tert-butyl)-2,6-diisopropylaniline (SI-12) as base and oxabicyclo[3.2.1]oct-3-ene-7-one (SI-13) as oxidant

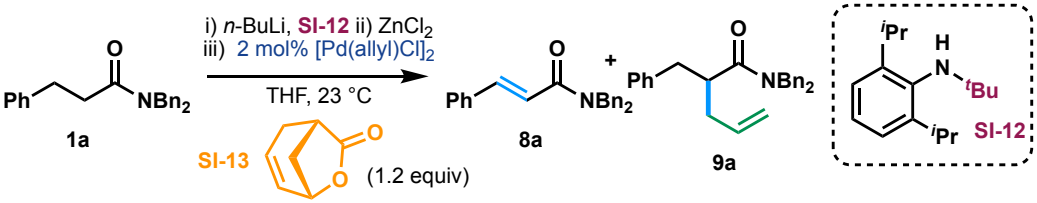

This reaction was run according to **General Procedure B**, using *N*-(tert-butyl)-2,6-diisopropylaniline (**SI-12**) (56 mg, 0.24 mmol, 1.2 equiv) instead of CyanH and 6-oxabicyclo[3.2.1]oct-3-ene-7-one (**SI-13**) (29.8 mg, 0.24 mmol, 1.2 equiv) instead of allyl acetate. The reaction was performed on a 0.2 mmol scale. The reaction mixture was warmed to ambient temperature and stirred for 1h. The reaction was quenched with sat. aq. NH_4Cl (1.0 mL) and diluted with EtOAc (1.0 mL). Yield was determined by ^1H NMR using 1,3,5-trimethoxybenzene as internal standard.

Table S3. Bulkier bases promote reductive elimination pathways.

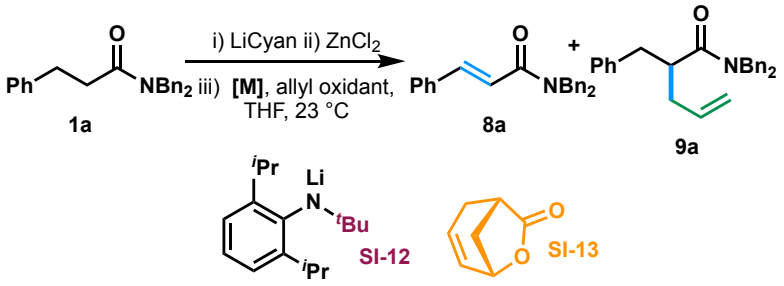

Entry	Variation	Yield 2a[a]	Yield 9a[a]	[M], allyl oxidant
1	none	83%	0%	2.5 mol% $[Pd(allyl)Cl]_2$ allyl acetate
2	SI-12	41%	42%	
3	SI-12 + SI-13	84%	0%	
4	none	92%	0%	5 mol % $Ni(dme)Br_2$ diethyl allyl phosphate
5	SI-12	29%	0%	

[a]Yield was determined by ^{1}H–NMR using 1,3,5-trimethoxybenzene as internal standard.

For the Ni- and Pd-catalyzed dehydrogenation of amide **1a**, the more hindered *tert*-butyl aniline (**SI-12**, compared to CyanH) was inefficient (Table SI-3).[9] Under Pd-catalyzed conditions this base (**SI-12**) generated a 1:1 mixture of dehydrogenation (**8a**) and allylation (**9a**) products (Table SI-3, entry 2). However, the yield could be recovered by using a bicyclic allyl-oxidant **SI-13** with bulky aniline **SI-12** (entry 3). Under Ni-catalyzed conditions when **SI-12** was used as base, a significant decrease in the yield was observed, but the allylation product was not detected (entry 5). This result is consistent with our previous findings that Ni is much less likely to promote allylation. The Ni-catalyzed conditions are less likely to lead to reductive elimination and afford the allylation product.

N,N,2-Tribenzylpent-4-enamide (9a)

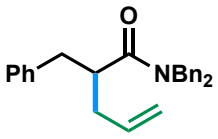

9a was prepared according to **General Procedure B** using *N*-(tert-butyl)-2,6-diisopropylaniline (**SI-12**) (56 mg, 0.24 mmol, 1.2 equiv) instead of CyanH (**3**). The reaction was performed on a 0.2 mmol scale. The reaction was stirred for 1 hour at ambient temperature then quenched with sat. aq. NH_4Cl (2.0 mL) and diluted with EtOAc (2.0 mL). The organic layer was separated, and the aqueous layer was extracted with EtOAc (3 x 1.0 mL). The organic layers were combined, washed with brine (5.0 mL), dried over anhydrous Na_2SO_4, filtered, and concentrated under reduced pressure by rotary evaporation. Purification by

flash column chromatography on silica gel (hexanes/EtOAc = 5:1) afforded **9a** as a white solid (29.6. mg, 40%). **R_f**: 0.29 (20% Et_2O/hexanes); **^{1}H NMR** (400 MHz, $CDCl_3$): δ 7.30 – 7.22 (m, 9H), 7.14 – 7.10 (m, 4H), 6.91 – 6.89 (m, 2H), 5.74 (ddt, *J* = 9.9, 7.3, 7.2 Hz, 1H), 5.09 (d, *J* = 17.2 Hz, 1H), 5.05 (d, *J* = 10.3 Hz, 1H), 4.63 (d, *J* = 14.6 Hz, 1H), 4.49 (d, *J* = 14.6 Hz, 1H), 3.08 – 2.96 (m, 2H), 2.81 (dd, *J* = 12.1, 4.3 Hz, 1H) 2.50 (ddd, *J* = 13.7, 6.9, 6.9 Hz, 1H), 2.31 (ddd, *J* = 13.7, 6.9, 6.9 Hz, 1H); **^{13}C{^{1}H} NMR** (101 MHz, $CDCl_3$): δ 175.3, 139.9, 137.4, 136.7, 135.6, 129.4, 128.9, 128.6, 128.5, 127.5, 127.3, 126.5, 126.4, 117.5, 49.6, 48.6, 44.2, 38.9, 37.7; **IR** (cm^{-1}): 3032, 2922, 1628, 1446, 1201, 915, 695; **ESI-HRMS (m/z)**: $[M+H]^+$ calc'd for $C_{26}H_{28}NO^+$: 370.2165; found: 370.2169. **m.p.** 78-79 °C

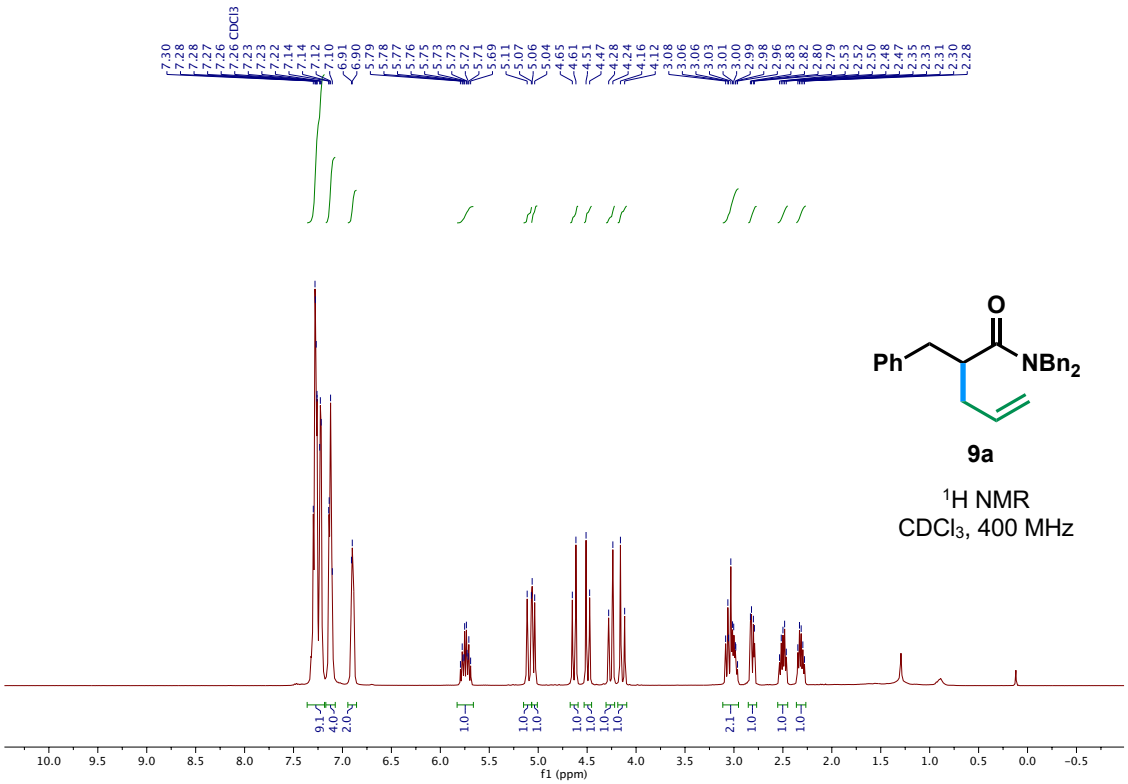

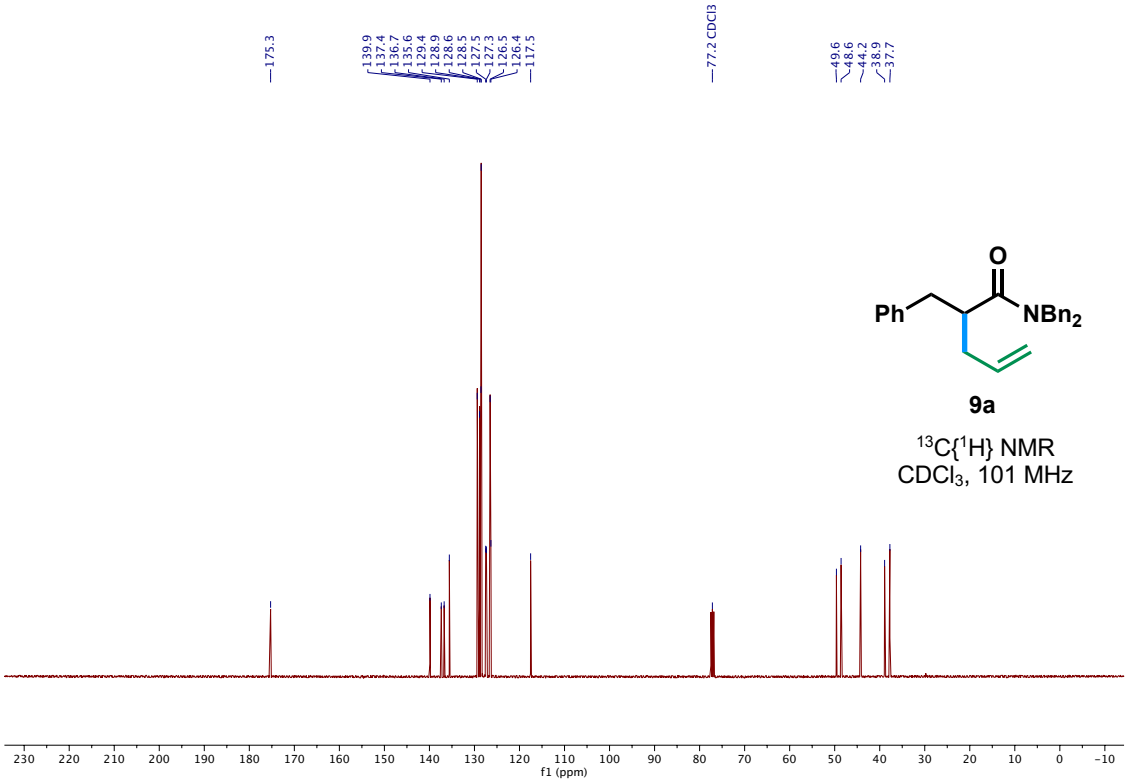

Table S4. Zn enolates and Ni catalysts suppress allylation.

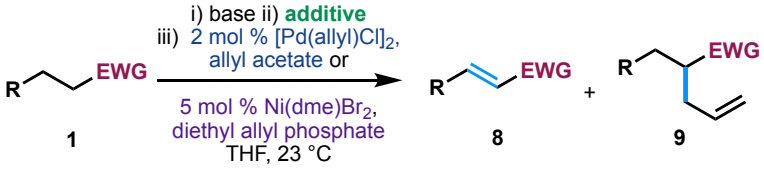

Entry	Catalyst/Base	Substrate	Additive	Yield 8[a]	Yield 9[a]
1	$[Pd(allyl)Cl]_2$	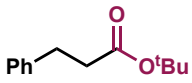	—	20%	20%
2	LiTMP		$ZnCl_2$	90%	n.d.
3	$Ni(dme)Br_2$	**1d**	—	n.d.	3%
4	LiCyan		$ZnCl_2$	86%	n.d.
5	$[Pd(allyl)Cl]_2$	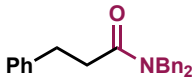	—	n.d.	n.d.
6	LiCyan		$ZnCl_2$	71%	n.d.
7[b]	$Ni(dme)Br_2$	**1a**	—	6%	13%
8[b]	LiCyan		$ZnCl_2$	90%	n.d.
9[c]	$[Pd(allyl)Cl]_2$	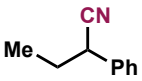	—	n.d.	80%
10[c]	LiCyan		$ZnCl_2$	11%	16%
11[b,d]	$Ni(dme)Br_2$	**1b**	—	n.d.	60%
12[b,d]	LiCyan		$ZnCl_2$	81%	n.d.

[a] Yields and conversions were determined by ^{1}H-NMR spectroscopy using 1,3,5-trimethoxybenzene as an internal standard. [b] 10 mol% Ni was used. [c] Diethyl allyl phosphate was used as oxidant instead of allyl acetate. [d] Reactions were run at 80 ºC in an oil bath.

For the dehydrogenation of ester **1d**, α-allylation was observed in the absence of $ZnCl_2$ (Table SI-4, entries 1 & 3), and at a greater extent for Pd than for Ni. However, in the presence of $ZnCl_2$, allylation was not observed with Ni or Pd (entries 2 & 4). For amide **1a**, allylation is not observed under Pd-catalyzed conditions without $ZnCl_2$, but is observed to a small extent under Ni-catalyzed conditions (entries 5 & 7). As we previously observed, addition of $ZnCl_2$ to the Ni- or Pd-catalyzed dehydrogenation of **1a** completely eradicated the allylation side-product (entries 6 & 8). For α-aryl nitrile **1b**, without the addition of $ZnCl_2$, allylation byproducts are observed in high yield (entries 9 & 11), which we attribute to its increased nucleophilicity. However, with the addition of $ZnCl_2$, allylation is observed to a lesser extent under Pd-catalyzed conditions and is eliminated under Ni-catalyzed conditions (entries 10 & 12).

In addition, allyl-Ni species are less electrophilic than allyl-Pd species due to differential

electronegativity[14] and are therefore less prone to yielding allylation products formed via outer-sphere attack.[15] Thus, the use of Ni along with $ZnCl_2$ inhibits undesired allylation and promotes dehydrogenation. It should be noted that this trend runs counter to the generally invoked expectation of Ni to favor C–C bond formation over β-hydride elimination for alkylnickel intermediates.

Results for the Evaluation of Zn Sources, Oxidants and Counterion Effects

Scheme S14: Dehydrogenation of 1a-ßd$_2$ using Cinnamyl Acetate (Ox 1) as Oxidant

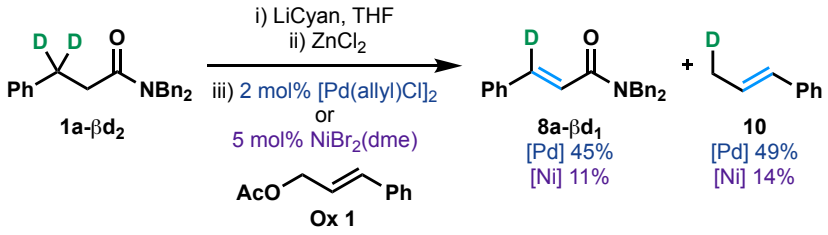

To a –40 °C solution of CyanH (31 mg, 0.12 mmol, 1.2 equiv) in THF (1.0 mL, 0.1 M) was added *n*-BuLi (2.5 M in hexanes, 48 µL, 0.12 mmol, 1.2 equiv). The reaction quickly became opaque and was stirred for 1h forming a pale-yellow mixture. Amide **1a-ßd$_2$** (33 mg, 0.1 mmol, 1.0 equiv) was added and the reaction was stirred for 30 min at 0 °C. $ZnCl_2$ (0.5 M in THF, 0.40 mL, 0.2 mmol, 2.0 equiv) was added and stirred for 30 min more at 0 °C. A solution of $[Pd(allyl)Cl]_2$ (0.73 mg, 0.002 mmol, 0.02 equiv) and cinnamyl acetate (20 µL, 0.12 mmol, 1.2 equiv) in THF (0.5 mL) was prepared and added to the reaction. The reaction mixture was warmed to ambient temperature. After stirring for 1h the reaction was quenched with sat. aq. NH_4Cl (1.0 mL) and diluted with EtOAc (1.0 mL). The yield of **8a-ßd$_1$** and **10** were determined by ^{1}H NMR using 1,3,5-trimethoxybenzene as internal standard. ^{13}C NMR and GC–MS were used to confirm the presence of **3** which matches previously reported literature values.[16]

Table S5. Effects of Zn sources

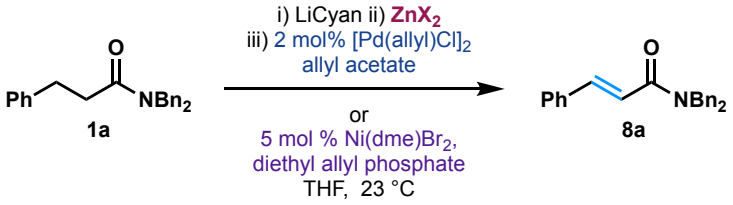

Entry	Zn Source	Yield (Pd)[a]	Yield (Ni)[a]
1	$ZnCl_2$	83% (89)	86% (88)
2	$ZnBr_2$	85% (90)	76% (85)
3	$Zn(OAc)_2$	5% (16)	5% (50)
4	$Zn(OTf)_2$	3% (69)	0% (2)
5	$Zn(TMP)_2$	trace (<5)	0% (<5)
6	none	3% (83)	1% (88)

[a]Yield and conversion were determined by ^{1}H NMR spectroscopy using 1,3,5-trimethoxybenzene as an internal standard.

Table S6. Effects of Allyl-Oxidants

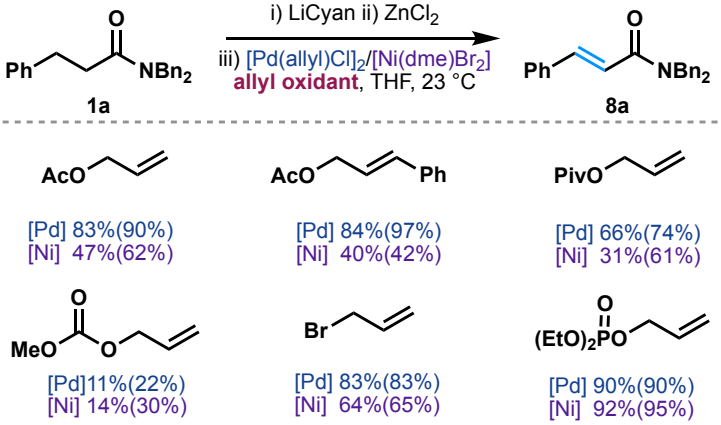

[a]Yield and conversion were determined by ^{1}H NMR spectroscopy using 1,3,5-trimethoxybenzene as an internal standard.

Table S7. Salts Effects

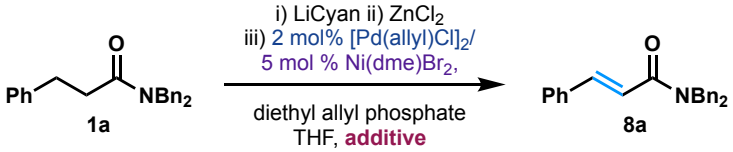

Entry	Additives	Yield (Pd)[a]	Yield (Ni)[a]
1	none	91% (91)	90% (95)
2	LiOAc (1.0 equiv)	83% (89)	41% (50)
3	LiO^tBu (1.0 equiv)	67% (92)	24% (88)
4	LiOH (1.0 equiv)	84% (86)	68% (70)
5	LiCl (1.0 equiv)	78% (80)	4% (21)
6	LiCl (3.0 equiv)	13% (75)	0% (0)

[a]Yield and conversion were determined by ^{1}H NMR spectroscopy using 1,3,5-trimethoxybenzene as an internal standard.

During early studies, we suspected that the solutions of *n*-BuLi used to generate LiCyan might be a source of potential reproducibility issues. Older or improperly stored bottles will contain a higher buildup of LiOH from *n*-BuLi being quenched by moisture. Different batches of *n*-BuLi also have variable amounts of lithium halide. Additionally, the concentrations of LiOH and LiCl may vary for solutions of *n*-BuLi in different solvents and from different suppliers. In order to test the effects of these potential lithium salt contaminants, we performed the dehydrogenation under standard conditions with the addition of various amounts of LiOH and LiCl in the presence of *sec*-BuLi (entries 4-6).[17] Under Pd-catalyzed conditions, 1 equivalent of LiOH and LiCl slightly suppressed the yield, but a significant side reaction was not observed. Increasing the equivalents of LiCl from one (entry 5) to three (entry 6) decreases the yield from 78% to 13%. Under Ni-catalyzed conditions, significant inhibition was observed. The primary side product of these reactions was a Michael adduct, which results from a Michael reaction between a zinc enolate and an unsaturated dehydrogenation product. This study highlights that these Ni- and Pd-catalyzed dehydrogenation reactions can be extremely sensitive to different counterions.

Additionally, proper storage of *n*-BuLi bottles is crucial to minimizing LiOH buildup. To resolve these issues, *n*-BuLi is routinely titrated with *N*-benzylbenzamide,[18] and bottles without sediment are used. If any cloudiness is observed, the bottle is discarded and a new bottle is used for the reaction. Additionally, the presence of LiOH and LiCl may promote the anionic pathway for the reaction, leading to depreciated yields.

Experimental Procedures and Characterization Data for Michael Addition Side Product

N^1,N^1,N^5,N^5,2-pentabenzyl-3-phenylpentanediamide (SI-14)

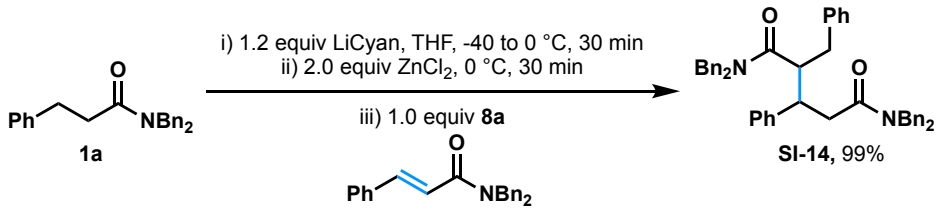

To a –40 °C solution of CyanH (31 mg, 0.12 mmol, 1.2 equiv) in THF (1.0 mL, 0.1 M) was added *n*-BuLi (2.5 M in hexanes, 48 µL, 0.12 mmol, 1.2 equiv). The reaction quickly became opaque and was stirred for 1h forming a pale-yellow mixture. Amide **1a** (33 mg, 0.1 mmol, 1.0 equiv) was added and the reaction was stirred for 30 min at 0 °C. $ZnCl_2$ (0.5 M in THF, 0.4 mL, 0.2 mmol, 2.0 equiv) was added and stirred for 30 min at 0 °C. A solution of **8a** (33 mg, 0.1 mmol, 1.0 equiv) added to the reaction. The reaction mixture was warmed to ambient temperature. After stirring for 1h the reaction was quenched with sat. aq. NH_4Cl (1.0 mL) and diluted with EtOAc (1.0 mL), and the organic phase was separated. The aqueous phase was extracted with EtOAc (3 × 2.0 mL) and the combined organic layers were washed with brine (5.0 mL), dried over anhydrous Na_2SO_4, filtered, and concentrated under reduced pressure by rotary evaporation. Purification by flash column chromatography on silica gel (10-20% EtOAc/hexanes) afforded the Michael addition product **SI-14** as a white foam (65 mg, 99%). **R_f**: 0.26 (40% Et_2O/hexanes); **^{1}H NMR** (400 MHz, $CDCl_3$) δ 7.41 – 7.29 (m, 3H), 7.29 – 7.07 (m, 19H), 7.07 – 7.00 (m, 2H), 7.00 – 6.92 (m, 2H), 6.85 – 6.78 (m, 2H), 6.48 – 6.42 (m, 2H), 4.63 (dd, *J* = 14.8, 7.9 Hz, 2H), 4.45 – 4.37 (m, 3H), 4.22 (d, *J* = 16.7 Hz, 1H), 4.01 (d, *J* = 14.8 Hz, 1H), 3.93 (ddd, *J* = 10.5, 6.9, 3.8 Hz, 1H), 3.80 (d, *J* = 16.7 Hz, 1H), 3.33 (ddd, *J* = 10.4, 6.8, 3.3 Hz, 1H), 3.22 – 3.09 (m, 2H), 3.02 (dd, *J* = 15.7, 10.3 Hz, 1H), 2.88 (dd, *J* = 12.6, 3.3 Hz, 1H); **^{13}C{^{1}H} NMR** (101 MHz, $CDCl_3$) δ 174.1, 171.9, 142.5, 139.9, 137.4, 137.0, 136.8, 136.2, 129.5, 129.1, 128.8, 128.6, 128.6, 128.5, 128.44, 128.41, 128.2, 127.7, 127.4, 127.3, 127.1, 126.92, 126.89, 126.6, 126.4, 50.1, 49.8, 49.7, 48.5, 48.0, 44.9, 35.9, 34.3; **IR** (cm^{-1}): 3027, 2925, 1630, 1471, 1209, 749, 729, 698; **ESI-HRMS (m/z)**: $[M+H]^+$ calc'd for $C_{46}H_{45}N_2O_2^+$: 657.3476; found: 657.3482.

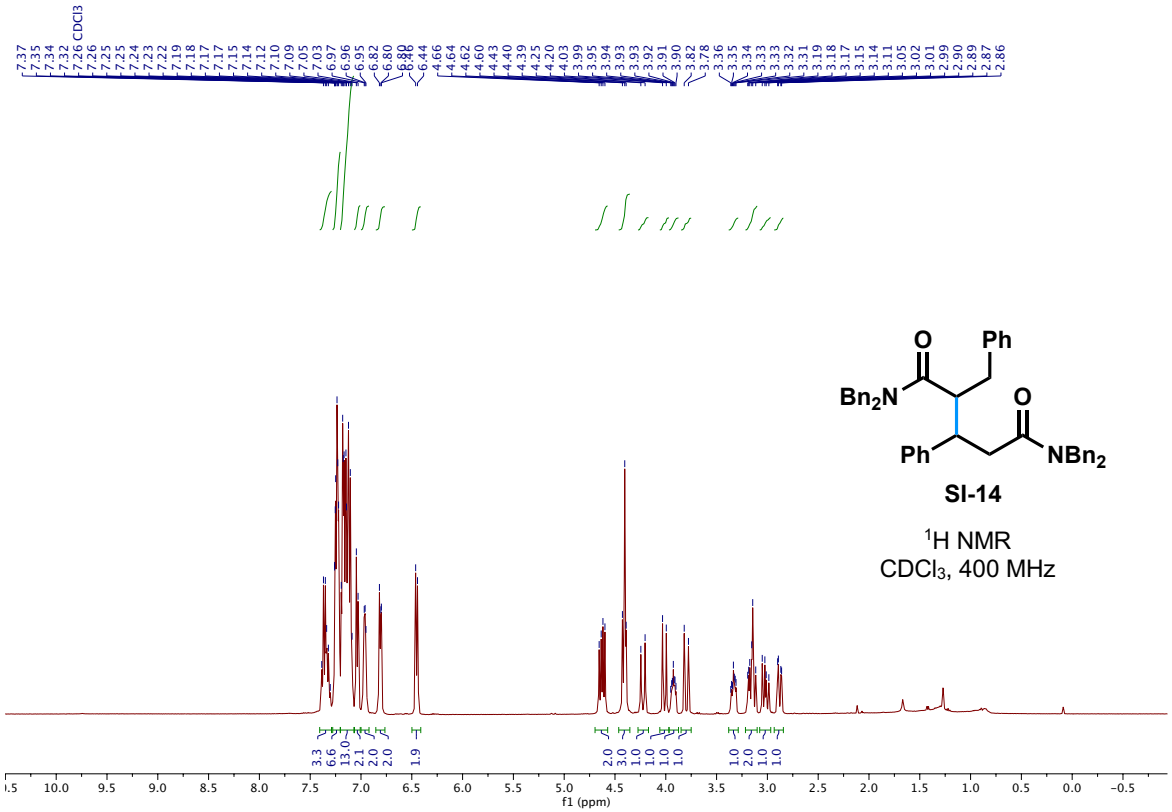

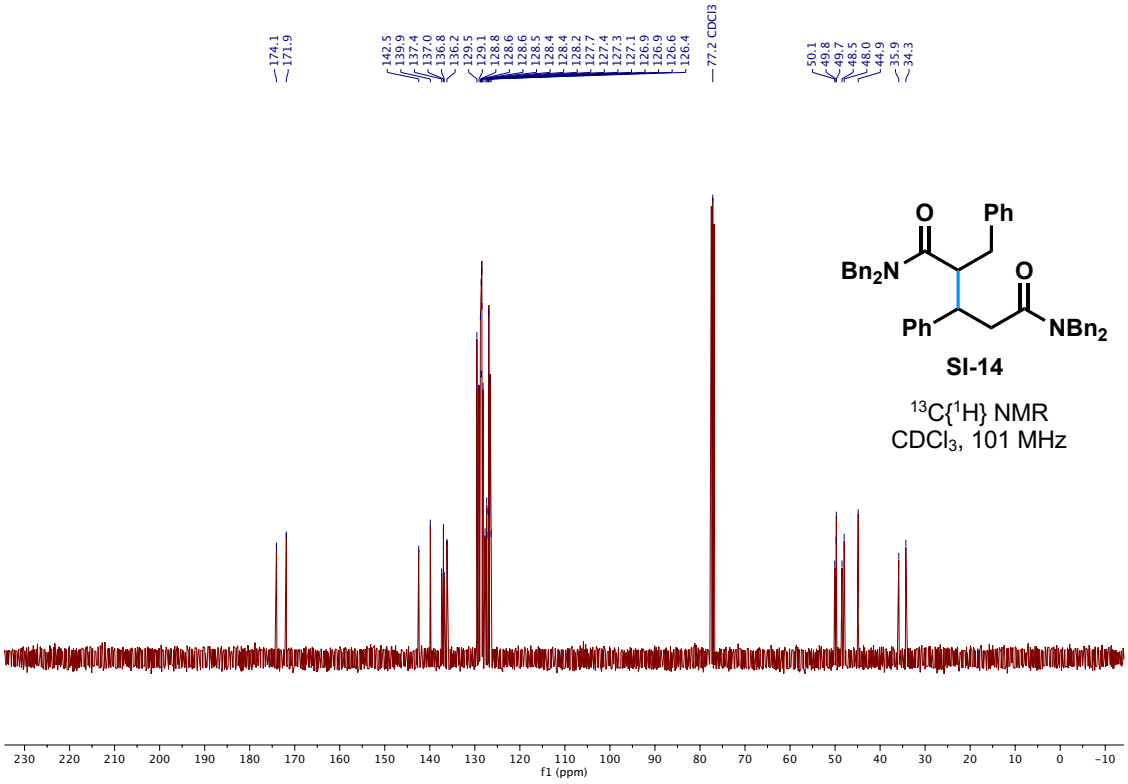

Experimental Procedures and Results for Catalyst Evaluation

Reactions were conducted according to **General Procedure B** on a 0.2 mmol scale.

Table S8. Effects of Palladium and Nickel Pre-catalysts

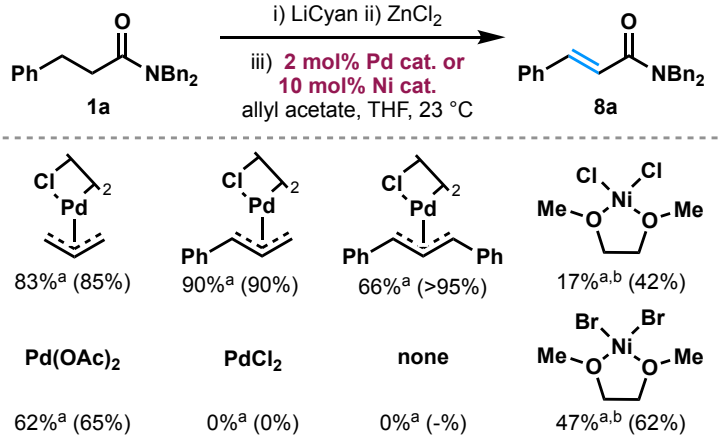

[a]Yields and conversions were determined by 1H NMR spectroscopy using 1,3,5-trimethoxybenzene as an internal standard. Conversion is indicated in parentheses. [b]1.2 equiv of diethyl allyl phosphate was used instead of allyl acetate.

Table S9. Effects of inhibitors.

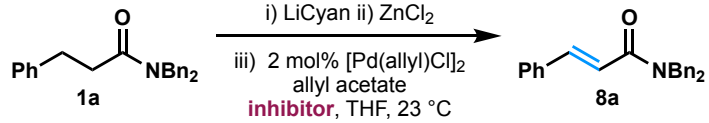

Entry	Inhibitor	Yield[a]
1	None	83% (85)
2	TEMPO	74% (95)
3[b]	TEMPO	trace (10)
4	Hg(0)	21% (23)
5	SMe_2	87% (94)
6	PVP	58% (58)

[a]Yields and conversions were determined by ^{1}H NMR spectroscopy using 1,3,5-trimethoxybenzene as an internal standard. Conversion is indicated in parentheses. [b]5 mol% Ni(dme)Br_2 and 1.2 equiv of diethyl allyl phosphate were used instead of $[Pd(allyl)Cl]_2$ and allyl acetate.

Computational Details

Computational Methods

All density functional theory (DFT) calculations were performed using the Gaussian 16 suite of programs (revision A3).[19] The ωb97X-D functional was used to investigate the reaction pathways.[20] Geometry optimizations for the ground states, transition states and products were performed with the LANL2DZ[21] pseudopotential for nickel (Ni) and palladium (Pd), and the 6-31G(d,p)[22] basis set for all other atoms. The stationary points are characterized via calculations of the analytical gradients and Hessians. Intermediates and transition states were identified by the observation of the correct number of negative eigenvalues in the Hessian matrix: zero (0) and one (1) respectively. The intrinsic reaction coordinate (IRC) method was used to authenticate the transition states connecting corresponding energy minima.[23] To refine the results, single point energy calculations and the solvent effects of THF were performed on the gas-phase optimized structures. This was performed using the ωb97X-D functional with the LANL2DZ pseudopotential for Ni and Pd and the Ahlrich's et al. triple-ζ (def2-TZVP)[24] basis set for all other atoms. All quoted free energies are reported at 298.15 K in THF and were calculated via the SMD continuum solvation model.[25]

Basis Sets and Functionals Screened for Ni- and Pd-Catalyzed β-Hydride Elimination

Table S10. Geometry optimization and frequency calculations for transition state barriers (kcal/mol) for β-hydride elimination for Ni and Pd in anionic and neutral pathways. Calculations were performed in the gas phase using the LANL2DZ pseudopotential (Ni, Pd).

		Anionic Pathway TS barriers		**Neutral Pathway TS barriers**	
Functional	Basis Set	Pd $\Delta G^{\ddagger}$	Ni $\Delta G^{\ddagger}$	Pd $\Delta G^{\ddagger}$	Ni $\Delta G^{\ddagger}$
B3LYP	6-31G(d,p) GD3	17.9	22.8	25.9	11.7
	6-31+G(d,p) GD3	17.2	21.6	13.1	10.4
M06	6-31G(d,p)	15.3	24.8	15.2	9.2
	6-31G(d,p) GD3	16.8	25.2	15.4	9.4
	6-31+G(d,p) GD3	16.4	24.1	14.6	8.7
WB97XD	6-31G(d,p)	18.3	16.3	14.4	12
	6-31+G(d,p)	17.1	14.7	13.6	10.8
	6-311+G(d,p)	15.9	13.4	12.1	9.1

Table S11. Single point energy calculations for transition state barriers (kcal/mol) for β-hydride elimination for Ni and Pd in anionic and neutral pathways. Geometry optimization and frequency calculations were performed using the ωb97X-D functional, LANL2DZ pseudopotential (Ni, Pd), and , 6-31G(d,p) basis set for all other atoms.

		Anionic Pathway TS Barriers			**Neutral Pathway TS Barriers**		
	Basis Set	Pd $\Delta G^{\ddagger}$	Ni $\Delta G^{\ddagger}$	difference in TS energies	Pd $\Delta G^{\ddagger}$	Ni $\Delta G^{\ddagger}$	difference in TS energies
Gas phase	6-311++g(d,p)	15.8	13.8	2	12	9.1	2.9
	def2TZVP	14.5	12.8	1.7	11.3	7.8	3.5

	CC-PVTZ	13.8	11.1	2.7	10.7	6.1	4.6
Solvated (THF)	6-311++g(d,p)	17.7	14.1	3.6	10.5	7.1	3.4
	def2TZVP	16.4	13.2	3.2	9.8	5.9	3.9
	CC-PVTZ	15.7	11.5	4.2	9.2	4.3	4.9

Basis Sets Screened for Pd-Catalyzed Reductive Elimination

Table S12. Transition state barriers (kcal/mol) for reductive elimination with Pd in the neutral pathway. Calculations were performed using the ωb97X-D functional and LANL2DZ pseudopotential (Pd).

Neutral Pathway Reductive Elimination TS Barrier (Pd)		
	Basis Set	$\Delta G^{\ddagger}$
Gas phase	6-311++g(d,p)	2.1
	def2TZVP	2.3
	CC-PVTZ	2.4
Solvated (THF)	6-311++g(d,p)	2.8
	def2TZVP	3
	CC-PVTZ	3.1

Figure S6. Free energy profile of the Pd-Catalyzed β-hydride elimination and reductive elimination via the neutral pathway comparing different basis sets. Calculations were performed using the ωb97X-D functional and LANL2DZ pseudopotential (Pd). Calculations were performed in THF via the SMD continuum solvation model. Energies are reported in kcal/mol.

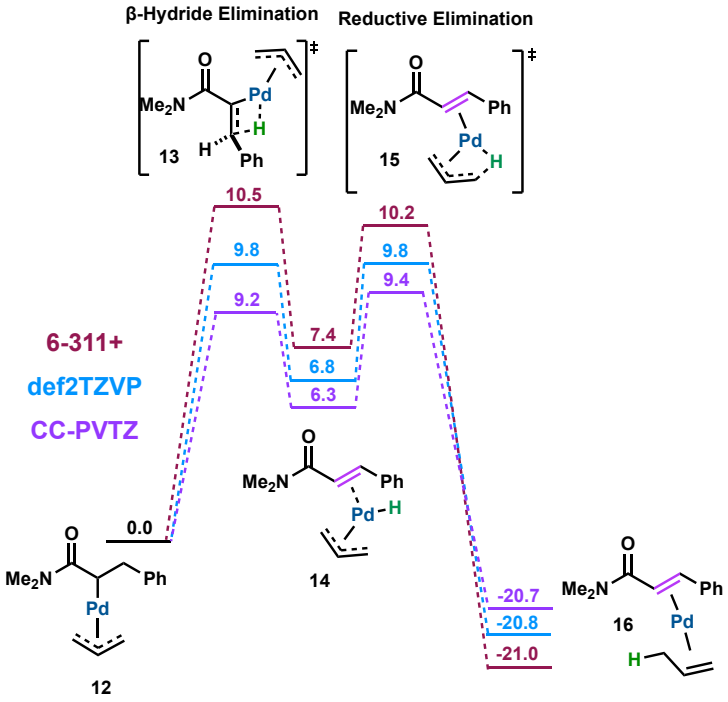

Free Energy Profile for the Ni- and Pd-Catalyzed β-Hydride Elimination of SI-15 and 12 via the Neutral Pathway

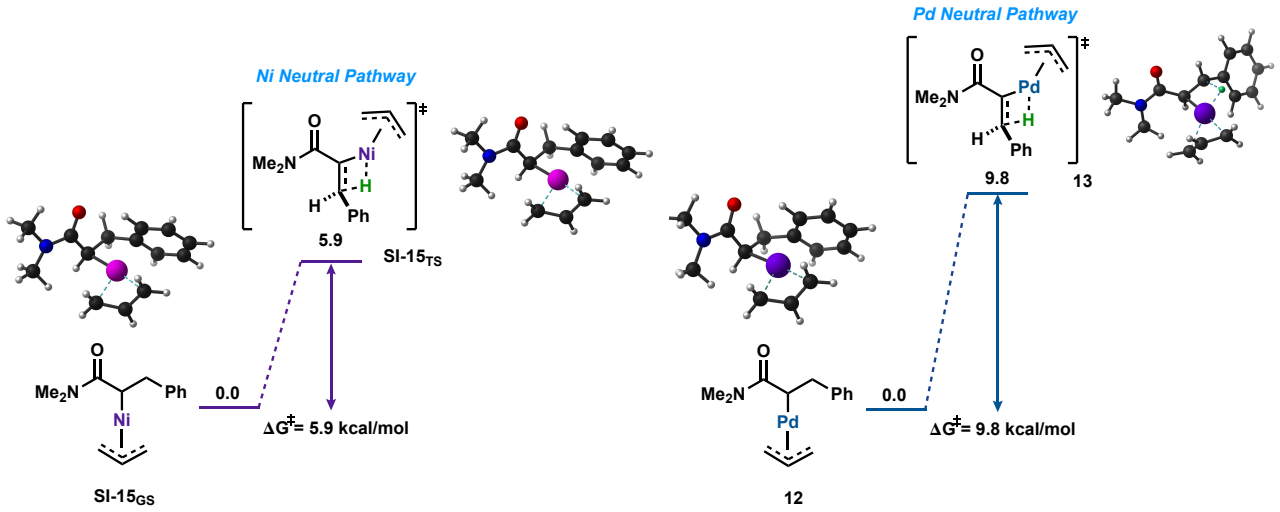

Figure S7. Free energy profile for β-hydride elimination of **SI-15** and **12**. All energies were calculated at the ωb97X-D/6-311+G(d,p)-LANL2DZ(Ni,Pd)//ωb97X-D/def2TZVP-LANL2DZ(Pd,Ni)-SMD-THF level of theory and are shown in kcal/mol.

Free Energy Profile for the Ni- and Pd-Catalyzed β-Hydride Elimination of SI-16 and SI-17 via the Anionic Pathway

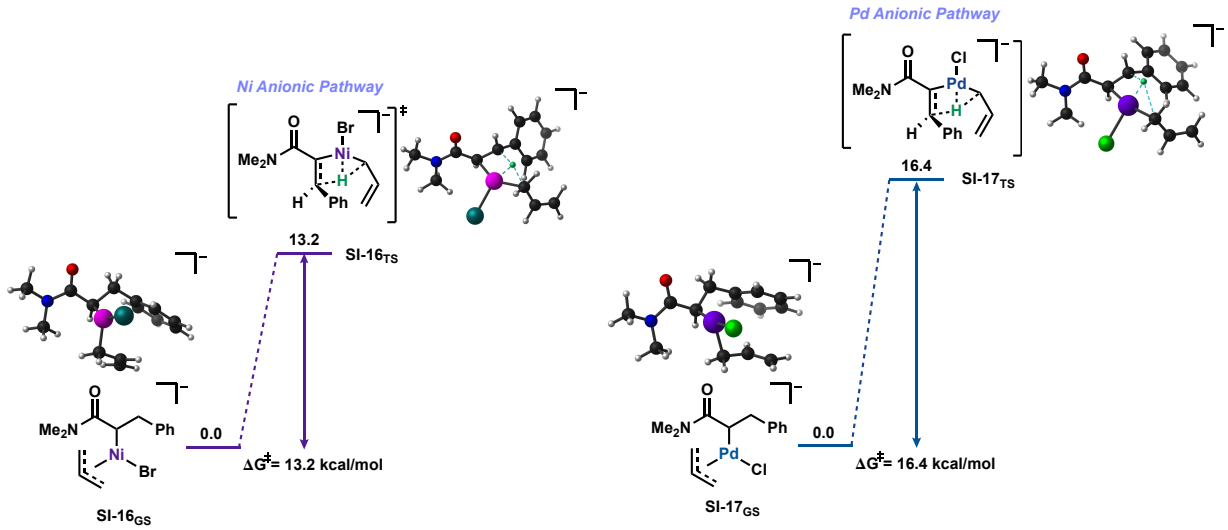

Figure S8. Free energy profile for β-hydride elimination of **SI-16** and **SI-17**. All energies were calculated at the ωb97X-D/6-311+G(d,p)-LANL2DZ(Ni,Pd)//ωb97X-D/def2TZVP-LANL2DZ(Pd,Ni)-SMD-THF level of theory and are shown in kcal/mol.

Free Energy Profile for the Pd-Catalyzed β-Hydride Elimination and Reductive Elimination via the Neutral Pathway

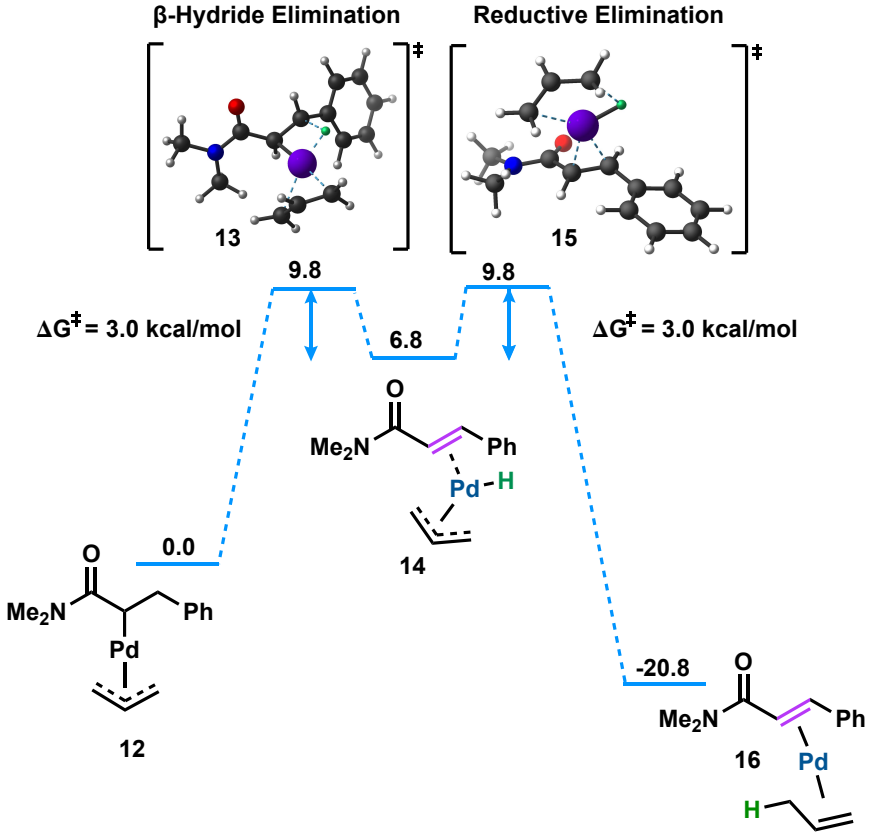

Figure S9. Free energy profile for the β-hydride elimination and reductive elimination of **12** and **14**. All energies were calculated at ωb97X-D/6-311+G(d,p)-LANL2DZ(Ni,Pd)//ωb97X-D/def2TZVP-LANL2DZ(Pd,Ni)-SMD-THF level of theory and are shown in kcal/mol.

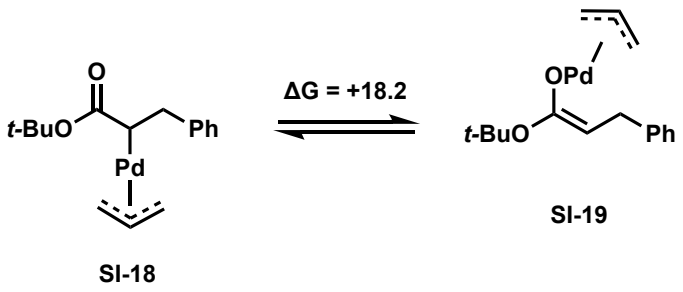

Figure S10. Free energy difference for the isomerization **SI-18** and **SI-19**. All energies were calculated at ωb97X-D/6-311+G(d,p)-LANL2DZ(Ni,Pd)//ωb97X-D/def2TZVP-LANL2DZ(Pd,Ni)-SMD-THF level of theory and are shown in kcal/mol.

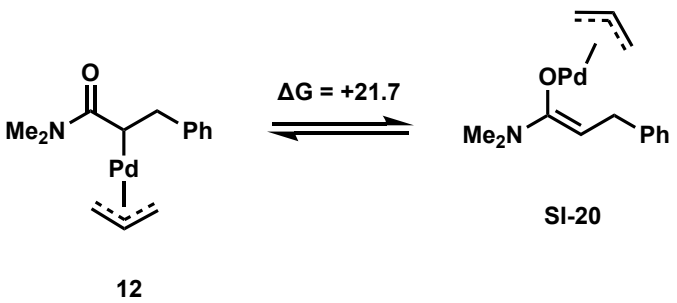

Figure S11. Free energy difference for the isomerization **12** and **SI-20**. All energies were calculated at ωb97X-D/6-311+G(d,p)-LANL2DZ(Ni,Pd)//ωb97X-D/def2TZVP-LANL2DZ(Pd,Ni)-SMD-THF level of theory and are shown in kcal/mol.

Cartesian Coordinates (Å) and Energies of Optimized Structures

SI-15$_{GS}$

Zero-point correction = 0.301802 (Hartree/Particle)
Thermal correction to Energy = 0.320070
Thermal correction to Enthalpy = 0.321014
Thermal correction to Gibbs Free Energy = 0.255072
Sum of electronic and zero-point Energies = -843.845063
Sum of electronic and thermal Energies = -843.826796
Sum of electronic and thermal Enthalpies = -843.825851
Sum of electronic and thermal Free Energies = -843.891794
E(RwB97XD) = -844.238134

Cartesian coordinates

ATOM	X	Y	Z
O	-1.69313	-1.85591	-0.79557
N	-3.16292	-0.25954	-0.16075
C	-1.96147	-0.92151	-0.036
C	-0.99283	-0.45555	0.98878
H	-1.44787	0.0211	1.85213
C	0.04778	-1.51068	1.37633
H	-0.27576	-2.5184	1.10037
H	0.2358	-1.48775	2.4522
C	1.33472	-1.17178	0.63932
C	1.3614	-1.22003	-0.76565
C	2.51091	-0.79352	1.31415
C	2.55425	-0.96797	-1.45929
H	0.47308	-1.56506	-1.28842
C	3.68088	-0.54383	0.62029
H	2.49843	-0.73293	2.39765
C	3.70909	-0.64433	-0.77341
H	2.56523	-1.04618	-2.54066

H	4.58132	-0.2754	1.16177
H	4.63203	-0.4612	-1.31204
C	-4.15134	-0.77647	-1.08613
H	-4.61902	0.04923	-1.6316
H	-3.66128	-1.44607	-1.78842
H	-4.93749	-1.33388	-0.55984
C	-3.65585	0.68927	0.8142
H	-4.12683	0.19508	1.67516
H	-2.85658	1.33337	1.17189
H	-4.40601	1.32557	0.33825
Ni	0.31255	0.69723	0.07885
C	1.47963	2.07506	-1.00458
H	2.56172	2.08047	-0.95933
H	1.03642	1.8537	-1.97268
C	-0.6639	2.40904	0.07405
H	-1.25452	2.34322	-0.83831
H	-1.20297	2.74885	0.95027
C	0.72962	2.66457	-0.00161
H	1.24092	3.06426	0.87097

SI-15$_{TS}$

Zero-point correction = 0.297444 (Hartree/Particle)
Thermal correction to Energy = 0.315654
Thermal correction to Enthalpy = 0.316598
Thermal correction to Gibbs Free Energy = 0.249120
Sum of electronic and zero-point Energies = -843.828967
Sum of electronic and thermal Energies = -843.810756
Sum of electronic and thermal Enthalpies = -843.809812
Sum of electronic and thermal Free Energies = -843.877290
E(RwB97XD) = -844.222836

Cartesian coordinates

ATOM	X	Y	Z
O	-1.87774	-1.22967	-1.71501
N	-2.71015	-1.5819	0.36583
C	-1.72523	-1.18504	-0.50039
C	-0.45602	-0.68488	0.10081
H	-0.25285	-0.88595	1.14495
C	0.6356	-0.43134	-0.75729
H	0.67999	1.34883	-1.27686
H	0.48297	-0.69219	-1.80049
C	2.03975	-0.51331	-0.27351
C	3.00667	-1.10052	-1.08818
C	2.42273	-0.04402	0.9852
C	4.32121	-1.2279	-0.65439
H	2.72492	-1.46376	-2.07109
C	3.73365	-0.17051	1.42076
H	1.6892	0.44108	1.62197
C	4.68919	-0.76535	0.60243
H	5.05865	-1.68949	-1.30157
H	4.01422	0.20334	2.39926
H	5.7144	-0.86095	0.94152
C	-0.33957	3.23894	-0.40607
Ni	-0.38707	1.24552	-0.30245
C	-3.91456	-2.18835	-0.16791
H	-3.96988	-3.24953	0.10157
H	-4.80161	-1.68157	0.2254
H	-3.89931	-2.09801	-1.25139
C	-2.54852	-1.6146	1.80671
H	-1.95499	-2.47393	2.14206
H	-2.08529	-0.69835	2.17471
H	-3.53702	-1.68904	2.26314

C	-1.75096	1.91556	1.08387
C	-1.61143	2.77357	-0.01263
H	-1.09718	2.01501	1.94795
H	-2.70483	1.43325	1.26064
H	-2.42595	2.82839	-0.73126
H	0.41679	3.46351	0.34316
H	-0.23654	3.77205	-1.34221

SI-16$_{GS}$

Zero-point correction = 0.301030 (Hartree/Particle)
Thermal correction to Energy = 0.322087
Thermal correction to Enthalpy = 0.323031
Thermal correction to Gibbs Free Energy = 0.246846
Sum of electronic and zero-point Energies = -3418.134508
Sum of electronic and thermal Energies = -3418.113451
Sum of electronic and thermal Enthalpies = -3418.112507
Sum of electronic and thermal Free Energies = -3418.188692
E(RwB97XD) = -3418.505224

Cartesian coordinates

ATOM	X	Y	Z
O	-2.35071	-1.19367	-1.91993
N	-2.96501	-1.92272	0.13715
C	-2.01243	-1.4253	-0.75027
C	-0.62648	-1.17766	-0.28602
H	-0.29787	-1.80872	0.54197
C	0.3602	-1.2525	-1.46533
H	0.11919	-0.4682	-2.1934
H	0.22186	-2.19954	-2.00853
C	1.80357	-1.13017	-1.04185
C	2.44298	0.11303	-1.00001
C	2.52956	-2.25974	-0.65457
C	3.76609	0.22212	-0.58055
H	1.88672	1.00763	-1.27105

C	3.85484	-2.15783	-0.23496
H	2.04309	-3.23286	-0.6778
C	4.47978	-0.91285	-0.19654
H	4.23704	1.20076	-0.54473
H	4.39777	-3.05032	0.06612
H	5.5115	-0.82683	0.1342
H	-0.66955	1.40884	2.41083
Br	-0.48424	3.02532	-0.33434
C	-0.26571	0.47065	2.01081
Ni	-0.63182	0.71146	0.15202
C	1.8792	-0.70768	2.56163
C	1.1991	0.37811	2.16334
H	1.76597	1.2655	1.87879
H	2.96506	-0.7271	2.57429
H	1.36226	-1.62719	2.83353
C	-4.35262	-1.86218	-0.2744
H	-4.83035	-0.92428	0.05118
H	-4.40278	-1.91458	-1.36103
H	-4.90305	-2.70276	0.16487
C	-2.76895	-1.94962	1.56915
H	-1.75145	-2.24643	1.82121
H	-2.96538	-0.97135	2.03243
H	-3.45338	-2.68605	2.00587
H	-0.77126	-0.38537	2.46323

SI-16$_{TS}$

Zero-point correction = 0.296457 (Hartree/Particle)
Thermal correction to Energy = 0.317333
Thermal correction to Enthalpy = 0.318278
Thermal correction to Gibbs Free Energy = 0.243445
Sum of electronic and zero-point Energies = -3418.113696
Sum of electronic and thermal Energies = -3418.092819

Sum of electronic and thermal Enthalpies = -3418.091875
Sum of electronic and thermal Free Energies = -3418.166707
E(RwB97XD) = -3418.590596

Cartesian coordinates

ATOM	X	Y	Z
O	-1.47227	-2.38937	-1.62368
N	-2.54851	-2.20226	0.363
C	-1.47812	-1.96347	-0.46692
C	-0.35584	-1.20003	0.11107
H	-0.18364	-1.28883	1.1792
C	0.78921	-0.94141	-0.73584
H	0.87299	0.49453	-1.27132
H	0.70749	-1.40891	-1.71773
C	2.16253	-1.02587	-0.14906
C	3.06851	-1.97112	-0.63346
C	2.57125	-0.18736	0.8906
C	4.34145	-2.08898	-0.08726
H	2.76419	-2.62491	-1.44503
C	3.84152	-0.30404	1.43912
H	1.89243	0.58164	1.24423
C	4.73334	-1.25598	0.95484
H	5.02932	-2.83193	-0.47865
H	4.14098	0.36535	2.23883
H	5.72815	-1.34129	1.3798
H	2.68929	3.91322	0.73302
C	2.43221	3.25446	-0.09037
C	0.67768	2.13609	-1.50143
C	1.15739	3.04517	-0.44267
H	0.37317	3.54689	0.12112
H	-0.2148	2.51431	-2.00482

H	1.4571	1.94861	-2.2479
H	3.25203	2.75024	-0.59706
Ni	-0.32565	0.67626	-0.46574
Br	-2.15672	1.88056	0.45061
C	-3.64948	-3.00602	-0.10808
H	-3.85337	-3.82857	0.59005
H	-4.56196	-2.40383	-0.20774
H	-3.38935	-3.41413	-1.08299
C	-2.6742	-1.62443	1.68528
H	-2.22037	-2.26037	2.45927
H	-2.23096	-0.62889	1.71336
H	-3.73625	-1.50938	1.91751

SI-17$_{GS}$

Zero-point correction = 0.302028 (Hartree/Particle)
Thermal correction to Energy = 0.322843
Thermal correction to Enthalpy = 0.323787
Thermal correction to Gibbs Free Energy = 0.249947
Sum of electronic and zero-point Energies = -1261.612097
Sum of electronic and thermal Energies = -1261.591281
Sum of electronic and thermal Enthalpies = -1261.590337
Sum of electronic and thermal Free Energies = -1261.664177
E(RwB97XD) = -1262.051182

Cartesian coordinates

ATOM	X	Y	Z
O	-2.3583	-1.8318	-1.50607
N	-3.00709	-1.51101	0.64633
C	-2.03238	-1.53082	-0.34857
C	-0.6282	-1.18638	-0.00026
H	-0.36185	-1.46282	1.02452
C	0.35023	-1.83626	-0.99091
H	0.12973	-1.48376	-2.00321
H	0.18658	-2.92492	-1.01368

C	1.79296	-1.5631	-0.65045
C	2.47858	-0.48519	-1.21878
C	2.46799	-2.35651	0.28265
C	3.79433	-0.20368	-0.86241
H	1.95701	0.16387	-1.91719
C	3.7851	-2.0791	0.64719
H	1.94667	-3.19756	0.73536
C	4.45419	-0.99828	0.07455
H	4.29653	0.65392	-1.30053
H	4.2872	-2.70437	1.38109
H	5.47764	-0.7728	0.36153
H	-0.32995	2.13069	1.89669
C	0.09256	1.15949	1.6219
C	2.32859	2.27572	1.4903
C	1.57017	1.17415	1.57576
H	2.06422	0.20255	1.59277
H	3.41185	2.20744	1.43552
Pd	-0.6278	0.88985	-0.25764
Cl	-0.77055	3.21533	-0.94895
H	1.87715	3.26226	1.41528
C	-2.7852	-0.86556	1.924
H	-1.85178	-1.20214	2.3779
H	-2.74578	0.22975	1.83238
H	-3.6013	-1.14033	2.60008
C	-4.38963	-1.52333	0.20907
H	-4.46299	-2.08713	-0.71982
H	-5.01283	-1.99326	0.97848
H	-4.76473	-0.50395	0.02681
H	-0.28503	0.37326	2.27977

SI-17$_{TS}$

Zero-point correction = 0.296282 (Hartree/Particle)
Thermal correction to Energy = 0.317187
Thermal correction to Enthalpy = 0.318131
Thermal correction to Gibbs Free Energy = 0.243639
Sum of electronic and zero-point Energies = -1261.586345
Sum of electronic and thermal Energies = -1261.565440
Sum of electronic and thermal Enthalpies = -1261.564496
Sum of electronic and thermal Free Energies = -1261.638989
E(RwB97XD) = -1262.027614

Cartesian coordinates

ATOM	X	Y	Z
O	-2.10325	-1.95449	-1.59761
N	-3.05117	-1.6034	0.43278
C	-1.98872	-1.57299	-0.43205
C	-0.6991	-1.09666	0.11601
H	-0.52792	-1.15455	1.18411
C	0.42722	-1.08574	-0.7482
H	0.7608	0.35704	-1.43531
H	0.2208	-1.49514	-1.73498
C	1.78714	-1.41701	-0.21467
C	2.29942	-2.69315	-0.4593
C	2.5471	-0.52114	0.5361
C	3.53618	-3.07266	0.04699
H	1.71471	-3.39404	-1.04725
C	3.78485	-0.90103	1.04294
H	2.17561	0.48644	0.69736
C	4.28413	-2.1762	0.8038
H	3.91749	-4.06907	-0.15211
H	4.36374	-0.18657	1.61857
H	5.25261	-2.46799	1.19671
H	3.21812	3.60214	1.05314
C	2.71625	3.27218	0.14871

C	0.57361	2.81007	-1.09051
C	1.37748	3.27718	0.04813
H	0.79972	3.61968	0.90632
H	-0.31031	3.43017	-1.25307
Pd	-0.2808	0.98466	-0.44182
Cl	-1.88493	2.19303	0.95669
H	1.16067	2.72469	-2.00718
H	3.34383	2.92063	-0.66757
C	-4.31362	-2.1421	-0.01406
H	-4.18612	-2.544	-1.01731
H	-4.65113	-2.94046	0.65936
H	-5.08391	-1.36136	-0.03862
C	-2.99824	-1.08483	1.78724
H	-2.61394	-1.83119	2.49687
H	-2.40045	-0.17379	1.83287
H	-4.01149	-0.81408	2.09272

12

Zero-point correction = 0.302085 (Hartree/Particle)
Thermal correction to Energy = 0.320460
Thermal correction to Enthalpy = 0.321404
Thermal correction to Gibbs Free Energy = 0.254767
Sum of electronic and zero-point Energies = -801.289984
Sum of electronic and thermal Energies = -801.271609
Sum of electronic and thermal Enthalpies = -801.270665
Sum of electronic and thermal Free Energies = -801.337302
E(RwB97XD) = -801.683940

Cartesian coordinates

ATOM	X	Y	Z
O	1.77307	-2.00965	0.86472
N	3.20649	-0.41003	0.15243
C	2.01962	-1.09873	0.07121
C	1.04018	-0.69474	-0.97513
H	1.50027	-0.29248	-1.87366
C	-0.00274	-1.77521	-1.28264

H	0.33422	-2.7616	-0.95106
H	-0.19476	-1.81921	-2.35724
C	-1.29776	-1.41332	-0.56772
C	-1.32612	-1.34311	0.8382
C	-2.4884	-1.1494	-1.27013
C	-2.52257	-1.04545	1.50799
H	-0.4356	-1.63177	1.38989
C	-3.66342	-0.86231	-0.59902
H	-2.47886	-1.19342	-2.35437
C	-3.68488	-0.81268	0.79704
H	-2.5301	-1.01978	2.59187
H	-4.5723	-0.67665	-1.16075
H	-4.60967	-0.59282	1.3184
C	4.21628	-0.84377	1.09514
H	4.57224	0.00599	1.68762
H	3.7803	-1.58869	1.75643
H	5.07513	-1.28799	0.57625
C	3.6153	0.59106	-0.80739
H	4.09778	0.15064	-1.69038
H	2.76317	1.18677	-1.12906
H	4.33288	1.26407	-0.33121
C	-1.44836	2.34934	0.97757
H	-2.53078	2.37945	0.94281
H	-0.99656	2.18226	1.95097
C	0.70141	2.56742	-0.16587
H	1.30417	2.59402	0.73928
H	1.22196	2.86692	-1.06855
C	-0.70151	2.83077	-0.08327
H	-1.22038	3.18265	-0.97109
Pd	-0.27794	0.7	-0.09276

13

Zero-point correction = 0.297015 (Hartree/Particle)
Thermal correction to Energy = 0.315306
Thermal correction to Enthalpy = 0.316250
Thermal correction to Gibbs Free Energy = 0.248687
Sum of electronic and zero-point Energies = -801.269782
Sum of electronic and thermal Energies = -801.251491
Sum of electronic and thermal Enthalpies = -801.250547
Sum of electronic and thermal Free Energies = -801.318110
E(RwB97XD) = -801.668162

Cartesian coordinates

ATOM	X	Y	Z

O	-1.43613	-1.92686	-1.64209
N	-2.35139	-2.09927	0.42679
C	-1.3815	-1.68205	-0.44316
C	-0.23543	-0.92392	0.14231
H	0.00243	-1.06837	1.18941
C	0.81933	-0.54492	-0.72965
H	0.70018	1.08392	-1.2766
H	0.69681	-0.88031	-1.75589
C	2.22706	-0.47944	-0.24371
C	3.21947	-1.12627	-0.97768
C	2.57843	0.16398	0.94379
C	4.53534	-1.14197	-0.52913
H	2.95832	-1.62546	-1.90499
C	3.8904	0.14698	1.39383
H	1.81855	0.69739	1.50667
C	4.8742	-0.50847	0.6593
H	5.29566	-1.65077	-1.11096
H	4.14964	0.65492	2.31605
H	5.90025	-0.51706	1.00904
C	-0.86479	3.3066	-0.42617
C	-3.42133	-2.94857	-0.0569
H	-3.42927	-3.90071	0.48493
H	-4.39288	-2.46108	0.0799
H	-3.26473	-3.13852	-1.11614
C	-2.34651	-1.79943	1.8445
H	-1.75562	-2.52167	2.4214
H	-1.96409	-0.79494	2.02738
H	-3.37468	-1.8352	2.21123
C	-2.17139	1.85491	1.06815
C	-2.06654	2.66069	-0.07746

H	-1.60275	2.09789	1.96194
H	-3.07353	1.27486	1.22087
H	-2.84117	2.57526	-0.83592
H	-0.19347	3.66886	0.34771
H	-0.79292	3.80783	-1.38278
Pd	-0.53975	1.14727	-0.27505

14

Zero-point correction = 0.299950 (Hartree/Particle)
Thermal correction to Energy = 0.318727
Thermal correction to Enthalpy = 0.319671
Thermal correction to Gibbs Free Energy = 0.250744
Sum of electronic and zero-point Energies = -801.116310
Sum of electronic and thermal Energies = -801.097532
Sum of electronic and thermal Enthalpies = -801.096588
Sum of electronic and thermal Free Energies = -801.165515
E(RwB97XD) = -801.66918

Cartesian coordinates

ATOM	X	Y	Z
O	-1.48097	-1.87886	-1.6471
N	-2.40502	-2.06068	0.42256
C	-1.41928	-1.6568	-0.43973
C	-0.25331	-0.93629	0.15612
H	-0.0215	-1.08682	1.20544
C	0.81405	-0.59503	-0.72235
H	0.62506	1.54855	-1.42478
H	0.68244	-0.9501	-1.74264
C	2.22244	-0.52581	-0.23684
C	3.22997	-1.11496	-1.00231
C	2.56262	0.07516	0.97903
C	4.54901	-1.11795	-0.55681
H	2.97734	-1.58012	-1.95103
C	3.87834	0.07316	1.42451

H	1.78976	0.56281	1.56793
C	4.87681	-0.52565	0.65823
H	5.32043	-1.58288	-1.16262
H	4.128	0.54726	2.36863
H	5.90531	-0.52349	1.00492
C	-0.87079	3.84066	-0.57242
C	-3.50125	-2.85837	-0.08794
H	-3.54257	-3.83045	0.41816
H	-4.4585	-2.34551	0.06616
H	-3.34391	-3.01108	-1.15421
C	-2.39965	-1.77827	1.84302
H	-1.82717	-2.5185	2.41798
H	-1.99638	-0.78257	2.03913
H	-3.43084	-1.79484	2.20635
C	-2.16673	2.44067	0.98504
C	-2.07988	3.2304	-0.17698
H	-1.56957	2.68798	1.86047
H	-3.07694	1.88165	1.17247
H	-2.87562	3.14395	-0.91516
H	-0.16934	4.20238	0.17651
H	-0.81309	4.32046	-1.54227
Pd	-0.5905	1.67726	-0.386

15

Zero-point correction = 0.297713 (Hartree/Particle)
Thermal correction to Energy = 0.316477
Thermal correction to Enthalpy = 0.317421
Thermal correction to Gibbs Free Energy = 0.248442
Sum of electronic and zero-point Energies = -801.131725
Sum of electronic and thermal Energies = -801.112961
Sum of electronic and thermal Enthalpies = -801.112017
Sum of electronic and thermal Free Energies = -801.180996
E(RwB97XD) = -801.662997

Cartesian coordinates

ATOM	X	Y	Z
O	-1.69925	-1.79889	-1.67718
N	-2.71564	-1.78977	0.35551
C	-1.64461	-1.56941	-0.47297
C	-0.39488	-1.04673	0.16818
H	-0.25315	-1.20915	1.23191
C	0.71427	-0.80606	-0.64762
H	0.61636	1.83577	-1.31308
H	0.57878	-1.01691	-1.70575
C	2.11634	-0.75591	-0.17162
C	3.14652	-0.96844	-1.09316
C	2.46009	-0.51979	1.1659
C	4.47892	-0.95197	-0.69436
H	2.8953	-1.14951	-2.13456
C	3.78997	-0.50389	1.56621
H	1.68045	-0.32869	1.89789
C	4.80676	-0.72045	0.63792
H	5.26205	-1.121	-1.427
H	4.03559	-0.31684	2.60718
H	5.84567	-0.70548	0.9518
C	-0.33451	3.19719	-0.52758
C	-3.90847	-2.4054	-0.18997
H	-4.13528	-3.34185	0.33365
H	-4.77106	-1.73481	-0.09276
H	-3.73306	-2.61244	-1.24416
C	-2.72267	-1.47747	1.77
H	-2.27802	-2.27433	2.38115
H	-2.19656	-0.54035	1.96616

H	-3.75914	-1.34676	2.09232
C	-1.78754	2.23404	1.25164
C	-1.62796	2.83178	0.01974
H	-1.02878	2.31818	2.02529
H	-2.76725	1.88682	1.56018
H	-2.48196	2.85235	-0.65445
H	0.42552	3.56871	0.15686
H	-0.34228	3.70537	-1.48547
Pd	-0.33789	1.07012	-0.2807

16

Zero-point correction = 0.301074 (Hartree/Particle)
Thermal correction to Energy = 0.320796
Thermal correction to Enthalpy = 0.321740
Thermal correction to Gibbs Free Energy = 0.248653
Sum of electronic and zero-point Energies = -801.315753
Sum of electronic and thermal Energies = -801.296032
Sum of electronic and thermal Enthalpies = -801.295087
Sum of electronic and thermal Free Energies = -801.368174
E(RwB97XD) = -801.711033

Cartesian coordinates

ATOM	X	Y	Z
O	-1.6841	-2.06949	-1.6441
N	-2.70049	-2.06037	0.38859
C	-1.62946	-1.84001	-0.43988
C	-0.37973	-1.31733	0.20126
H	-0.238	-1.47975	1.26499
C	0.72942	-1.07666	-0.61453
H	0.59393	-1.28751	-1.67267
C	2.13149	-1.02651	-0.13854
C	3.16167	-1.23904	-1.06008
C	2.47524	-0.79039	1.19898

C	4.49407	-1.22257	-0.66128
H	2.91044	-1.42011	-2.10148
C	3.80512	-0.77449	1.59929
H	1.69559	-0.59929	1.93098
C	4.8219	-0.99105	0.671
H	5.2772	-1.3916	-1.39391
H	4.05074	-0.58744	2.64027
H	5.86081	-0.97608	0.98489
C	-0.33439	3.26995	-0.53603
C	-3.89332	-2.676	-0.15689
H	-4.12013	-3.61245	0.36673
H	-4.75591	-2.00541	-0.05967
H	-3.71791	-2.88304	-1.21107
C	-2.70752	-1.74807	1.80308
H	-2.26288	-2.54493	2.41423
H	-2.18141	-0.81095	1.99924
H	-3.74399	-1.61736	2.12541
C	-1.78754	2.23404	1.25164
C	-1.69827	2.93287	0.02869
H	-1.02878	2.31818	2.02529
H	-2.76725	1.88682	1.56018
H	-2.52266	2.84817	-0.68993
H	0.55488	3.48416	0.01915
H	-0.06631	3.30053	-1.57145
Pd	-0.50445	0.91052	-0.07113
H	-0.62881	4.29864	-0.5398

SI-18

Zero-point correction = 0.345060 (Hartree/Particle)
Thermal correction to Energy = 0.365831

Thermal correction to Enthalpy = 0.366775
Thermal correction to Gibbs Free Energy = 0.294585
Sum of electronic and zero-point Energies = -899.757104
Sum of electronic and thermal Energies = -899.736333
Sum of electronic and thermal Enthalpies = -899.735389
Sum of electronic and thermal Free Energies = -899.807580
E(RwB97XD) = -900.102165

Cartesian coordinates

ATOM	X	Y	Z
O	-1.69313	-1.85591	-0.79557
C	-1.96147	-0.92151	-0.036
C	-0.99283	-0.45555	0.98878
H	-1.44787	0.0211	1.85213
C	0.04778	-1.51068	1.37633
H	-0.27576	-2.5184	1.10037
H	0.2358	-1.48775	2.4522
C	1.33472	-1.17178	0.63932
C	1.3614	-1.22003	-0.76565
C	2.51091	-0.79352	1.31415
C	2.55425	-0.96797	-1.45929
H	0.47308	-1.56506	-1.28842
C	3.68088	-0.54383	0.62029
H	2.49843	-0.73293	2.39765
C	3.70909	-0.64433	-0.77341
H	2.56523	-1.04618	-2.54066
H	4.58132	-0.2754	1.16177
H	4.63203	-0.4612	-1.31204
C	-4.15134	-0.77647	-1.08613
C	1.47963	2.07506	-1.00458
H	2.56172	2.08047	-0.95933
H	1.03642	1.8537	-1.97268
C	-0.6639	2.40904	0.07405
H	-1.25452	2.34322	-0.83831
H	-1.20297	2.74885	0.95027
C	0.72962	2.66457	-0.00161
H	1.24092	3.06426	0.87097
O	-3.16292	-0.25954	-0.16075
C	-3.4571	-1.72506	-2.08103
H	-2.59154	-1.24467	-2.48714

H	-3.1633	-2.62051	-1.57432
H	-4.13411	-1.96907	-2.87287
C	-5.2539	-1.55823	-0.34802
H	-5.59153	-0.99011	0.4935
H	-6.07388	-1.73225	-1.01303
H	-4.86235	-2.49549	-0.01168
C	-4.80936	0.38526	-1.85359
H	-5.67318	0.02582	-2.37274
H	-5.10033	1.14928	-1.1633
H	-4.11175	0.78786	-2.55799
Pd	0.31255	0.69723	0.07885

SI-19

Zero-point correction = 0.345735 (Hartree/Particle)

Thermal correction to Energy = 0.366142

Thermal correction to Enthalpy = 0.367086

Thermal correction to Gibbs Free Energy = 0.294377

Sum of electronic and zero-point Energies = -899.720627

Sum of electronic and thermal Energies = -899.700220

Sum of electronic and thermal Enthalpies = -899.699276

Sum of electronic and thermal Free Energies = -899.771985

E(RwB97XD) = -900.066362

Cartesian coordinates

ATOM	X	Y	Z
O	-0.18736	-1.06421	0.32251
C	0.21656	0.03828	0.88968
C	1.33548	0.25914	1.59415
H	1.51105	1.23273	2.03043
C	2.39097	-0.80865	1.72085
H	1.90856	-1.79075	1.66558
H	2.88011	-0.74283	2.69911
C	3.4377	-0.71097	0.626

C	4.75546	-0.34715	0.89791
C	3.07315	-0.95996	-0.7033
C	5.69234	-0.22911	-0.12857
H	5.05347	-0.15083	1.92515
C	4.00441	-0.84428	-1.72831
H	2.04547	-1.24402	-0.91769
C	5.31996	-0.47658	-1.44498
H	6.71412	0.05715	0.10366
H	3.70591	-1.04471	-2.75349
H	6.0477	-0.38639	-2.24581
C	-0.4943	2.15526	-0.21225
Pd	-2.17508	-0.55338	0.06296
C	-4.29762	-0.13863	0.02916
C	-3.27529	-2.29134	-0.32714
C	-3.98867	-1.18378	-0.85486
H	-4.02798	-1.02111	-1.92905
H	-4.64329	0.81268	-0.36262
H	-2.81999	-3.00589	-1.00531
H	-3.50951	-2.66934	0.66636
H	-4.55523	-0.34754	1.06547
O	-0.77103	1.06753	0.73215
C	0.45873	3.1594	0.43466
H	1.46217	2.74204	0.5286
H	0.5206	4.05772	-0.18674
H	0.09555	3.44482	1.42572
C	-1.85519	2.8015	-0.44918
H	-2.306	3.09958	0.50154
H	-1.74694	3.68841	-1.07951
H	-2.53191	2.1046	-0.95452
C	0.09251	1.60511	-1.51026

H	1.04682	1.10513	-1.32519
H	-0.59127	0.88902	-1.97672
H	0.26399	2.42878	-2.20959

SI-20

Zero-point correction = 0.301905 (Hartree/Particle)
Thermal correction to Energy = 0.320001
Thermal correction to Enthalpy = 0.320946
Thermal correction to Gibbs Free Energy = 0.254032
Sum of electronic and zero-point Energies = -801.249929
Sum of electronic and thermal Energies = -801.231832
Sum of electronic and thermal Enthalpies = -801.230888
Sum of electronic and thermal Free Energies = -801.297801
E(RwB97XD) = -801.648599

Cartesian coordinates

ATOM	X	Y	Z
O	-1.30497	0.32588	-1.06403
N	-2.53176	1.45531	0.53243
C	-1.4123	1.42917	-0.33161
C	-0.49711	2.42333	-0.41313
H	-0.63172	3.34756	0.13436
C	0.75861	2.23587	-1.21375
H	1.1305	3.21125	-1.55432
H	0.53224	1.65722	-2.11558
C	1.90009	1.53786	-0.48541
C	1.98785	1.53174	0.90839
C	2.91272	0.90102	-1.21065
C	3.05863	0.92229	1.5588
H	1.19323	2.00163	1.48063
C	3.98306	0.28474	-0.56718
H	2.85702	0.88842	-2.29667
C	4.06157	0.29429	0.8249

H	3.10817	0.93579	2.64409
H	4.75716	-0.20341	-1.15241
H	4.8956	-0.18301	1.33021
C	-3.79995	1.09307	-0.08279
H	-4.24005	1.93088	-0.65009
H	-3.64613	0.2593	-0.76668
H	-4.51289	0.79094	0.6913
C	-2.64946	2.59233	1.41728
H	-1.72818	2.71145	1.9934
H	-2.85016	3.53831	0.88433
H	-3.47342	2.41549	2.11518
Pd	-0.818	-1.43231	-0.28172
C	-0.72576	-3.33489	0.75866
C	1.05675	-1.72516	0.59465
C	0.5209	-2.99086	0.22264
H	0.92093	-3.52522	-0.63506
H	-1.2789	-4.17281	0.34534
H	1.88792	-1.30261	0.03842
H	0.93952	-1.35242	1.6097
H	-1.00445	-3.02528	1.76338

References

(1) Bodnar, A. K.; Turlik, A.; Huang, D.; Butcher, W.; Lew, J. K.; Newhouse, T. R. Preparation of Hindered Aniline CyanH and Application in the Allyl-Ni-Catalyzed α,β-Dehydrogenation of Carbonyls. *Org. Synth.* **2021**, *98*, 263–288.

(2) Ishii, S.; Zhao, S.; Helquist, P. Stereochemical Probes of Intramolecular C−H Insertion Reactions of Iron-Carbene Complexes. *J. Am. Chem. Soc.* **2000**, *122*, 5897–5898.

(3) Chen, Y.; Romaire, J. P.; Newhouse, T. R. Palladium-Catalyzed α,β-Dehydrogenation of Esters and Nitriles. *J. Am. Chem. Soc.* **2015**, *137*, 5875–5878.

(4) Lim, K. M.-H.; Hayashi, T. Rhodium-Catalyzed Asymmetric Arylation of Allyl Sulfones under the Conditions of Isomerization into Alkenyl Sulfones. *J. Am. Chem. Soc.* **2015**, *137*, 3201–3204.

(5) Lang, K.; Li, C.; Kim, I.; Zhang, X. P. Enantioconvergent Amination of Racemic Tertiary C–H Bonds. *J. Am. Chem. Soc.* **2020**, *142*, 20902–20911.

(6) Yao, H.; Yamamoto, K. Aerobic Amide Bond Formation with *N*-Hydroxysuccinimide. *Chem. Asian J.* **2012**, *7*, 1542–1545.

(7) Hargrave, J. D.; Allen, J. C.; Kociok-Kohn, G.; Bish, G.; Frost, C. G. Catalytic Enantioselective Dieckmann-Type Annulation: Synthesis of Pyrrolidines with Quaternary Stereogenic Centers. *Angew. Chem. Int. Ed.* **2010**, *49*, 1825—1829.

(8) Ozeki, M.; Egawa, H.; Kuse, A.; Takano, T.; Yasuda, N.; Mizutani, H.; Izumiya, S.; Nakashima, D.; Arimitsu, K.; Miura, T. Practical and Highly Stereoselective Synthesis of Trisubstituted (*E*)- α,β-Unsaturated Esters. *Synthesis,* **2015**, *47*, 3392–3402.

(9) Chen, Y.; Turlik, A.; Newhouse, T. R. Amide A,B-Dehydrogenation Using Allyl-Palladium Catalysis and a Hindered Monodentate Anilide. *J. Am. Chem. Soc.* **2016**, *138*, 1166–1169.

(10) Davies, S. G.; Ichihara, O.; Walters, I. A. Asymmetric Synthesis of Syn-α-Alkyl-β-Amino Acids. *J. Chem. Soc., Perkin Trans. 1,* **1994**, *9*, 1141—1147.

(11) Jacobs, B. P.; Wolczanski, P. T.; Lobkovsky, E. B. Oxidatively Triggered Carbon–Carbon Bond Formation in Ene-Amide Complexes. *Inorg. Chem.* **2016**, *55*, 4223–4232.

(12) Zha, G.-F.; Fang, W.-Y.; Li, Y.-G.; Leng, J.; Chen, X.; Qin, H.-L. SO_2F_2-Mediated Oxidative Dehydrogenation and Dehydration of Alcohols to Alkynes. *J. Am. Chem. Soc.* **2018**, *140*, 17666–17673.

(13) Kojima, S.; Inai, H.; Hidaka, T.; Fukuzaki, T.; Ohkata, K. *Z*-Selective Synthesis of α,β-Unsaturated Amides with Triphenylsilylacetamides. *J. Org. Chem.* **2002**, *67*, 4093–4099.
(14) Tasker, S. Z.; Standley, E. A.; Jamison, T. F. Recent Advances in Homogeneous Nickel Catalysis. *Nature,* **2014**, *509*, 299-309.
(15) Billington, D. C. Π-Allylnickel Halides as Selective Reagents in Organic Synthesis. *Chem. Soc. Rev.* **1985**, *14*, 93–120.
(16) Takada, Y.; Caner, J.; Kaliyamoorthy, S.; Naka, H.; Saito, S. Photocatalytic Transfer Hydrogenolysis of Allylic Alcohols on Pd/TiO_2: A Shortcut to (*S*)-(+)-Lavandulol. *Chem. Eur. J.* **2017**, *23*, 18025–18032.
(17) Eckert, P.; Sharif, S.; Organ, M. G. Salt to Taste: The Critical Roles Played by Inorganic Salts in Organozinc Formation and in the Negishi Reaction. *Angew. Chem. Int. Ed.* **2021**, *60*, 12224–12241.
(18) Burchat, A. F.; Chong, J. M.; Nielsen, N. Titration of Alkyllithiums with a Simple Reagent to a Blue Endpoint. *J. Organomet. Chem.* **1997**, *542*, 281–283.
(19) Frisch, M. J.; Trucks, G. W.; Schlegel, H. B.; Scuseria, G. E.; Robb, M. A.; Cheeseman, J. R.; Scalmani, G.; Barone, V.; Petersson, G. A.; Nakatsuji, H.; Li, X.; Caricato, M.; Marenich, A. V.; Bloino, J.; Janesko, B. G.; Gomperts, R.; Mennucci, B.; Hratchian, H. P.; Ortiz, J. V.; Izmaylov, A. F.; Sonnenberg, J. L.; Williams; Ding, F.; Lipparini, F.; Egidi, F.; Goings, J.; Peng, B.; Petrone, A.; Henderson, T.; Ranasinghe, D.; Zakrzewski, V. G.; Gao, J.; Rega, N.; Zheng, G.; Liang, W.; Hada, M.; Ehara, M.; Toyota, K.; Fukuda, R.; Hasegawa, J.; Ishida, M.; Nakajima, T.; Honda, Y.; Kitao, O.; Nakai, H.; Vreven, T.; Throssell, K.; Montgomery Jr., J. A.; Peralta, J. E.; Ogliaro, F.; Bearpark, M. J.; Heyd, J. J.; Brothers, E. N.; Kudin, K. N.; Staroverov, V. N.; Keith, T. A.; Kobayashi, R.; Normand, J.; Raghavachari, K.; Rendell, A. P.; Burant, J. C.; Iyengar, S. S.; Tomasi, J.; Cossi, M.; Millam, J. M.; Klene, M.; Adamo, C.; Cammi, R.; Ochterski, J. W.; Martin, R. L.; Morokuma, K.; Farkas, O.; Foresman, J. B.; Fox, D. J. Gaussian 16 Rev. C.01. **2016**.
(20) Chai, J.-D.; Head-Gordon, M. Long-Range Corrected Hybrid Density Functionals with Damped Atom–Atom Dispersion Corrections. *Phys. Chem. Chem. Phys.* **2008**, *10*, 6615–6620.
(21) (a) Hay, P. J.; Wadt, W. R. Ab Initio Effective Core Potentials for Molecular Calculations. Potentials for the Transition Metal Atoms Sc to Hg. *J. Chem. Phys.* **1985**, *82*, 270–283. (b) Wadt, W. R.; Hay, P. J. Ab Initio Effective Core Potentials for Molecular Calculations. Potentials for

Main Group Elements Na to Bi. *J. Chem. Phys.* **1985**, *82*, 284–298. (c) Hay, P. J.; Wadt, W. R. Ab Initio Effective Core Potentials for Molecular Calculations. Potentials for K to Au Including the Outermost Core Orbitals. *J. Chem. Phys.* **1985**, *82*, 299–310.

(22) Hehre, W. J.; Ditchfield, R.; Pople, J. A. Self-Consistent Molecular Orbital Methods. Xii. Further Extensions of Gaussian-Type Basis Sets for Use in Molecular Orbital Studies of Organic Molecules. *J. Chem. Phys.* **1972**, *56*, 2257–2261.

(23) Hratchian, H.; Schlegel, H. Using Hessian Updating to Increase the Efficiency of a Hessian Based Predictor-Corrector Reaction Path Following Method. *J. Chem. Thoery Comput.* **2005**, *1*, 61–69.

(24) Schäfer, A.; Horn, H.; Ahlrichs, R. Fully Optimized Contracted Gaussian Basis Sets for Atoms Li to Kr. *J. Chem. Phys.* **1992**, *97*, 2571–2577.

(25) Marenich, A. V.; Cramer, C. J.; Truhlar, D. G. Universal Solvation Model Based on Solute Electron Density and on a Continuum Model of the Solvent Defined by the Bulk Dielectric Constant and Atomic Surface Tensions. *J. Phys. Chem. B,* **2009**, *113*, 6378–6396.